JOINT INSTITUTE FOR AERONAUTICS AND ACOUSTICS

NASA/CR- 1998 208351

National Aeronautics and
Space Administration
Ames Research Center

JIAA TR 121

Stanford University

SELF-SIMILAR COMPRESSIBLE FREE VORTICES

Karl von Ellenrieder

Department of Aeronautics and Astronautics
Stanford University
Stanford, CA 94305

March 1998

Abstract

Lie group methods are used to find both exact and numerical similarity solutions for compressible perturbations to an incompressible, two-dimensional, axisymmetric vortex reference flow. The reference flow vorticity satisfies an eigenvalue problem for which the solutions are a set of two-dimensional, self-similar, incompressible vortices. These solutions are augmented by deriving a conserved quantity for each eigenvalue, and identifying a Lie group which leaves the reference flow equations invariant. The partial differential equations governing the compressible perturbations to these reference flows are also invariant under the action of the same group. The similarity variables found with this group are used to determine the decay rates of the velocities and thermodynamic variables in the self-similar flows, and to reduce the governing partial differential equations to a set of ordinary differential equations. The ODE's are solved analytically and numerically for a Taylor vortex reference flow, and numerically for an Oseen vortex reference flow. The solutions are used to examine the dependencies of the temperature, density, entropy, dissipation and radial velocity on the Prandtl number. Also, experimental data on compressible free vortex flow are compared to the analytical results, the evolution of vortices from initial states which are not self-similar is discussed, and the energy transfer in a slightly-compressible vortex is considered.

Acknowledgements

This work was supported, in part, by the NASA Graduate Student Researchers Program and the NASA Ames-Stanford Joint Institute for Aeronautics and Acoustics NCC 2-55.

Nomenclature

Spatial/temporal coordinates

r	Radial coordinate
t	Time
$\hat{t}$	Acoustic time
τ	Viscous time
τ_t	Time constant of angular momentum transport

Flow variables

u	Radial velocity
v	Tangential velocity
ω	Vorticity
$\mathcal{M}$	Total angular momentum
A_m	m^{th} moment of vorticity
Υ	Dissipation function
p	Pressure
ρ	Density
T	Temperature
e	Internal energy (italic font)
s	Entropy
q	Radial heat flux

Subscripts & superscripts

$(\,)_\infty$	Far-field values (constant)
$(\,)_i$	Initial value ($\tau = 0$)
$(\,)_h$	Homogeneous part of solution
$(\,)_p$	Particular part of solution
$(\,)_s$	Series solution
$(\,)_e$	Exact solution
$(\,)_{ss}$	Self-similar part of solution
$(\,)_{ns}$	Non-self-similar part of solution
$(\,)_d$	Diffusion-related value
$(\,)_{obs}$	Observed value
$\hat{(\,)}$	Acoustic scaling
$\tilde{(\,)}$	Viscous scaling
$\tilde{(\,)}_0$	Incompressible reference flow quantities, viscous scaling
$\tilde{(\,)}_1$	Compressible perturbation quantities, viscous scaling
$\bar{(\,)}$	Angular momentum scaling
$\vec{(\,)}$	Vector quantity

Dimensionless parameters

Pr	Prandtl number
Re	Reynolds number
M	Mach number
Re^*	Time-dependent Reynolds number
M^*	Time-dependent Mach number

Group parameters

a, b, c	Stretching parameters
j	Eigenvalue of vorticity equation, stretching parameter
$m = j/2$	Eigenvalue, stretching parameter
τ_i	Translation-in-time parameter (corresponds to initial time)

Similarity variables

$\eta = r^2/4(\tau+\tau_i)$	Similarity coordinate
$\eta_1 = \eta Pr$	Similarity coordinate scaled by Pr
$\Omega(\eta) = \tilde{\omega}_0/(\tau+\tau_i)^{m+1}$	Self-similar reference flow vorticity
$V(\eta) = \tilde{v}_0/(\tau+\tau_i)^{m+1/2}$	Self-similar reference flow velocity
$\mathcal{P}(\eta) = \tilde{p}_0/(\tau+\tau_i)^{2m+1}$	Self-similar reference flow pressure
$\sigma(\eta) = \tilde{T}_1/(\tau+\tau_i)^{2m+1}$	Self-similar temperature perturbation
$\beta(\eta) = \tilde{\rho}_1/(\tau+\tau_i)^{2m+1}$	Self-similar density perturbation
$\alpha(\eta) = \tilde{u}_1^*/(\tau+\tau_i)^{2m+3/2}$	Self-similar radial velocity perturbation
$\phi(\eta) = \tilde{v}_1/(\tau+\tau_i)^{3m+3/2}$	Self-similar tangential velocity perturbation
$\psi(\eta) = \tilde{p}_1/(\tau+\tau_i)^{4m+2}$	Self-similar pressure perturbation
$\zeta(\eta) = \tilde{s}_1/(\tau+\tau_i)^{2m+1}$	Self-similar entropy perturbation
$\delta(\eta) = (\partial\tilde{s}_1/\partial\tau)/(\tau+\tau_i)^{2(m+1)}$	Self-similar dissipation perturbation
$\varpi(\eta) = \tilde{\omega}_1/(\tau+\tau_i)^{3m+2}$	Self-similar vorticity perturbation

Physical constants

R	Specific gas constant
C_p	Specific heat at constant pressure
C_v	Specific heat at constant volume
$\gamma = C_p/C_v$	Ratio of specific heats
a_∞	Far-field sound speed

Viscosity/conductivity

μ	Shear viscosity
μ_ν	Bulk viscosity
$\nu = \mu/\rho$	Kinematic viscosity
κ	Thermal conductivity

Mathematical functions/symbols

$\frac{\partial}{\partial r}$	Partial derivative wrt. r
$\frac{\mathrm{d}}{\mathrm{d}r}$	Total derivative wrt. r
$\frac{\partial}{\partial t}$	Partial derivative wrt. t
$\frac{\mathrm{d}}{\mathrm{d}t}$, or $\frac{\mathrm{D}}{\mathrm{D}t}$	Total (material) derivative wrt. t
$\vec{\nabla}$	Gradient operator
$\bar{\mathrm{M}}(\ )$	Hypergeometric function
$\mathrm{L}_m(\ )$	m^{th} Laguerre polynomial
$O(*)$	Order of magnitude of $*$
$\max(*)$	Maximum value of $*$
$\Delta *$	Maximum variation of $*$
e, exp	Base of the natural logarithm (roman font)
π	Pi, $\pi = 3.14159\ldots$
dS	Differential surface element
dV	Differential volume element
f	Generic flow variable/function

Mathematical constants

C	Integration constant for $\tilde{T}_1$
$\bar{C}_j, \bar{D}_j$	Integration constants for Ω
$C_m = \bar{C}_{j/2}$	Integration constant for Ω
B_m	Integration constant for σ
B_{1s}	Integration constant for σ when $m = 1$, series soln.
B_{1e}	Integration constant for σ when $m = 1$, exact soln.

D_n	Frobenius series coefficients
G_m	Integration constant for α
Q_m	Integration constant for ϕ
W_m	Integration constant for ϖ

Abbreviations

ODE	Ordinary differential equation
PDE	Partial differential equation
wrt.	with respect to

Miscellaneous symbols

$\tilde{u}_1^*$	Perturbed radial velocity scaled by $\tilde{Re}$
$\Delta\rho^*$	$(\rho_\infty - \rho(r=0))/\rho_\infty$ Normalized density-well depth
l	Vortex core size

Contents

Abstract iii

Acknowledgements iv

Nomenclature v

1 Introduction 1

1.1 Orientation 2

1.2 Literature survey 10

1.3 Overview 12

2 Similarity and the Navier-Stokes Equations 13

2.1 Two-dimensional, axisymmetric, Navier-Stokes equations 13

2.1.1 Simplifications 14

2.2 Non-dimensional forms and perturbation expansions 16

2.2.1 The viscous timescale equations 16

2.2.2 The low Mach number approximation 20

3 The Reference Flow 23

3.1 Derivation 23

3.2 Physical description of reference flow solutions 26

3.2.1 Tangential velocity 27

3.2.2 Pressure 28

3.2.3 Decay rates 30

3.2.4 Superposed solutions 31
3.3 The Oseen vortex, the Taylor vortex and Mandella's vortex 32

4 Similarity Forms **39**
4.1 Perturbation variables 39
4.1.1 Decay rates 41
4.2 Perturbed entropy, dissipation, and vorticity 41
4.2.1 Entropy and dissipation 41
4.2.2 Vorticity 44
4.2.3 Similarity forms 44
4.3 Perturbation equations 45
4.3.1 The behavior of the solutions 47

5 Solutions **48**
5.1 Analytical solutions for the slightly-compressible Taylor vortex 48
5.1.1 Initial/boundary conditions 50
5.1.2 Convergence rates 55
5.1.3 Prandtl number dependence 58
5.1.4 Entropy production 61
5.2 Numerical solutions 62

6 Discussion **67**
6.1 Radial velocity 67
6.2 Vortex energetics 69
6.3 The entropy distribution 72
6.4 Entropy production 73
6.5 Similarity and decay rates 76

7 Conclusions & Recommendations **80**
7.1 Conclusions 80
7.2 Future work 82

A Angular Momentum 84
A.1 Angular momentum transport 84
A.1.1 Convective 85
A.1.2 Convective/diffusive 86
A.1.3 Diffusive 86
A.2 Discussion 86

B Introduction to One-Parameter Lie Groups 88
B.1 Basic definitions 88
B.2 Simplifying/solving equations 95

C The Integral Invariants 97

D Similarity at Higher Orders 99

Bibliography 102

List of Tables

5.1 C_m and τ_i for $m \in \{0, \ldots, 4\}$ 62

A.1 Physical constants characteristic of the experimental vortex 85

D.1 Similarity forms 100

List of Figures

1.1 (a,b) Structure of a two-dimensional, compressible, free vortex 5
1.1 (c,d) 6
1.1 (e) 7
1.2 Coordinate system and flow-field 8
1.3 Flow-field around an experimentally-created vortex (shadowgraph) . . 9
1.4 Flow-field around an experimentally-created vortex (schlieren) 10

2.1 Acoustic and viscous flow regions 18

3.1 (a,b) Reference flow vorticity, tangential velocity, and pressure 29
3.1 (c) 30
3.2 Creation of a free two-dimensional vortex 35
3.3 Free vortex formation sequence 36

5.1 (a,b) Exact solutions for a slightly-compressible Taylor vortex 52
5.1 (c,d) 53
5.1 (e,f) 54
5.1 (g) 55
5.2 (a,b) Variation of the exact solution with B_{1e} 56
5.2 (c,d) 57
5.3 Convergence of the series solution vs. N 58
5.4 Convergence of the series solution vs. η 59
5.5 (a,b) Pr dependence of the Taylor vortex solution 60
5.5 (c) 61

5.6 (a,b) Pr dependence of the Oseen vortex solution 64
5.6 (c,d) 65
5.7 Pr dependence of the radial velocity in a Taylor vortex 66

6.1 (a,b) Pressure, density, temperature and entropy in Mandella's vortex 74
6.1 (c,d) 75
6.2 Entropy production in the Taylor vortex 77
6.3 Entropy produced by heat transfer and viscous work for $m = 1$ 78

B.1 An invariant curve 91
B.2 A family of rays 94

Chapter 1

Introduction

A *compressible flow* is one in which a change in pressure over some characteristic length scale of the flow results in a corresponding change in density. Similarly, a *compressible vortex* is a vortex containing large tangential velocities which create strong pressure gradients; these pressure gradients, in turn, produce substantial density variations across the vortex. The main objective of this thesis is to present analytical self-similar solutions of the equations describing the viscous decay of a two-dimensional, axisymmetric, slightly-compressible, free vortex. A quantitative characterization of the problem at hand is given in § 1.1. However, let us first consider the current state of basic research on this subject.

Vortices have long fascinated fluid dynamicists and although the total number of investigations involving vortices is quite large, there has been relatively little work on compressible vortex flow. For example, a search of the citations in Stanford University's science journal holdings reveals that, since 1969, the university has collected about 18,500 articles on vortices. A similar search shows that, during the same time period, the university libraries acquired around 330 compressible vortex articles. Assuming these numbers are representative of the general state of vortex research, slightly less than 2% of the work on vortex flow takes into account the effects of compressibility. Further, studies of flows containing compressible vortices do not usually focus on the basic physics or structure of a vortex, but concentrate on other aspects

of the flow — such as shock/vortex interaction, blade/vortex interaction, or vortex breakdown.

The dearth of basic research on compressible vortices is especially surprising given the fact that they play a key role in many fluid flows of physical interest: turbulent combustion in piston and turbine engines, strong wing-tip vortices, flows with aerodynamically generated noise, shock diffraction around sharp corners, and astrophysical flows such as those occurring in the solar corona or in the gaseous disks of spiral galaxies. Most fluid dynamicists are surprised to find that there are no simple analytical solutions describing the viscous decay of a compressible free vortex. The mathematical solutions to the equations of compressible vortex flow are complicated and must usually be numerically obtained. The primary goal of this thesis is to describe a set of simple analytical solutions for compressible free vortex flow. This work is motivated by the fact that such solutions can yield a great amount of insight into the fundamental physical behavior of compressible vortices, as well as provide a quick and easy means of validating computational and experimental results.

The next section further describes the flow under consideration and is followed by a brief literature survey of work on compressible vortices and an overview of the thesis.

1.1 Orientation

The lack of work on compressible free vortices is partly due to their complexity. In contrast, the two-dimensional motion of an isolated free vortex in an incompressible flow is well understood. Conservation of mass requires that there is no radial velocity in the vortex, and the Reynolds number Re, governs the vortex's evolution. For very large Reynolds numbers, $Re \to \infty$, the flow is essentially inviscid, and the vortex motion is nearly steady. Otherwise, for $Re \sim O(1)$ or smaller, one finds that the viscous diffusion of angular momentum is the process which dominates the flow.

When the compressibility of fluid within the vortex is important, the flow has an analogous dependence on the Reynolds number, but analyzing the flow becomes more complicated. In studying a two-dimensional, compressible vortex one must

examine the effects of heat conduction, viscous dissipation, compressibility, and radial convection on the motion and structure of the vortex [7]. In addition to Re, solutions for compressible vortex flow require that four other parameters be considered: the Mach number M, the Prandtl number Pr, and the temperature dependent values of viscosity μ, and thermal conductivity κ.

To get a quantitative feel for the nature of the compressible vortices under investigation, consider the vortex pictured in figure 1.1(a–e). In general, the radial profiles of the velocities and thermodynamic variables (pressure, density, temperature, etc.) in such a vortex may be slightly different, but the sketch illustrates the main structural features of a compressible vortex. Here r is the radial coordinate and the origin of the system is the center of the vortex (see figure 1.2). Since the present work is limited to two-dimensional axisymmetric vortices, the flow does not vary in the tangential or axial directions. Here we will also assume that the far-field ($r \rightarrow \infty$) flow conditions are constant.

The maximum tangential velocity v_m occurs at the radial location l_i (figure 1.1a); l_i will be called the *core size* of the vortex. In the following analysis, l_i and v_m are the length scale and the velocity scale, respectively. Together with the far-field viscosity, density, and sound speed, l_i and v_m are used to form the Reynolds number and Mach number of the vortex.

As a rule of thumb, the maximum tangential velocity can be considered "large" when its magnitude is greater than or equal to about 30% of the far-field speed of sound. Thus, for a Mach number of $M \gtrsim 0.30$ the vortex will be considered compressible; when the Mach number is lower than $M \approx 0.3$ a simplified analysis which assumes the flow is completely incompressible should generally suffice. However, the vortex studied here is *slightly-compressible* and so v_m cannot be too large either. As will be further explained in §2.2 the present study uses the Rayleigh-Janzen expansion [38] to derive equations describing compressible perturbations to an incompressible vortex reference flow. Colonius, Lele, & Moin [12] compare the results of computations of the full Navier-Stokes equations and numerical solutions for a slightly compressible vortex flow (found using the Rayleigh-Janzen expansion). They show that the

approximation is valid for Mach numbers as large as $M \approx 0.67$. The same flow conditions apply to the vortices in this work, so we will take the range of Mach numbers under consideration to be $0.30 \lesssim M \lesssim 0.67$.

The centrifugal force in the rotating vortex flow produces a pressure minimum at the center of the vortex. The corresponding density variation in the vortex is regarded as significant when the non-dimensional *depth of the density well* $\Delta\rho^*$, which is the difference between the density in the center of the vortex and the density in the far-field ρ_∞, normalized by the far-field density, is $\Delta\rho^* \gtrsim 0.3$.

Consider the vortex studied by Mandella & Bershader [26]. A two-dimensional, compressible, free vortex was created in a shock tube by the diffraction of a shock around a 3.7 cm chord-length NACA 0018 airfoil (see §3.3). The strength of the incident shock was $M_s \approx 1.8$, and the airfoil's angle of attack was 30°. The vortex was embedded in a free stream with a Mach number of $M_\infty \approx 0.52$ and a Reynolds number, based on airfoil chord-length, of $Re_\infty \approx 4.4 \times 10^5$. Holographic interferometry and pressure transducers were used to measure the density and pressure, respectively, in the vortex studied. The measured density and pressure distributions in the vortex and the estimated tangential velocity in the flow give $l_i \approx 9.3 \times 10^{-1}$ mm, $v_m \approx 2.3 \times 10^2$ m s^{-1}, $M \approx 6.7 \times 10^{-1}$, and $\Delta\rho^* \approx 5.5 \times 10^{-1}$. The vortex Reynolds number (based on l_i, v_m, and a far-field kinematic viscosity of $\nu_\infty \approx 1.1 \times 10^{-5}$) is $\tilde{Re} \approx 2.0 \times 10^4$. The magnitude of the radial velocity in a compressible free vortex is generally very small (figure 1.1*e*). Mandella & Bershader estimate the magnitude of the maximum radial velocity in the vortex they studied to be $(\max|u|)/v_m \approx 1.3 \times 10^{-3}$. However, Colonius *et al.* [12] have shown that if the far-field flow conditions are assumed to be constant, Mandella's estimate of the radial velocity is too large and therefore violates the Second Law of Thermodynamics. They suggest the radial velocity should be around two orders of magnitude smaller. Nevertheless, the vortex in Mandella & Bershader's experiments clearly exhibits the tangential velocity, density, and pressure profiles characteristic of a compressible vortex. The issues of the entropy distribution and the entropy production in a compressible vortex will be discussed in §§ 6.3 and 6.4.

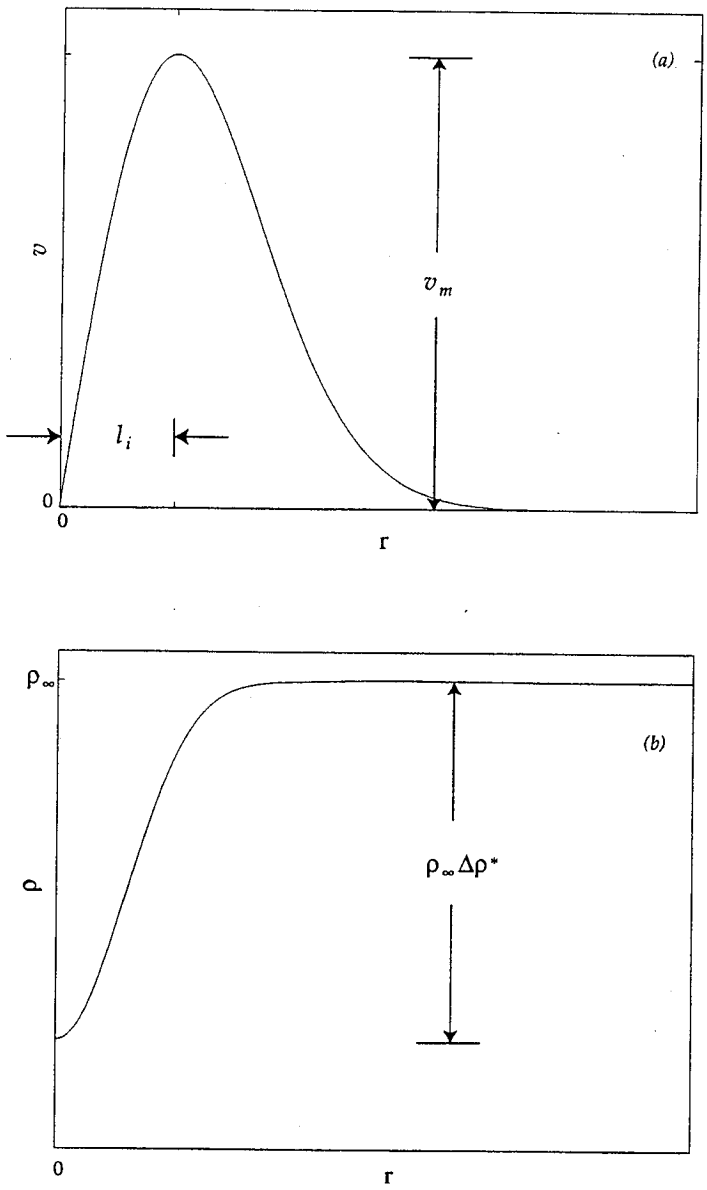

Figure 1.1: a, b

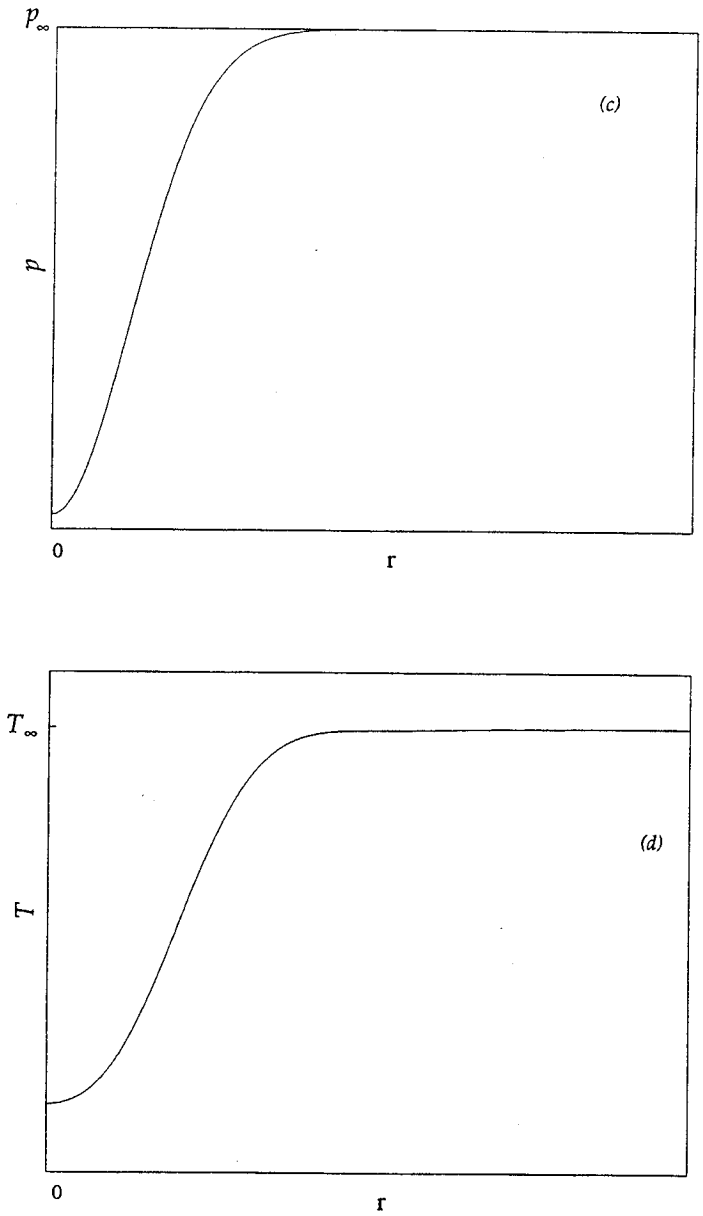

Figure 1.1: c, d

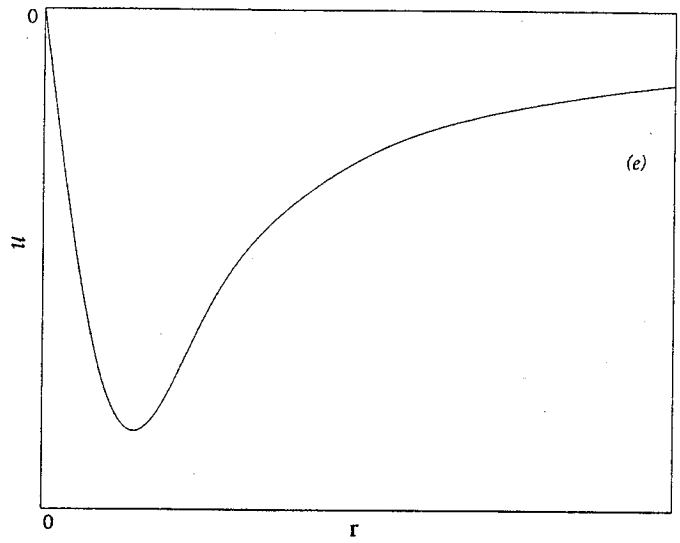

Figure 1.1: The structure of a two-dimensional, compressible, free vortex — radial profiles of (a) tangential velocity, (b) pressure, (c) density, (d) temperature, (e) radial velocity.

The vortices considered in this work are called *free vortices* because there are no boundaries in the flow for $0 \leq r/l_i < \infty$. Therefore, the fluid's motion is only determined by its internal shear stresses and the exhange of momentum between neighboring fluid particles. This is in contrast to a *driven vortex* in which the movement is influenced by an externally controlled surface — such as a rotating cylinder centered at the origin of the flow [6], [23]. Additionally, we will assume that there are no acoustic waves present in the flow (see §2.2.1).

Note that in this work the interferograms and data obtained in the experiments of Mandella [25] will be used to describe the formation of compressible free vortices, study their entropy distributions, and to construct initial conditions for our self-similar vortex solutions. However, one must be careful to remember that the vortex solutions presented in this theoretical study correspond to idealized flow conditions. The flow-field in the experiments is less "hospitable" and less well-characterized. The

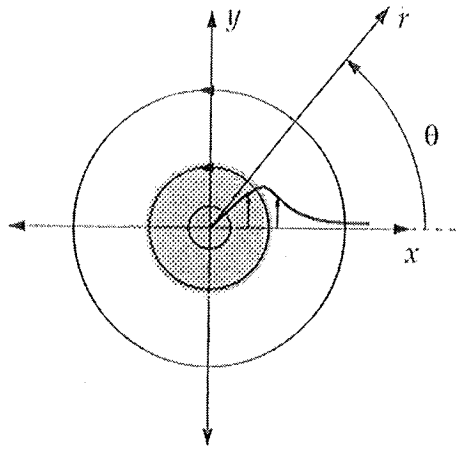

Figure 1.2: Sketch of the coordinate system and flow-field. Circular lines depict the rotating fluid in the vortex. The curved line radially emanating from the origin schematically represents the tangential velocity profile of a Taylor vortex [36].

timescale of diffusion for the vortex studied by Mandella would be $t_d \approx 7.9 \times 10^{-2}$ s, based on a coresize of $l_i \approx 9.3 \times 10^{-1}$ mm, a viscosity of $\mu \approx 1.9 \times 10^{-5}$ N s m^{-2}, and a density of $\rho_\infty \approx 1.8$ kg m^{-3}; the observation period in Mandella's experiments[1], $t_{obs} \approx 500$ μs, is about two orders of magnitude smaller than t_d. In comparison, the acoustic timescale for the vortex is $t_a \approx 2.7\mu$s based on the same value of l_i and a far-field sound speed of $a_\infty \approx 3.4 \times 10^2$m s^{-1}. At early times in the motion of the vortex in Mandella's experiment, the presence of acoustic waves in the flow may affect the vortex's evolution. Figures 1.3 and 1.4 show a compressible free vortex which has been created using the same conditions as the vortices studied by Mandella & Bershader [26]. Notice the weak circular shockwave, the non-linear acoustic waves, and the rolled up vortex sheet surrounding the vortex. The experimental flow is quite complex and the far-field flow conditions may be time dependent [2]. The acoustic waves propagate away from the vortex just after the vortex has formed. In this experiment, and in

[1] During this observation period, the free vortex travels a distance of ≈ 9.0 cm and executes about 130 rotations or "eddy turnovers".

[2] Over the short observation time of Mandella's experiment, the distributions of radial velocity and entropy may be very sensitive to small changes in the far-field pressure and density; see von Ellenrieder, Kao, & Bershader [40] and Appendix A.

the experiments of Mandella & Bershader the observations are made within 500 μsecs of the vortex's formation. Because of the presence of these waves, and the short observation period of Mandella's experiments, a direct comparison cannot be made between the time evolution of the vortex studied by Mandella and the viscous decay of the self-similar vortex solutions developed here.

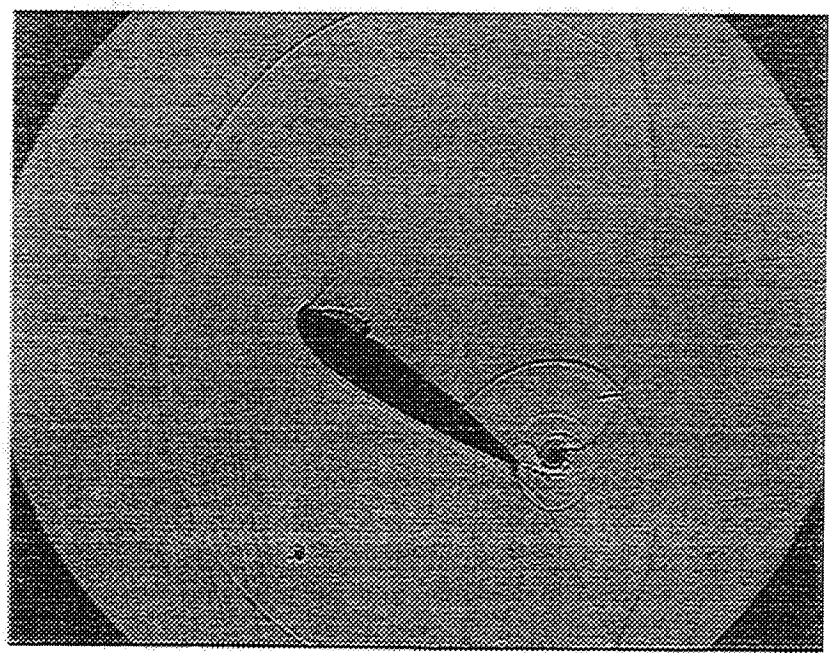

Figure 1.3: A shadowgraph of the flow-field around a vortex created under the same conditions used in the experiments of [26]. There are several acoustic waves present in the flow (circular waves centered near the vortex center). Also, one can see several contact surfaces and a slip-line, which extends from the trailing-edge of the airfoil, being wrapped around the vortex.

The final approximations made in the following analysis are that the coefficients of viscosity and thermal conductivity are constant. In summary, the following assumptions have been made: The vortex is a two-dimensional, axisymmetric, slightly-compressible, viscously-decaying, free vortex; the far-field flow conditions and the coefficients of viscosity and thermal conductivity are constant.

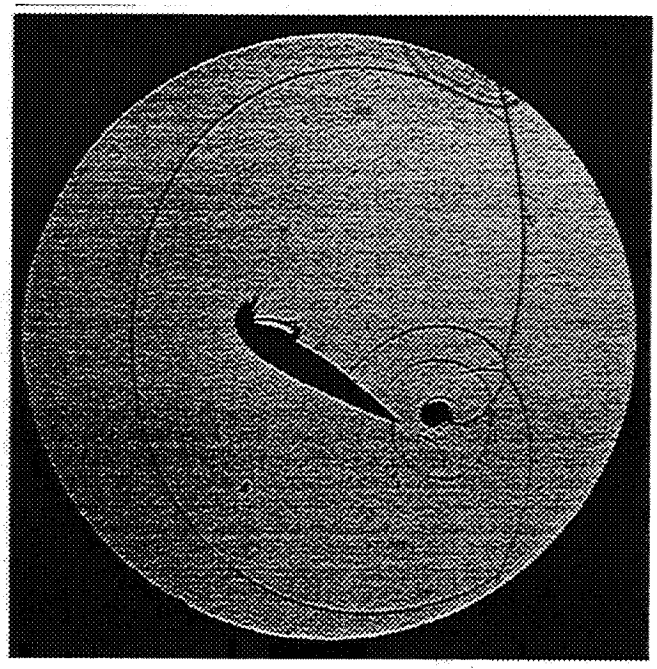

Figure 1.4: Two-color (yellow & blue) schlieren image of the flow-field around a vortex created under the same conditions used in the experiments of [26]. This image corresponds to a slightly later experimental time than shown in figure 1.3. The density variations in the separation bubble and vortex at the nose of the airfoil, as well as the shock system, are more apparent in this image than in the preceding picture. However, the shadowgraph in figure 1.3 more clearly captures the slipstreams present in the flow.

1.2 Literature survey

This section discusses only previous work on viscous two-dimensional free vortices. The reader interested in steady inviscid vortices [11], [2], driven vortex flow [23], [6], three-dimensional compressible vortices [27], or in compressible leading-edge vortices [9] is referred to the cited works and to the fairly comprehensive review written by Bershader [7].

Mandella [25] and Mandella & Bershader [26] discuss a compressible free vortex which is produced by shock diffraction in a shock tube. Interferometric density measurements are used to develop empirical formulae for the evolution of the density

and radial velocity in the vortex. The pressure in this vortex is measured at one location along its trajectory. Using these data, and assuming that the radial pressure gradient is balanced by centrifugal forces, the distributions of temperature and tangential velocity in the vortex are calculated. Mandella & Bershader conclude that: the compressible free vortex studied in their experiments is not homentropic; the radial velocities present in the vortex arise to counteract the viscous diffusion of angular momentum[3]; and the primary effects of compressibility are the inward convection and compression of rotating fluid.

Sibulkin [33] investigates the transfer of total energy within a decaying, two-dimensional, viscous rotating flow. Low Mach number flows of both liquids and gases are considered. Analytical solutions for the perturbations to the total energy in a Taylor vortex [36] reference flow are given for early times in the evolution of the vortex (when $Pr = 1$ and $\gamma = 2$). Sibulkin also considers the Pr variation of the driving terms in the perturbed energy equation. Unfortunately, in Sibulkin's approach, velocity perturbations which are on the order of the Mach number squared are neglected in the analysis, and so the radial velocity in the vortex is assumed to be zero. This leads to a contradiction in the overall solution. The solution predicts that the total mass in the vortex increases in time, yet aside from radial convection there is no physical mechanism to cause the accretion of mass in the vortex. Additionally, with the omission of the radial and tangential velocity perturbations Sibulkin's solutions for the total energy are incomplete.

Colonius *et al.* [12] perform an analytical and numerical study of compressible free vortices. Viscosity and heat conductivity are taken into account with the simplifying assumption that both are constant. The Navier-Stokes equations are expanded in powers of Re^{-1} to determine the evolution of the flow on a viscous and on an acoustic time-scale. An ordinary differential equation (ODE) for the vortex's radial velocity is found using the viscous timescale equations. Estimates of the radial velocity for the vortex described in the experiments of Mandella & Bershader are made using the ODE. The estimates are compared to both the empirical formulas mentioned above

[3]See appendix A for a further discussion of angular momentum conservation in a compressible vortex.

and to computational solutions of the full Navier-Stokes equations. Colonius *et al.* find that the experimentally determined radial velocity is too large, and that the empirical formulas violate the Second Law of Thermodynamics — the net amount of entropy generated in the flow would be negative. Additionally, the viscous timescale equations are expanded in powers of Mach number squared (M^2) to derive a set of equations describing compressible perturbations to an incompressible reference flow. Solutions for the case of an Oseen vortex reference flow are determined using numerical integration. Two different initial conditions, which are not self-similar, are used for the calculations. In the first case the vortex initially has a constant density; in the second case the vortex is initially homentropic. Colonius *et al.* find that the radial velocity in a slightly-compressible vortex is generated by viscous effects and that the vortex is compressed, regardless of the initial distributions of density and entropy.

1.3 Overview

This thesis presents a set of self-similar solutions for the compressible perturbations to an incompressible, two-dimensional, axisymmetric vortex. A discussion of the perturbation equations is given chapter 2 and is followed in chapter 3 by a description of the reference flow solutions, the corresponding conserved quantities, and a discussion of how compressible free vortices may be formed. Similarity variables which transform both the reference flow equations and the perturbation equations from partial differential equations (PDE's) to ODE's are derived in chapter 4, and some of the properties of the new equation set are discussed. In chapter 5 exact solutions and numerical solutions for the Taylor vortex [36] temperature, density and entropy perturbations are presented. Numerical solutions for the Oseen vortex [30] and the Taylor vortex base flows are compared and the influence of the Prandtl number on the temperature, density, entropy, and radial velocity distributions is also investigated. In chapter 6 we discuss the dissipation produced in the Taylor vortex, examine the decay of vortices from initial conditions which are not self-similar, and investigate the nature of the radial velocity and the energy transfer in a slightly compressible vortex. A brief summary of this thesis and some concluding remarks are given in chapter 7.

Chapter 2

Similarity and the Navier-Stokes Equations

2.1 Two-dimensional, axisymmetric, Navier-Stokes equations

For a two-dimensional, cylindrically-symmetrical fluid flow, the conservation equations for mass, radial momentum, tangential momentum, and internal energy, respectively, are

$$\frac{\partial \rho}{\partial t} + \frac{1}{r}\frac{\partial}{\partial r}(\rho u r) = 0, \tag{2.1a}$$

$$\frac{\partial u}{\partial t} + u\frac{\partial u}{\partial r} + \frac{1}{\rho}\frac{\partial p}{\partial r} = \frac{v^2}{r} + \frac{2\mu}{\rho}\frac{\partial}{\partial r}\left[\frac{1}{r}\frac{\partial}{\partial r}(ru)\right] + \frac{\partial}{\partial r}\left[\left(\mu_\nu - \frac{2\mu}{3}\right)\frac{1}{r}\frac{\partial}{\partial r}(ru)\right], \tag{2.1b}$$

$$\frac{\partial v}{\partial t} + u\frac{\partial v}{\partial r} + \frac{uv}{r} = \frac{\mu}{\rho}\frac{\partial}{\partial r}\left[\frac{1}{r}\frac{\partial}{\partial r}(rv)\right], \tag{2.1c}$$

$$\rho\frac{\partial e}{\partial t} + \rho u\frac{\partial e}{\partial r} = -\frac{p}{r}\frac{\partial}{\partial r}(ru) + \Upsilon + \frac{1}{r}\frac{\partial}{\partial r}\left(\kappa r\frac{\partial T}{\partial r}\right). \tag{2.1d}$$

The radial coordinate r, is the distance from the center of the vortex, and t represents time. The radial and tangential velocities u and v (respectively), as well as the thermodynamic variables (internal energy e, pressure p, density ρ, and temperature T) are functions of r and t. The bulk viscosity μ_ν, the shear viscosity μ, the thermal

conductivity κ, and the ratio of specific heats γ, are assumed constant in this analysis. Additionally, the fluid under consideration is taken to be an ideal gas with equation of state $p = \rho RT$, where R is the specific (molar) gas constant. The term Υ in the energy equation is the dissipation function given by

$$\Upsilon = 2\mu \left\{ \left(\frac{\partial u}{\partial r}\right)^2 + \left(\frac{u}{r}\right)^2 + \frac{r^2}{2}\left[\frac{\partial}{\partial r}\left(\frac{v}{r}\right)\right]^2 \right\} + \left(\mu_\nu - \frac{2\mu}{3}\right)\frac{1}{r^2}\left[\frac{\partial}{\partial r}(ru)\right]^2. \qquad (2.2)$$

The quantity Υ is positive definite and corresponds to the part of the viscous work used to deform (not accelerate) a fluid particle [37].

The fluid under consideration is thermally and calorically perfect, so the internal energy is linearly proportional to the temperature: $e = C_v T$. C_v is the the specific heat at constant volume, and is related to the specific heat at constant pressure C_p by $R = C_p - C_v$ and alternatively by $\gamma = C_p/C_v$. Using these relations, (2.1a), and the equation of state, the internal energy equation (2.1d) can be written in terms of the pressure

$$\frac{\partial p}{\partial t} + u\frac{\partial p}{\partial r} + \frac{\gamma p}{r}\frac{\partial}{\partial r}(ru) = (\gamma - 1)\Upsilon + \frac{(\gamma - 1)}{r}\frac{\partial}{\partial r}\left(\kappa r \frac{\partial T}{\partial r}\right). \qquad (2.3)$$

2.1.1 Simplifications

The large number of parameters and the nonlinearity of the equations shown above makes them difficult to solve analytically. In general, analytical solutions require substantial simplification of the boundary conditions, the initial conditions, and the form of the equations. For example, Chiocchia [11] and Ardalan *et al.* [2] assumed steady, inviscid flow and applied hodograph transformations to solve ideal-fluid, compressible vortex problems. Earlier, Mack [23] and Bellamy-Knights [6] investigated steady, viscous, compressible vortex flows. In both of the latter two works, the boundary conditions at the center of the vortex were simplified by driving the flow with a rotating circular cylinder.

In order to describe unsteady, viscous, compressible vortex flow, Colonius *et al.* [12] made several simplifications to (2.1a–c) and (2.3). The initial conditions were specified at all radial locations by assuming that the flow starts in a state where the vortex has either a constant density distribution or a constant entropy distribution. The complexity of the equations is reduced by assuming a high Reynolds number flow and using low Mach number perturbation expansions.

Among techniques for finding analytical solutions to compressible vortex flow, the search for symmetry under a Lie group seems like a natural approach[1]. But note that for a free vortex in an unbounded domain the far-field pressure, density, and temperature asymptotically converge to non-zero constant values. However, similarity solutions require the system of governing equations to be invariant under translations of the thermodynamic variables. For example consider the following boundary condition for the far-field density:

$$\lim_{r\to\infty} \rho = \rho_\infty,$$

where ρ_∞ is a constant. A simple test to determine if a given transformation leaves an equation invariant is to re-write the equation in terms of the transformed variable. If the equation reads exactly the same in the new variables, then the equation is invariant under the transformation. The boundary condition above is invariant under the following translation group

$$\rho' = \rho - \rho_\infty, \tag{2.4}$$

if ρ' can be found such that

$$\lim_{r\to\infty} \rho' = 0.$$

But, on substituting the transformation (2.4) into (2.1a), we see that the transformation does not leave the continuity equation invariant. An extra term containing ρ_∞ appears in the transformed equation, but is not present in the original equation

$$\frac{\partial \rho'}{\partial t} + \frac{1}{r}\frac{\partial}{\partial r}(\rho' u r) + \frac{1}{r}\frac{\partial}{\partial r}(\rho_\infty u r) = 0.$$

[1] A brief introduction to Lie groups is given in appendix B.

Since the full Navier-Stokes equations are not invariant under translations of the thermodynamic variables they will not admit similarity solutions for compressible free vortex flow; this is the main reason why analytical solutions for fully-compressible free vortices do not exist. However, as shown in chapters 3 and 4, the perturbation equations and the incompressible reference flows presented by Colonius *et al.* [12] are invariant under a three-parameter Lie group. This group allows a rich set of similarity solutions to be found for a slightly compressible vortex. In general, similarity transformations are used to decrease the number of dimensions in a problem by combining independent variables [8], [10]. This provides two main benefits: 1) The number of initial or boundary conditions required to solve the problem is reduced. For the vortex under consideration, the use of similarity transformations makes it unnecessary to explicitly assign initial conditions for each flow variable at every point in the flow. For example, if the temperature at the center of a self-similar vortex is specified at a given time, the value of the temperature at all other radial locations (for the same time) is fixed. 2) The PDE's describing compressible perturbations of the vortex are reduced to ODE's which are, in this case, relatively easy to solve.

2.2 Non-dimensional forms and perturbation expansions

The similarity solutions for a slightly compressible vortex are developed from the perturbation equations formulated by Colonius *et al.* [12]. We summarize the derivation of these equations for completeness, and make some additional remarks concerning the bulk viscosity, initial conditions, and boundary conditions.

2.2.1 The viscous timescale equations

Solutions of (2.1a–c) and (2.3) vary on three time scales: viscous, convective, and acoustic. If it is assumed that the radial velocity in the vortex arises to counteract the viscous diffusion of angular momentum, the convective and the diffusive timescales are equivalent. The flow variables are written as functions of an acoustic timescale

$\hat{t}$, a slower viscous timescale τ, where $\mathrm{d}\tau = \mathrm{d}\hat{t}/Re$, and a non-dimensional radial coordinate $\hat{r}$. The flow quantities in (2.1a–c) and (2.3) are then expanded in terms of the viscous time τ, and the resulting expressions are collected in powers of Re^{-1}. The non-dimensional parameters used in the timescale expansions are

$$\left.\begin{aligned} \hat{r} = \frac{r}{l_i}, \quad \hat{t} = \frac{a_\infty t}{l_i}, \quad \hat{v} = \frac{v}{a_\infty}, \\ \hat{u} = \frac{u}{a_\infty}, \quad \hat{\rho} = \frac{\rho}{\rho_\infty}, \quad \hat{p} = \frac{p}{\rho_\infty a_\infty^2}, \\ \hat{T} = \frac{C_p T}{a_\infty^2}, \quad Re = \frac{\rho_\infty a_\infty l_i}{\mu}, \quad Pr = \frac{\mu C_p}{\kappa}. \end{aligned}\right\} \tag{2.5}$$

l_i is the core size of the vortex's initial velocity profile. Here, we define the core size as the radial position of maximum tangential velocity. The specific heat at constant pressure is C_p, the far-field speed of sound is a_∞, and all far-field flow conditions are denoted by the subscript ∞.

Under the further assumption that $\hat{u} \sim O(1/Re)$ and with $\hat{u}^* = \hat{u}Re$, the viscous timescale equations are found to be

$$\frac{\partial \hat{\rho}}{\partial \tau} + \frac{1}{\hat{r}}\frac{\partial}{\partial \hat{r}}(\hat{\rho}\hat{u}^*\hat{r}) = 0, \tag{2.6a}$$

$$\frac{\partial \hat{p}}{\partial \hat{r}} = \frac{\hat{\rho}\hat{v}^2}{\hat{r}}, \tag{2.6b}$$

$$\hat{\rho}\frac{\partial \hat{v}}{\partial \tau} + \frac{\hat{\rho}\hat{u}^*}{\hat{r}}\frac{\partial}{\partial \hat{r}}(\hat{r}\hat{v}) = \frac{\partial}{\partial \hat{r}}\left[\frac{1}{\hat{r}}\frac{\partial}{\partial \hat{r}}(\hat{r}\hat{v})\right], \tag{2.6c}$$

$$\frac{\partial \hat{p}}{\partial \tau} + \hat{u}^*\frac{\partial \hat{p}}{\partial \hat{r}} + \frac{\gamma \hat{p}}{\hat{r}}\frac{\partial}{\partial \hat{r}}(\hat{r}\hat{u}^*) = (\gamma - 1)\left[\hat{r}\frac{\partial}{\partial \hat{r}}\left(\frac{\hat{v}}{\hat{r}}\right)\right]^2 + \frac{(\gamma - 1)}{Pr}\frac{1}{\hat{r}}\frac{\partial}{\partial \hat{r}}\left(\hat{r}\frac{\partial \hat{T}}{\partial \hat{r}}\right). \tag{2.6d}$$

The equation of state has the form:

$$\hat{p} = \frac{(\gamma - 1)}{\gamma}\hat{\rho}\hat{T}. \tag{2.6e}$$

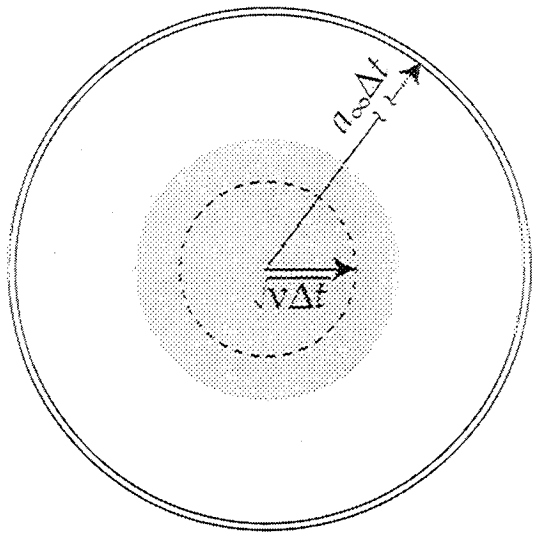

Figure 2.1: Acoustic and viscous (shaded area) flow regions; $a_\infty \Delta t \gg (\nu \Delta t)^{1/2}$.

Assuming that there are no acoustic waves propagating into the region of interest, the Re^{-1} timescale expansion has the effect of separating the events occurring on an acoustic timescale from those events which occur over a longer viscous timescale. To see this, compare the acoustic propagation of a disturbance starting at $r = 0$ and the viscous diffusion of a disturbance also starting at the origin. During a time Δt the acoustic disturbance travels a distance $\approx a_\infty \Delta t$, and the viscously diffusing disturbance travels a distance $\approx (\nu \Delta t)^{1/2}$, where $\nu = \mu/\rho_\infty$. The velocity of the acoustic wave is around a_∞, whereas the time dependent velocity of the diffusing disturbance is about $(\nu/2\Delta t)^{1/2}$. If we assume that at very early times $\Delta t < \nu/a_\infty^2$ the fluid can be treated as a continuum[2], the diffusing disturbance travels faster than

[2]Strictly speaking, one cannot treat the fluid as a continuum at such short times. For air at standard atmospheric temperature and pressure $\nu/a_\infty^2 \approx 1.3 \times 10^{-10}$ s. In comparison, the time between successive collisions of the air molecules would be around 1.4×10^{-10} s. So for $\Delta t < \nu/a_\infty^2$ the gas will not reach thermal equilibrium after the disturbance's occurence. To properly model the situation, one would have to invoke the kinetic theory of gases; for example see the work concerning an impulsively-started plate performed by Howarth [17] and Yang & Lees [42].

the acoustic disturbance. However, here we are only interested in times $\Delta t \gg \nu/a_\infty^2$ when $a_\infty \Delta t \gg (\nu \Delta t)^{1/2}$ and the acoustic wave is traveling much more rapidly than the diffusing disturbance. For these times the viscous region of the flow is confined to a relatively small area which contains no acoustic waves[3] (see figure 2.1). Using l_i as a lengthscale, the dimensionless viscous time is given by $\Delta\tau = \nu \Delta t / l_i^2$ and the dimensionless acoustic time is given by $\Delta \hat{t} = a_\infty \Delta t / l_i$. The ratio of these two timescales is

$$\frac{\Delta\tau}{\Delta\hat{t}} = \frac{\nu \Delta t / l_i^2}{a_\infty \Delta t / l_i} = \frac{\nu}{a_\infty l_i} = \frac{1}{Re}.$$

This result shows that, for $Re \gg 1$, an event occurring over a time Δt seems much longer to an observer measuring time on the acoustic timescale than it does to an observer measuring events based on a viscous timescale. For this reason the viscous timescale equations (2.6*a–e*) are stationary with respect to the acoustic time $\hat{t}$ (there are no $d\hat{t}$ derivatives) and the relevant velocity scale for Re is a_∞.

Another approximation made in the derivation of (2.6*b*, *d*) is that we have assumed that the terms involving $(\mu_\nu - 2\mu/3)$ in (2.1*b*) and (2.3) are $O(1/Re^2)$ or smaller. For dilute monatomic gases ($\mu_\nu/\mu \approx 0$) and air ($\mu_\nu/\mu \approx 0.6$) [37] this assumption is valid. However, for gases such as CO_2 ($\mu_\nu/\mu \approx 1000$) and H_2 ($\mu_\nu/\mu \approx 32$) one must be careful in applying the approximation.

Using the viscous timescale equations all of the necessary boundary conditions can be specified to $O(1/Re)$. Since the flow is symmetrical about the origin, the tangential velocity, radial velocity, and heat flux vanish at the center of the vortex. Therefore, as can be shown with (2.6*b*), the radial pressure gradient must be zero at the origin. Since both the temperature and pressure gradients are zero at the center of the vortex, the ideal gas law requires the density gradient to be zero at $\hat{r} = 0$ as well. The flow domain is unbounded, and we will assume that both components of velocity vanish in the far-field. The pressure, temperature, and density are assumed to approach the constant values p_∞, T_∞, and ρ_∞, respectively, as $\hat{r} \to \infty$.

[3]Note that Lagerstrom [22], Stewartson [34], Howarth [17], and Van Dyke [39] have investigated flows in which both acoustic waves and heat/viscous diffusion are simultaneously present.

2.2.2 The low Mach number approximation

To derive the equations for the compressible perturbations to an incompressible vortex, the viscous timescale equations are first re-written using the following non-dimensional parameters

$$\left.\begin{aligned} \tilde{r} = \frac{r}{l_i}, \quad \tilde{t} = \frac{v_m t}{l_i}, \quad \tilde{v} = \frac{v}{v_m}, \\ \tilde{u} = \frac{u}{v_m}, \quad \tilde{\rho} = \frac{\rho}{\rho_\infty}, \quad \tilde{p} = \frac{p - p_\infty}{\rho_\infty v_m^2}, \\ \tilde{T} = \frac{T}{T_\infty}, \quad \tilde{Re} = \frac{\rho_\infty v_m l_i}{\mu}, \quad Pr = \frac{\mu C_p}{\kappa}, \\ M = \frac{v_m}{a_\infty}, \quad \tau = \frac{\tilde{t}}{\tilde{Re}} = \frac{\hat{t}}{Re}. \end{aligned}\right\} \tag{2.7}$$

v_m is a reference velocity — the maximum tangential velocity in the vortex's initial velocity profile. The term $\tilde{p}$ is similar to the standard definition of the dynamic pressure coefficient in aerodynamics [19] and represents the normalized deviation of the local pressure p from the far-field pressure p_∞. Note that the transformation from p to $\tilde{p}$ is similar to the example transformation from ρ to ρ' shown in (2.4) above, and is simply a translation in pressure.

The equations which are obtained after applying the change of variables in (2.7) are expanded in powers of M^2 with the Rayleigh-Janzen expansion[4]. In this method the dependent flow variables are approximated as

$$\tilde{f} = \tilde{f}_0 + M^2 \tilde{f}_1 + O(M^4), \tag{2.8}$$

[4]This expansion has been used by many researchers for examining low Mach number compressible flow (Van Dyke [38], Lagerstrom [22]). Several combustion studies [28], [24], use a slightly modified form of (2.8) in which the expansion parameter is γM^2. A justification for expanding the flow variables in terms of M^2, rather than in odd powers of M, is given by Mahalingam [24]. He shows that as $M \to 0$, M^2 appears as a small parameter in the equations for the relative changes in velocity, pressure, density, and temperature in a one dimensional inviscid flow.

where $\tilde{f}$ may represent any of the dependent flow variables. Terms of $O(1)$ are collected to yield equations describing an incompressible reference flow, and $O(M^2)$ terms are collected to give expressions for the compressible perturbations to the reference flow. The reference flow terms are designated with a subscript 0 and the $O(M^2)$ perturbations are denoted by the subscript 1.

In the reference flow the radial velocity is necessarily zero $\tilde{u}_0 = 0$, the density and temperature are uniform $\tilde{\rho}_0 = \tilde{T}_0 = 1$, the pressure gradient balances the centrifugal forces created by the tangential velocity, and the tangential velocity is governed by a diffusion equation

$$\frac{\partial \tilde{p}_0}{\partial \tilde{r}} = \frac{\tilde{v}_0^2}{\tilde{r}}, \tag{2.9a}$$

$$\frac{\partial \tilde{v}_0}{\partial \tau} = \frac{\partial}{\partial \tilde{r}}\left[\frac{1}{\tilde{r}}\frac{\partial}{\partial \tilde{r}}(\tilde{r}\tilde{v}_0)\right]. \tag{2.9b}$$

The corresponding boundary conditions are

$$\tilde{r} = 0 \qquad \begin{cases} \tilde{v}_0 = 0, \\ \\ \dfrac{\partial \tilde{p}_0}{\partial \tilde{r}} = 0, \end{cases} \tag{2.10a}$$

and

$$\tilde{r} \to \infty \qquad \begin{cases} \tilde{v}_0 \to 0, \\ \\ \tilde{p}_0 \to 0. \end{cases} \tag{2.10b}$$

To $O(M^2)$ the equations for conservation of mass, radial momentum, tangential momentum, energy, and the equation of state, respectively, are

$$\frac{\partial \tilde{\rho}_1}{\partial \tau} + \frac{1}{\tilde{r}}\frac{\partial}{\partial \tilde{r}}(\tilde{r}\tilde{u}_1^*) = 0, \tag{2.11a}$$

$$\frac{\partial \tilde{p}_1}{\partial \tilde{r}} = \frac{\tilde{\rho}_1 \tilde{v}_0^2}{\tilde{r}} + \frac{2\tilde{v}_1\tilde{v}_0}{\tilde{r}}, \tag{2.11b}$$

$$\tilde{\rho}_1\frac{\partial \tilde{v}_0}{\partial \tau} + \frac{\partial \tilde{v}_1}{\partial \tau} + \tilde{u}_1^*\frac{\partial \tilde{v}_0}{\partial \tilde{r}} + \frac{\tilde{v}_0\tilde{u}_1^*}{\tilde{r}} = \frac{\partial}{\partial \tilde{r}}\left[\frac{1}{\tilde{r}}\frac{\partial}{\partial \tilde{r}}(\tilde{r}\tilde{v}_1)\right], \tag{2.11c}$$

$$\frac{\partial \tilde{T}_1}{\partial \tau} + \frac{(\gamma-1)}{\tilde{r}}\frac{\partial}{\partial \tilde{r}}(\tilde{r}\tilde{u}_1^*) = \gamma(\gamma-1)\left(\frac{\partial \tilde{v}_0}{\partial \tilde{r}} - \frac{\tilde{v}_0}{\tilde{r}}\right)^2 + \frac{\gamma}{Pr}\frac{1}{\tilde{r}}\frac{\partial}{\partial \tilde{r}}\left(\tilde{r}\frac{\partial \tilde{T}_1}{\partial \tilde{r}}\right), \qquad (2.11d)$$

$$\gamma \tilde{p}_0 = \tilde{\rho}_1 + \tilde{T}_1, \qquad (2.12)$$

where $\tilde{u}_1^* = \tilde{u}_1 \tilde{Re}$. Note that (2.12) implies that, for a slightly compressible vortex, the $O(M^2)$ density and temperature perturbations are of the same order of magnitude as the $O(1)$ pressure variation.

Using (2.11a, d), and (2.12) we can derive a partial differential equation for the evolution of $\tilde{T}_1$ in terms of the known reference flow velocity $\tilde{v}_0$ and pressure $\tilde{p}_0$

$$\frac{\partial \tilde{T}_1}{\partial \tau} - \frac{1}{\tilde{r}Pr}\frac{\partial}{\partial \tilde{r}}\left(\tilde{r}\frac{\partial \tilde{T}_1}{\partial \tilde{r}}\right) = (\gamma-1)\left[\left(\frac{\partial \tilde{v}_0}{\partial \tilde{r}} - \frac{\tilde{v}_0}{\tilde{r}}\right)^2 + \frac{\partial \tilde{p}_0}{\partial \tau}\right]. \qquad (2.13)$$

The equation set (2.11a–c), (2.12), and (2.13) will be used to to describe the evolution of the $O(M^2)$ quantities; the related boundary conditions are

$$\tilde{r} = 0 \qquad \begin{cases} \tilde{u}_1 = 0, \quad \tilde{v}_1 = 0, \\ \dfrac{\partial \tilde{p}_1}{\partial \tilde{r}} = 0, \quad \dfrac{\partial \tilde{T}_1}{\partial \tilde{r}} = 0, \\ \dfrac{\partial \tilde{\rho}_1}{\partial \tilde{r}} = 0, \end{cases} \qquad (2.14a)$$

and

$$\tilde{r} \to \infty \qquad \begin{cases} \tilde{u}_1 \to 0, \quad \tilde{v}_1 \to 0, \\ \tilde{p}_1 \to 0, \quad \tilde{T}_1 \to 0, \\ \tilde{\rho}_1 \to 0. \end{cases} \qquad (2.14b)$$

After the reference flow variables $\tilde{p}_0$ and $\tilde{v}_0$ are determined, one can solve for all of the $O(M^2)$ perturbation quantities.

Chapter 3

The Reference Flow

One can completely determine the reference flow pressure and velocity from knowledge of the vorticity $\tilde{\omega}_0$. Therefore, we begin this chapter by discussing the reference flow vorticity equation. In the process of solving this equation we will find a group which leaves it invariant and identify a set of conserved quantities for the solutions.

3.1 Derivation

Taking the curl of (2.9*b*) we obtain an equation for the diffusion of vorticity

$$\frac{\partial \tilde{\omega}_0}{\partial \tau} = \frac{1}{\tilde{r}} \frac{\partial}{\partial \tilde{r}} \left(\tilde{r} \frac{\partial \tilde{\omega}_0}{\partial \tilde{r}} \right), \tag{3.1}$$

where

$$\tilde{\omega}_0 = \frac{1}{\tilde{r}} \frac{\partial}{\partial \tilde{r}} (\tilde{r} \tilde{v}_0). \tag{3.2}$$

Here we assume that $\tilde{\omega}_0$ is bounded at $\tilde{r} = 0$, and that $\tilde{\omega}_0 \to 0$ as $\tilde{r} \to \infty$.

Based on the form of the integral invariants involved in self-similar solutions of the one-dimensional heat equation [5], we expect the following area-integrated, positive-integer moments of vorticity to be conserved

$$\bar{A}_j = 2\pi \int_0^\infty \tilde{r}^j \tilde{\omega}_0 \tilde{r} \mathrm{d}\tilde{r}. \tag{3.3}$$

Consider the invariance of (3.1) and (3.3) under dilations in $\tilde{\omega}_0$, $\tilde{r}$, and τ, and translation in τ

$$\tilde{r}' = \mathrm{e}^a \tilde{r}, \quad \tau' = \mathrm{e}^b \tau + (\mathrm{e}^b - 1)\tau_i, \quad \tilde{\omega}_0' = \mathrm{e}^c \tilde{\omega}_0.$$

The invariance of (3.1) and (3.3) requires that $b = 2a$ and $c = -(j+2)a$. The group is

$$\tilde{r}' = \mathrm{e}^a \tilde{r}, \quad \tau' = \mathrm{e}^{2a} \tau + (\mathrm{e}^{2a} - 1)\tau_i, \quad \tilde{\omega}_0' = \mathrm{e}^{-(j+2)a} \tilde{\omega}_0, \tag{3.4}$$

and $a = 0$ is the identity element of the transformation. The associated characteristic equations are

$$\frac{\mathrm{d}\tilde{r}}{\tilde{r}} = \frac{\mathrm{d}\tau}{2(\tau + \tau_i)} = -\frac{\mathrm{d}\tilde{\omega}_0}{(j+2)\tilde{\omega}_0}. \tag{3.5}$$

Note that this group has three parameters: a, j, and τ_i. The resulting similarity variables are

$$\eta = \frac{\tilde{r}^2}{4(\tau + \tau_i)}, \tag{3.6}$$

and

$$\Omega(\eta) = \tilde{\omega}_0 (\tau + \tau_i)^{(j+2)/2}. \tag{3.7}$$

Substituting these group invariants into (3.1), we obtain an ordinary differential equation in the variable η

$$\eta \frac{\mathrm{d}^2\Omega}{\mathrm{d}\eta^2} + (\eta + 1)\frac{\mathrm{d}\Omega}{\mathrm{d}\eta} + \frac{(j+2)}{2}\Omega = 0, \quad (0 \le \eta \le \infty). \tag{3.8}$$

We require that Ω is bounded at $\eta = 0$, and that $\Omega \to 0$ as $\eta \to \infty$. Bateman [4] shows that the two-dimensional diffusion equation is satisfied by a separated solution in the variables τ and η, and his solution method also leads to (3.8). For arbitrary values of j, he gives the general solution of (3.8) as

$$\Omega(\eta) = \bar{C}_j \exp(-\eta) \bar{\mathrm{M}}(-\frac{j}{2}; 1; \eta), \tag{3.9}$$

where $\bar{C}_j$ is a constant and $\bar{\mathrm{M}}(-\frac{j}{2}; 1; \eta)$ is a confluent hypergeometric function. Note that an overbar and an upright font are used to distinguish this function from the previously defined Mach number M.

Using (3.6) and (3.7) the integral (3.3) becomes

$$\bar{A}_j = 4^{(j+2)/2}\pi \int_0^\infty \eta^{j/2}\Omega(\eta)\mathrm{d}\eta, \tag{3.10}$$

where j is a positive integer. Using (3.9) in this integral we find that $\bar{A}_j$ is unbounded for odd values of j (see Appendix C). Therefore, we will only consider even values of j. Taking $j = 2m$, the confluent hypergeometric function reduces to the Laguerre polynomial

$$\bar{\mathrm{M}}(-m;1;\eta) = \mathrm{L}_m(\eta) = \frac{\mathrm{e}^\eta}{m!}\frac{\mathrm{d}^m}{\mathrm{d}\eta^m}\left(\eta^m \mathrm{e}^{-\eta}\right) = \sum_{k=0}^{m} \frac{m!(-\eta)^k}{(k!)^2(m-k)!}. \tag{3.11}$$

This solution for $\Omega(\eta)$ agrees with the vortex solutions found by de Neufville [13]. For reference, the first five Laguerre polynomials are

$$\mathrm{L}_0 = 1, \quad \mathrm{L}_1 = 1-\eta, \quad \mathrm{L}_2 = \frac{1}{2}\left(\eta^2 - 4\eta + 2\right), \quad \mathrm{L}_3 = -\frac{1}{6}\left(\eta^3 - 9\eta^2 + 18\eta - 6\right),$$

$$\mathrm{L}_4 = \frac{1}{24}(\eta^4 - 16\eta^3 + 72\eta^2 - 96\eta + 24).$$

In the even-integer case the conserved quantity $\bar{A}_j$ converges to a finite value for every m. Taking $\bar{A}_j \to A_m$ for $j = 2m$, (3.3) reduces to

$$A_m = 2\pi \int_0^\infty \tilde{r}^{2m}\tilde{\omega}_0 \tilde{r}\mathrm{d}\tilde{r}. \tag{3.12}$$

Each A_m is the $2m^{th}$ area-moment of the m^{th} vorticity solution. As pointed out by de Neufville [13], when $m = 0$ the total circulation of the fluid is invariant and when $m = 1$ the total angular momentum of the flow $\mathcal{M}$ is invariant. These two invariants are a subset of the more general expression for the reference flow integral invariants (3.12) developed here. When $m = 0$, $A_m = A_0$, which is the total circulation of the reference flow, and for $m = 1$ the integral invariant is related to the total angular momentum $A_1 = -2\mathcal{M}$.

In (3.9) let $\bar{C}_j \to C_m$ for $j = 2m$. The constant C_m is related to the integral invariant A_m and is found by evaluating (3.10). Using (3.9) and (3.11), we can re-write (3.10) in the following form

$$A_m = \frac{4^{(m+1)}\pi C_m}{m!}\int_0^\infty \eta^m \frac{\mathrm{d}^m}{\mathrm{d}\eta^m}\left(\eta^m \mathrm{e}^{-\eta}\right)\mathrm{d}\eta. \tag{3.13}$$

Integrating this equation by parts several times and then applying mathematical induction to the results, we can reduce A_m to the following expression

$$A_m = (-1)^m 4^{(m+1)}\pi C_m \int_0^\infty \eta^m \mathrm{e}^{-\eta}\mathrm{d}\eta. \tag{3.14}$$

The integral in (3.14) is the Gamma function [1], and for integer powers of m, C_m and A_m are related in the following way,

$$C_m = \frac{A_m}{(-1)^m 4^{(m+1)}(m!)\pi}. \tag{3.15}$$

Using(3.7), (3.9), and (3.11) the solution for the reference flow vorticity can be written as

$$\tilde{\omega}_0 = \frac{C_m \mathrm{e}^{-\eta}\mathrm{L}_m(\eta)}{(\tau+\tau_i)^{(m+1)}}, \tag{3.16}$$

where $C_m/\tau_i^{(m+1)}$ corresponds to the amplitude (at $\tilde{\tau} = 0$) of the m^{th} self-similar vorticity solution (when $\tau = 0$). The velocity and pressure corresponding to (3.16) are given in the following section.

3.2 Physical description of reference flow solutions

Each eigenfunction (solution for $\tilde{\omega}_0$) satisfying (3.1) corresponds to a different radial profile of tangential velocity and pressure. Using (3.4) in (3.2) and (2.9a), we can find the transformation group for $\tilde{v}_0$ and $\tilde{p}_0$

$$\tilde{v}_0' = \mathrm{e}^{-(2m+1)a}\tilde{v}_0, \quad \tilde{p}_0' = \mathrm{e}^{-2(2m+1)a}\tilde{p}_0. \tag{3.17}$$

These transformations leave the boundary conditions (2.10a,b) invariant, and yield the following self-similar forms

$$V(\eta) = \tilde{v}_0(\tau + \tau_i)^{(m+1/2)}, \tag{3.18a}$$

and

$$\mathcal{P}(\eta) = \tilde{p}_0(\tau + \tau_i)^{(2m+1)}, \tag{3.18b}$$

and the corresponding boundary conditions

$$\eta = 0 \qquad \begin{cases} V = 0, \\ \\ \eta^{\frac{1}{2}} \dfrac{\mathrm{d}\mathcal{P}}{\mathrm{d}\eta} = 0, \end{cases} \tag{3.19a}$$

$$\eta \to \infty \qquad \begin{cases} V \to 0, \\ \mathcal{P} \to 0. \end{cases} \tag{3.19b}$$

For each eigenvalue m, a completely self-similar solution can be found for the reference flow. The mathematical form of each solution may be used to describe the physical nature of the flow it represents.

3.2.1 Tangential velocity

Integrating (3.2), one obtains a solution for the reference flow velocity

$$\tilde{v}_0 = \begin{cases} \dfrac{2C_0}{\tilde{r}} \left[1 - \exp(-\eta)\right], & m = 0 \\ \\ -\dfrac{2C_m}{\tilde{r}(\tau + \tau_i)^m} \exp(-\eta) \left[\mathrm{L}_m(\eta) - \mathrm{L}_{m-1}(\eta)\right], & m \geq 1. \end{cases} \tag{3.20}$$

When ($m \geq 1$), the term in square brackets in (3.20) is a polynomial which has one root at $\eta = 0$ and $(m-1)$ roots for $\eta > 0$. Therefore, the tangential velocity for the m^{th} eigenvalue will change direction $(m-1)$ times as one varies $\tilde{r}$ from the origin

to $\tilde{r} \to \infty$ (e.g. figure 3.1b). Self-similar vortices corresponding to values of $m \geq 2$, would consist of $(m-1)$ concentric shear layers.

3.2.2 Pressure

From (2.9a) we see that $\partial\tilde{p}_0/\partial\tilde{r} \geq 0$. Therefore, $\tilde{p}_0$ increases monotonically from its minimum value, at the center of the vortex ($\tilde{r} = 0$), to $\tilde{p}_0 = 0$, as $\tilde{r} \to \infty$. Using (3.20) in (2.9a) gives $\tilde{p}_0$

$$\tilde{p}_0 = -\int_{\tilde{r}}^{\infty} \frac{\tilde{v}_0^2}{\tilde{r}} \mathrm{d}\tilde{r} = \frac{-C_m^2}{2(\tau+\tau_i)^{(2m+1)}} \int_{\eta}^{\infty} \frac{\exp(-2\eta)\left[\mathrm{L}_m(\eta) - \mathrm{L}_{m-1}(\eta)\right]^2}{\eta^2} \mathrm{d}\eta. \tag{3.21}$$

The pressure for the first few eigenvalues is

$$\tilde{p}_0 = \begin{cases} -\dfrac{C_0^2}{(\tau+\tau_i)}\left[\dfrac{1+\exp(-2\eta)-2\exp(-\eta)}{2\eta} + \mathrm{E}_1(\eta) - \mathrm{E}_1(2\eta)\right], & m=0 \\ -\dfrac{C_1^2\exp(-2\eta)}{4(\tau+\tau_i)^3}, & m=1 \\ -\dfrac{C_2^2\exp(-2\eta)}{2(\tau+\tau_i)^5}\left[\dfrac{\eta^2}{8} - \dfrac{3\eta}{8} + \dfrac{5}{16}\right], & m=2 \\ -\dfrac{C_3^2\exp(-2\eta)}{2(\tau+\tau_i)^7}\left[\dfrac{\eta^4}{72} - \dfrac{5\eta^3}{36} + \dfrac{11\eta^2}{24} - \dfrac{13\eta}{24} + \dfrac{11}{48}\right], & m=3, \end{cases} \tag{3.22}$$

where $\mathrm{E}_1(\eta)$ is the exponential integral

$$\mathrm{E}_1(\eta) = \int_{\eta}^{\infty} \frac{\mathrm{e}^{-\eta}}{\eta} \mathrm{d}\eta.$$

The radial distributions of vorticity, tangential velocity, and pressure are plotted in figure 3.1(a–c) for the first three eigenvalues m, with $C_m = 1, \tau = 0$, and $\tau_i = 1$. Notice that $\tilde{\omega}_0 = 1$ at $\tilde{r} = 0$ for all three solutions shown. However, as m increases both the corresponding maximum tangential velocity, and maximum pressure drop decrease.

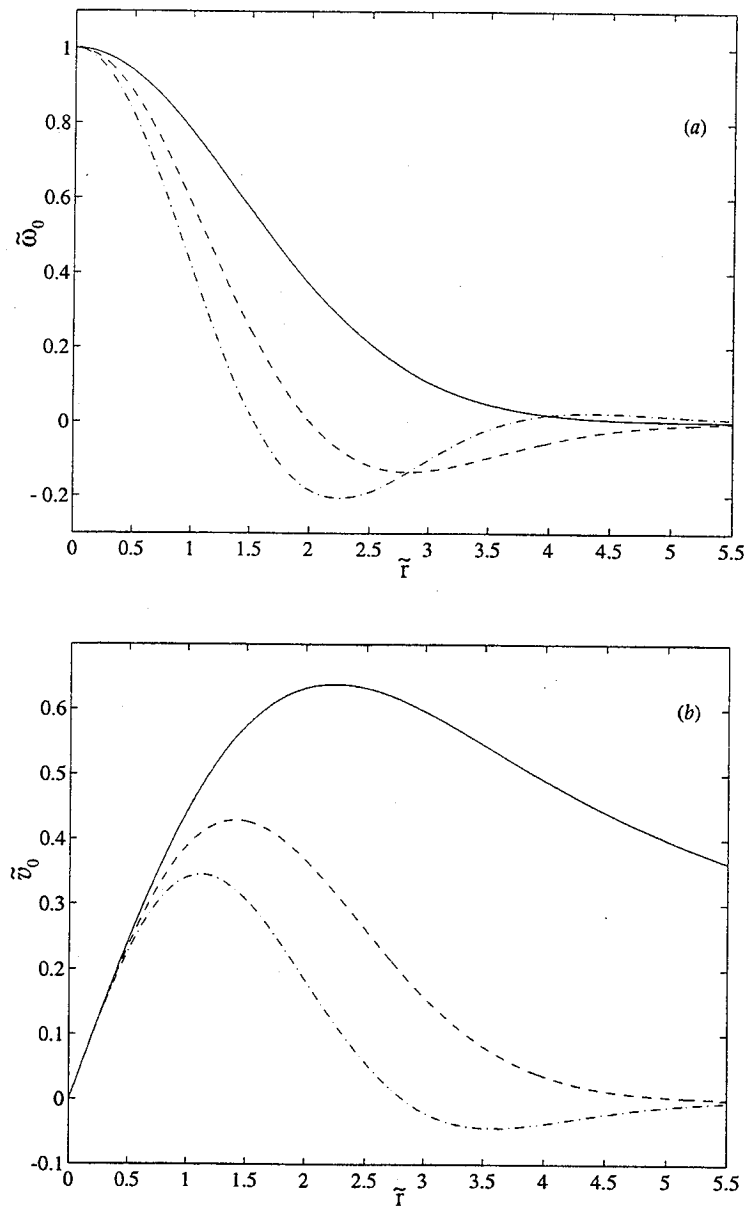

Figure 3.1: a, b

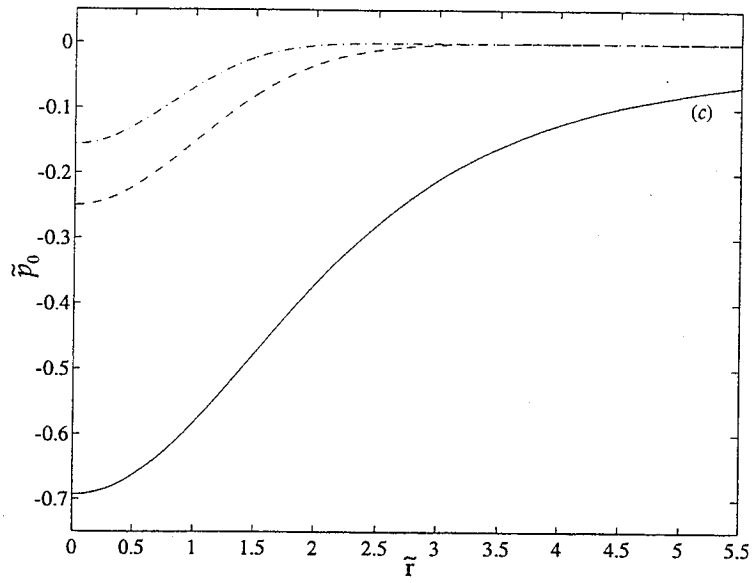

Figure 3.1: Radial distributions of (a) vorticity $\tilde{\omega}_0$, (b) tangential velocity $\tilde{v}_0$, and (c) pressure $\tilde{p}_0$, for $C_m = 1, \tau = 0$, and $\tau_i = 1$ ——, $m = 0$; – – – –, $m = 1$; —·—, $m = 2$.

3.2.3 Decay rates

The solutions of the reference flow vorticity (3.16), tangential velocity (3.20), and pressure (3.21) can each be factored into two parts. The first part corresponds to an inverse power of τ, and the second part is purely a function of η. The η-dependent part of each solution governs the spreading of its radial profile by viscous diffusion, whereas the other factor governs the solution's time rate of decay.

For arbitrary values of m, the vorticity, tangential velocity, and pressure have the following inverse time dependence

$$\tilde{\omega}_0 \propto \tau^{-(m+1)}, \quad \tilde{v}_0 \propto \tau^{-(m+1/2)}, \quad \tilde{p}_0 \propto \tau^{-(2m+1)}. \qquad (3.23a, b, c)$$

Note that the incompressible pressure decays like $\tilde{p}_0 \sim \tilde{v}_0^2$.

In §2.2 the governing equations were scaled by l_i and v_m, which are determined from the initial velocity profile in a vortex. However, the core size and maximum

tangential velocity in a vortex are functions of time. As a self-similar incompressible vortex decays, its core size l (radial location of maximum tangential velocity), grows at a rate governed by viscous diffusion: $l \propto \tau^{\frac{1}{2}}$. Using this lengthscale and the time dependent maximum tangential velocity $v_m(\tau)$, we can show that the Reynolds number $\tilde{Re}^*$ and the Mach number M^*, at the core radius of a vortex vary in time as

$$\tilde{Re}^* \propto \tau^{-m} \quad \text{and} \quad M^* \propto \tau^{-(m+1/2)}. \qquad (3.24a, b)$$

Interestingly, for $m = 0$ both the circulation (based on maximum tangential velocity v_m and core size l) and $\tilde{Re}^*$ are constant. If $m > 0$, both $\tilde{Re}^*$ and M^* decrease in time — with the Mach number decreasing more rapidly than the Reynolds number. This time-dependent behavior is consistent with the underlying assumption that the Mach number of the vortex remains small.

In the next section we will show that the inverse time dependence of the reference flow quantities has important implications for the form of the solutions we can use to model a self-similar vortex.

3.2.4 Superposed solutions

The Laguerre polynomials are a complete set of orthogonal eigenfunctions, and (3.1) is a linear equation. Therefore, an infinite series of Laguerre polynomials could be used to construct a description of any arbitrary vortex reference flow with $\tilde{\omega}_0 \to 0$ as $\tilde{r} \to \infty$. However, as de Neufville [13] notes, the convergence of these polynomials is slow, and in order to approximate a particular vortex, a very large number of terms may be required. In the present work superposed solutions will be avoided, not because of their slow convergence properties, but because such solutions are not self-similar. In order to find similarity solutions to the $O(M^2)$ perturbation equations (2.11a–c), (2.12), and (2.13), the reference flow solutions (which form the forcing terms in these equations) must be self-similar.

To see that superposed solutions are not self-similar, let a superscript enclosed in parentheses denote the m^{th} vorticity solution and consider the sum of the $m1^{th}$ and

the $m2^{th}$ vorticity solutions

$$\omega_0^{(m1)} + \omega_0^{(m2)} = \frac{C_{m1}\mathrm{e}^{-\eta}\mathrm{L}_{m1}(\eta)}{(\tau+\tau_i)^{(m1+1)}} + \frac{C_{m2}\mathrm{e}^{-\eta}\mathrm{L}_{m2}(\eta)}{(\tau+\tau_i)^{(m2+1)}}. \tag{3.25}$$

Multiplying each term by $(\tau+\tau_i)^{(m1+1)}$ we get

$$\begin{aligned}(\tau+\tau_i)^{(m1+1)}\left(\omega_0^{(m1)} + \omega_0^{(m2)}\right) &= C_{m1}\mathrm{e}^{-\eta}\mathrm{L}_{m1}(\eta) \\ &+ C_{m2}\mathrm{e}^{-\eta}\mathrm{L}_{m2}(\eta)\,(\tau+\tau_i)^{(m1-m2)}.\end{aligned} \tag{3.26}$$

If the vorticity distribution in (3.26) is self-similar, all terms on the right hand side of the equation must be a function of η alone. This is only true if $m1 = m2$; therefore, superpositions of self-similar solutions are not self-similar.

From a physical standpoint, a time-dependent quantity is self-similar if the spatial distributions of the quantity, at different instants in time, can be obtained from each other by the same group transformation. Each term (eigenfunction) in the solution of a vortex composed of superposed eigenfunctions will decay at its own, distinct, rate. The parts of the solution corresponding to large eigenvalues will become negligible long before the terms corresponding to small eigenvalues have decayed.

3.3 The Oseen vortex, the Taylor vortex and Mandella's vortex

The similarity equations we will develop in chapter 4 are valid for any eigenvalue m. However, in §§5.1 and 5.2 we will focus on the solutions for the Oseen vortex ($m = 0$) and the Taylor vortex ($m = 1$). This section describes these two types of vortex, and qualitatively explores the formation of the vortex studied by Mandella [25].

The reference flow solution for $m = 0$ is the classical Oseen vortex [30], which is sometimes also called the Lamb vortex [20], or the Lamb-Oseen vortex [31],[15]. The solution when $m = 1$ is Taylor's vortex [36] and has also been referred to as a

"Taylor swirl"[1] [12]. Radial profiles of vorticity, tangential velocity, and pressure are given for both vortex solutions in figures 3.1a–c. Note that, the tangential velocity profiles of both the Oseen vortex and the Taylor vortex have $\tilde{v}_0$ of the same sign (direction) at all values of $\tilde{r}$. However, as $\tilde{r} \to \infty$ the Oseen vortex has an infinite total angular momentum, and a finite circulation; the Taylor vortex has a finite total angular momentum and zero circulation. Also, note that the reference flow solutions for all higher order eigenvalues $m \geq 2$ have zero total angular momentum, and zero circulation for $\tilde{r} \to \infty$ [13].

The Oseen vortex is often used to model the viscous decay of vortex pairs such as those found far downstream from the wingtips of an airplane in steady, level flight. Assuming the vortices have the same circulation strength, but rotate in opposite directions, they move along parallel linear paths. Each member of such a vortex pair contains an infinite amount of angular momentum about its own center. However, the total angular momentum along a symmetry plane, equidistant from each vortex, and parallel to their motion, is zero — the circulation and angular momentum of each vortex in the pair are equal in magnitude, but opposite in sign. For the Oseen vortex $\tilde{Re}$ is constant; see equation (3.24a).

Now consider the vortex studied by Mandella [25],[26]. As shown in figures 3.2-3.3, this vortex is created by shock diffraction. A shock of strength $M_s \approx 1.8$ travels from left to right and passes over an airfoil. The airfoil has an angle of attack of 30°, and a thickness-to-chord ratio of 18%. How can the resulting flow be described?

Currently there do not seem to be any reports, either computational or experimental, which give the vorticity, velocity, density, and pressure fields present in such a flow[2]. However, many features of the flow may be identified from the schematics shown on the left side of figure 3.2. In these diagrams the heavy lines represent shocks, the thinner lines represent contact surfaces, the direction of propagation of

[1]The use of this expression may have arisen to prevent confusion with the three dimensional vortices found in circular Taylor-Couette flow [14]. Such vortices are also often called Taylor vortices.

[2]Moon & Yee [29] use a TVD scheme to numerically determine the pressure and density of the flow for the early stages of Mandella & Bershader's experiment [26]. Unfortunately, their computations do not capture the complete formation of the free vortex.

each shock is marked with arrows, and vorticity of positive and negative sign is denoted by + and −, respectively. The accompanying holographic interferograms on the right hand side of figure 3.2 were provided courtesy of Dr. M. J. Mandella.

The incoming shock first contacts the airfoil near the airfoil's leading-edge. A reflected shock is produced which propagates away from the airfoil in a circular pattern (figure 3.2*a*). The incoming shock is split (into two parts) by the airfoil, forming an upper shock, which travels over the top surface of the airfoil, and a lower shock, which moves along the airfoil's bottom surface. The circular, reflected shock is connected to the upper and lower shocks by Mach stem configurations. The upper shock diffracts and expands over the leading-edge of the airfoil and so becomes curved and weaker. As a result, the upper shock slows with respect to the lower shock, which is compressed and strengthened due to the airfoil's high angle of attack. The lower shock reaches the sharp trailing-edge of the airfoil before the upper shock and diffracts around the tip. The diffraction produces a vortex of strong, predominately-positive (counter-clockwise) vorticity (figure 3.2*b*). The curved upper shock and the small boundary layer on the upper surface of the airfoil both create negative (clockwise) vorticity. When the diffracted lower shock (now curving around to the upper surface of the airfoil) and the upper shock collide, the resulting shock structure continues to move from left to right. This shock structure then passes through the vortex at the airfoil's trailing-edge, causing the vortex to shed from the airfoil and convect with the free-stream flow. In this free-vortex formation process, the strong, positive vorticity at the tail of the airfoil is encircled by negative vorticity of smaller magnitude (figure 3.2*c*).

The schematic is highly simplified, and figure 3.3 shows that some elements of the real flow have been omitted: 1) The formation of a second, weaker vortex by shock diffraction at the leading-edge of the airfoil. This second vortex remains attached at the airfoil's nose by a slip-line and seems to be accompanied by a small separation bubble. 2) A series of slip-lines or contact surfaces are present near the free vortex [26]. 3) When the upper and lower shocks collide near the trailing-edge of the airfoil, a focusing effect seems to occur. This focusing effect causes the resulting shock configuration to resemble the three-shock intersection structures reported by Sturtevant & Kulkarny [32]. This structure is visible in figure 3.3 as a triangular

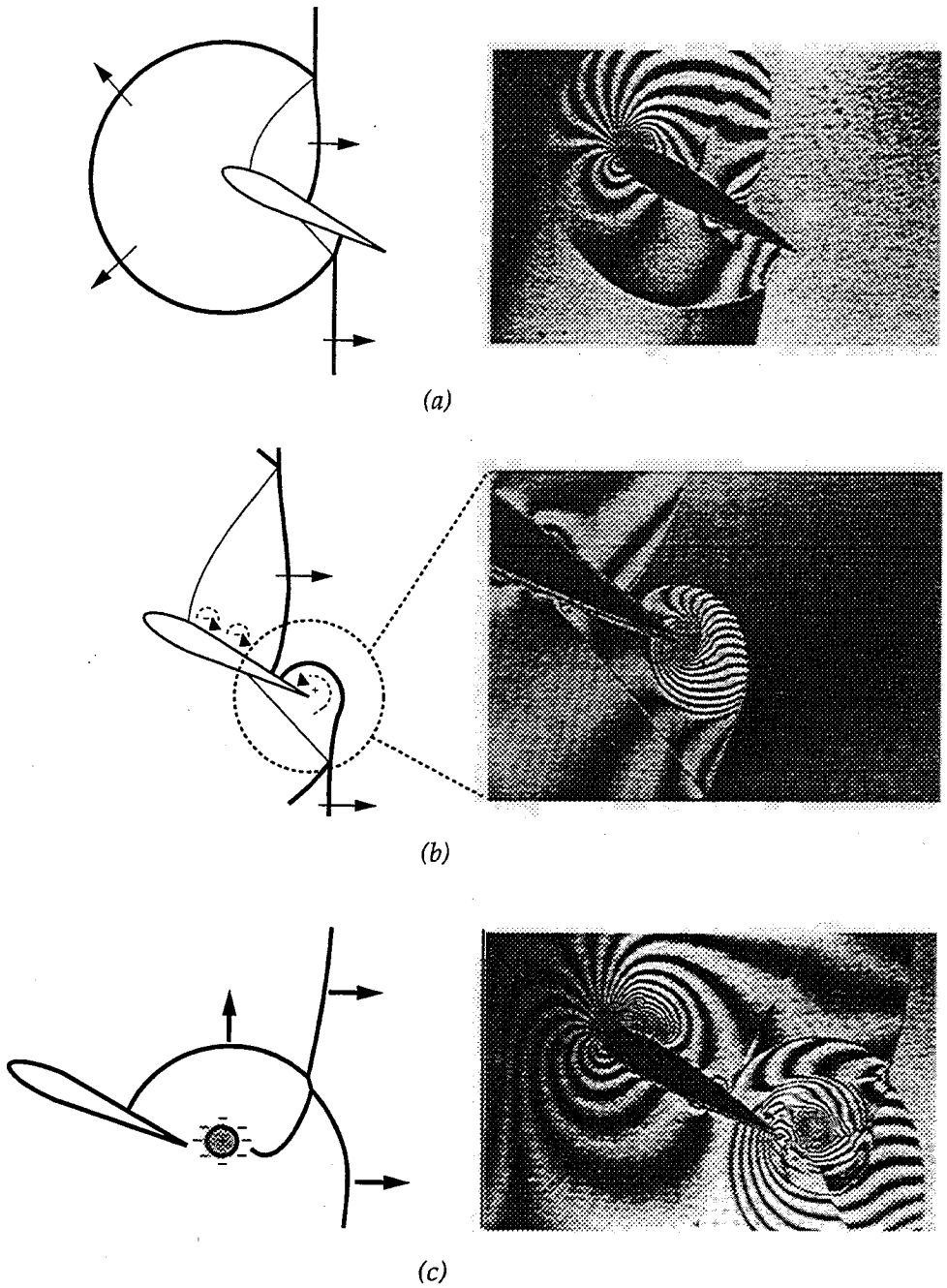

Figure 3.2: Three stages in the creation of a free two-dimensional vortex: (a) incident and reflected shocks, (b) diffraction around the airfoil's trailing-edge, and (c) free convection of a vortex which contains both positive and negative vorticity.

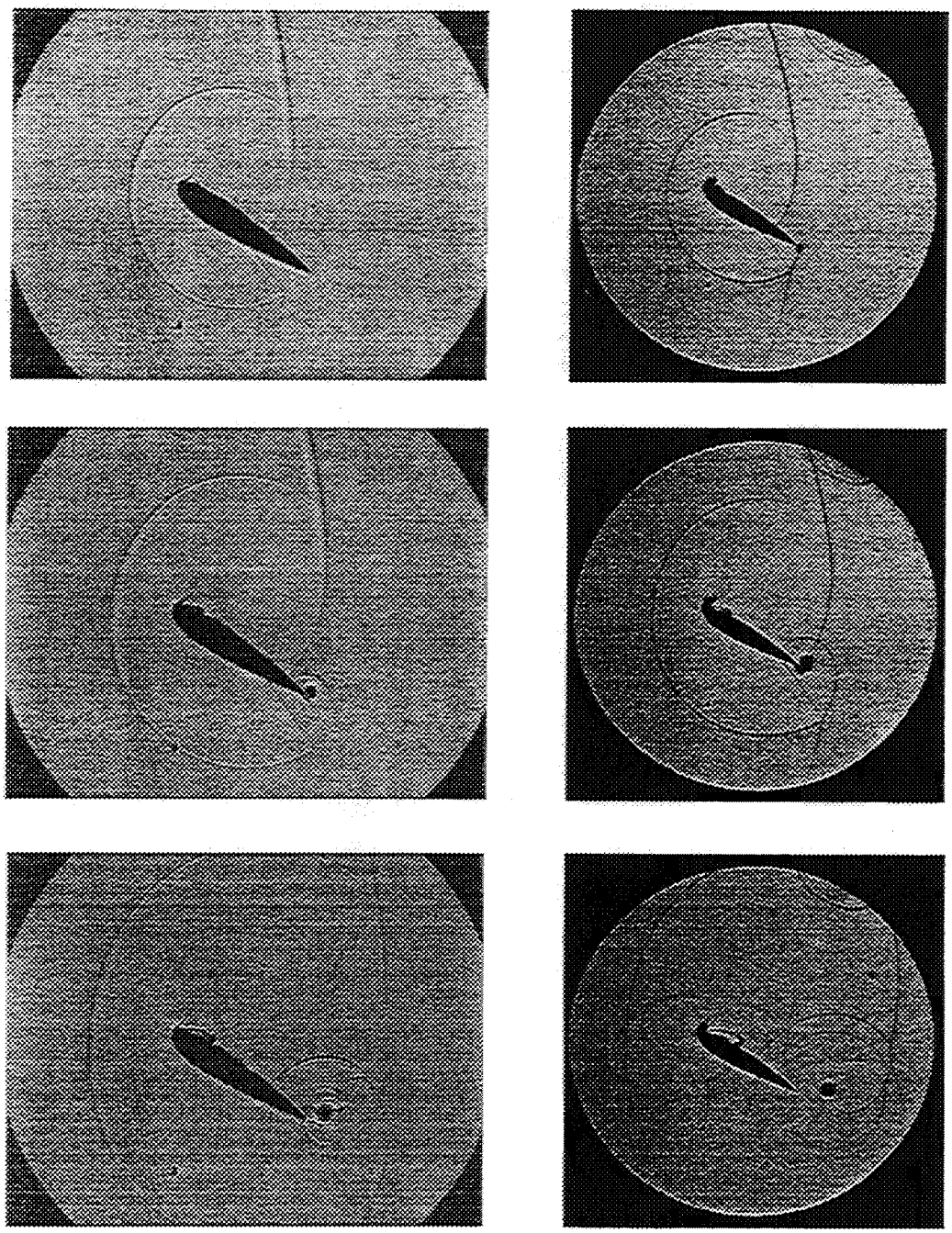

Figure 3.3: Shadowgraph (left) and yellow & blue two-color schlieren (right) pictures showing the formation of Mandella's vortex. The sequence is ordered from left to right and top to bottom.

system of contact surfaces and shocks (located slightly above and to the right of the free vortex).

Despite their simplicity, the schematics in figure 3.2 capture one of the main features involved in the formation of a free vortex by shock diffraction: from physical reasoning, we expect such a vortex to contain vorticity of both positive and negative sign. This idea motivates the examination of self-similar solutions for the Taylor vortex. Taylor's vortex ($m = 1$), corresponds to the lowest and most stable eigenfunction which satisfies the reference flow and possesses vorticity of both signs. For this reason, we will focus on analytical solutions for compressible perturbations to an incompressible Taylor vortex in §5.1.

However, remember from § 1.1 that the flow in Mandella's experiments is fairly complex, and that there may be acoustic waves present in the vicinity of the vortex. Again, the slightly-compressible vortex solutions developed in this thesis correspond to an idealized flow situation in which there are no acoustic waves and the far-field flow conditions are constant. Here, the Oseen vortex and the Taylor vortex are used as the base flows for the development of weakly-compressible vortex solutions. In a strict mathematical sense, there are shortcomings to representing a lone, two dimensional vortex with either the Oseen vortex or the Taylor vortex. If one assumes that the flow domain is completely unbounded and calculates the total circulation and the total angular momentum by performing integrations for $0 \leq \tilde{r} \leq \infty$, then: 1) Oseen's vortex has a non-zero total circulation but an infinite amount of total angular momentum — it would require an infinite amount of energy to create such a vortex, 2) Taylor's vortex has a finite total angular momentum, but zero total circulation — such a vortex could not be produced by a lifting body, such as an airfoil, because it would necessarily shed vortices with nonzero total circulation[3]. In

[3]The lift on the airfoil and the distribution of circulation in the vortices in Mandella's experiments has not been fully determined. As demonstrated by Taneda [35], the correlation between the lift on an impulsively started body and the presence of an isolated starting vortex is complex. He has shown that an impulsively started elliptical cylinder (2 : 1 aspect ratio), at angles of attack of 20° and 45°, experiences two peaks in lift magnitude. The first peak is associated with the development of a boundary layer and occurs in the absence of a visible starting vortex; the second peak arises just after the shedding of isolated vortices from both the leading- and trailing-edges of the body.

reality, these vortex solutions are only rough approximations of vortices existing in flows which can never be truly unbounded.

These facts should be kept in mind when using the slightly-compressible vortex solutions developed in chapter 5. In the next chapter, the reference flow solutions are used to derive a set of equations which govern the self-similar forms of the compressible perturbations.

Chapter 4

Similarity Forms

In §3.1 it is shown that the reference flow is invariant under the three-parameter group a, τ_i, and j. Since the reference flow involves only even values of the integer j, $j = 2m$, we can alternatively use m as the third group parameter. It will now be shown that the compressible perturbation equations (2.11a–c), (2.12–2.13) and the corresponding boundary conditions (2.14a–b) are also invariant under this three-parameter group. We will use this group to find invariant forms of the $O(M^2)$ flow variables and the governing perturbation equations.

4.1 Perturbation variables

The similarity forms of the $O(M^2)$ compressible perturbation quantities are found by substituting the reference flow terms (3.7) and (3.18a–b) into the compressible equations (2.11a–c), and (2.12–2.13) and looking for a transformation group which leaves them invariant. We also require that this group yield the similarity variable η. Therefore, the $O(M^2)$ similarity solutions will have an $\tilde{r}$ and τ dependence of the

same form as the $O(1)$ similarity solutions. The relevant group is

$$\left.\begin{aligned} \tilde{r}' = \mathrm{e}^{a}\tilde{r}, \quad \tau' = \mathrm{e}^{2a}\tau + (\mathrm{e}^{2a}-1)\tau_i, \quad \tilde{\rho}_1' = \mathrm{e}^{-2(2m+1)a}\tilde{\rho}_1, \\ \tilde{u}_1^{*\prime} = \mathrm{e}^{-(4m+3)a}\tilde{u}_1^*, \quad \tilde{p}_1' = \mathrm{e}^{-4(2m+1)a}\tilde{p}_1, \\ \tilde{v}_1' = \mathrm{e}^{-3(2m+1)a}\tilde{v}_1, \quad \tilde{T}_1' = \mathrm{e}^{-2(2m+1)a}\tilde{T}_1, \\ \gamma' = \gamma, \quad Pr' = Pr. \end{aligned}\right\} \tag{4.1}$$

The gas properties γ and Pr are treated as invariant quantities, and are assumed constant for this analysis. The characteristic equations of this group are

$$\begin{aligned} \frac{\mathrm{d}\tilde{r}}{\tilde{r}} &= \frac{\mathrm{d}\tau}{2(\tau+\tau_i)} = -\frac{\mathrm{d}\tilde{\rho}_1}{2(2m+1)\tilde{\rho}_1} = -\frac{\mathrm{d}\tilde{u}_1^*}{(4m+3)\tilde{u}_1^*} \\ &= -\frac{\mathrm{d}\tilde{p}_1}{4(2m+1)\tilde{p}_1} = -\frac{\mathrm{d}\tilde{v}_1}{3(2m+1)\tilde{v}_1} = -\frac{\mathrm{d}\tilde{T}_1}{2(2m+1)\tilde{T}_1}, \end{aligned} \tag{4.2}$$

and are used to find similarity variables corresponding to the $O(M^2)$ perturbed quantities

$$\left.\begin{aligned} \sigma(\eta) &= \tilde{T}_1(\tau+\tau_i)^{(2m+1)}, \\ \beta(\eta) &= \tilde{\rho}_1(\tau+\tau_i)^{(2m+1)}, \\ \alpha(\eta) &= \tilde{u}_1^*(\tau+\tau_i)^{(2m+3/2)}, \\ \phi(\eta) &= \tilde{v}_1(\tau+\tau_i)^{(3m+3/2)}, \\ \psi(\eta) &= \tilde{p}_1(\tau+\tau_i)^{(4m+2)}. \end{aligned}\right\} \tag{4.3a–e}$$

4.1.1 Decay rates

The decay rates of the $O(M^2)$ terms can be determined by inspection of (4.3a–e)

$$\tilde{T}_1 \propto \tau^{-(2m+1)}, \quad \tilde{\rho}_1 \propto \tau^{-(2m+1)}, \quad \tilde{u}_1^* \propto \tau^{-(2m+3/2)}, \qquad (4.4a, b, c)$$

$$\tilde{v}_1 \propto \tau^{-(3m+3/2)}, \quad \tilde{p}_1 \propto \tau^{-(4m+2)}. \qquad (4.4d, e)$$

Comparing (4.4a–e) with (3.23a–c) we see that $\tilde{T}_1$ and $\tilde{\rho}_1$ decay at the same rate as the reference flow pressure (3.23c); this result could have also been inferred from the $O(M^2)$ ideal gas law (2.12). The other $O(M^2)$ terms decay faster than the reference flow terms because the Mach number of the vortex decreases in time (3.24b), and so the compressibility of the vortex also decreases. When $m \geq 1$, $\tilde{v}_1$ and $\tilde{p}_1$ decay more rapidly than the other $O(M^2)$ variables.

4.2 Perturbed entropy, dissipation, and vorticity

The solutions to (2.11a–c) and (2.12–2.13), form a minimum set of equations which can be used to completely describe the state of a compressible vortex — to $O(M^2)$. However, we can learn more about compressible vortices by explicitly investigating the entropy, dissipation, and vorticity within them. For this reason, we derive the equations which govern these quantities before giving the invariant forms of the $O(M^2)$ perturbation equations (§4.3).

4.2.1 Entropy and dissipation

Using the Gibbs equation [37], the entropy (here in non-dimensional form) is related to the pressure and density in an ideal gas as follows:

$$\tilde{s} = \frac{s - s_\infty}{C_p} = \frac{1}{\gamma} \ln\left(\frac{p}{p_\infty}\right) - \ln\left(\frac{\rho}{\rho_\infty}\right). \qquad (4.5)$$

After writing p and ρ in non-dimensional form using (2.7), expanding (4.5) in a Rayleigh–Janzen expansion (2.8), and then approximating logarithmic terms as

$$\ln(x) = (x-1) + \frac{1}{2}(x-1)^2 + \cdots, \quad (0 < x \leq 2), \tag{4.6}$$

[1] one can show [12]:

$$\tilde{s} = (\tilde{p}_0 - \tilde{\rho}_1)M^2 + O(M^4). \tag{4.7}$$

Hence, the $O(1)$ entropy variation of the reference flow is $\tilde{s}_0 = 0$ — which is expected since $\tilde{T}_0$ and $\tilde{\rho}_0$ are both constant. The $O(M^2)$ compressible entropy perturbation is

$$\tilde{s}_1 = \tilde{p}_0 - \tilde{\rho}_1. \tag{4.8}$$

To find the dissipation, we take the total derivative of $\tilde{s}$, which is, to $O(M^2)$:

$$\frac{D\tilde{s}_1}{D\tau} = \frac{\partial \tilde{s}_1}{\partial \tau} + \tilde{R}e\tilde{u}_1 \underbrace{\frac{\partial \tilde{s}_0}{\partial \tilde{r}}}_{=0}. \tag{4.9}$$

Therefore, differentiating (4.5) by τ gives the total derivative of the entropy, to $O(M^2)$, as

$$\frac{D\tilde{s}_1}{D\tau} = \frac{\partial \tilde{s}_1}{\partial \tau} = \frac{\partial \tilde{p}_0}{\partial \tau} - \frac{\partial \tilde{\rho}_1}{\partial \tau}. \tag{4.10}$$

Using (2.11a), (2.12), and (2.13), the local rate of change of entropy is given by [12]

$$\frac{\partial \tilde{s}_1}{\partial \tau} = (\gamma - 1)\left(\frac{\partial \tilde{v}_0}{\partial \tilde{r}} - \frac{\tilde{v}_0}{\tilde{r}}\right)^2 + \frac{1}{\tilde{r}Pr}\frac{\partial}{\partial \tilde{r}}\left(\tilde{r}\frac{\partial \tilde{T}_1}{\partial \tilde{r}}\right). \tag{4.11}$$

The first term on the right hand side of (4.11) is proportional to the rate of entropy production by viscous dissipation, and the second term is proportional to the rate of change of entropy due to heat conduction. In §6.4 we will use analytical solutions of the self-similar equations to investigate the relative magnitude of the terms in this equation.

Before proceeding, note that (4.11) has an interesting consequence for the total heat flux in a slightly-compressible vortex. Using the fact that $\tilde{s}_1 \to 0$ in the far-field,

together with the $O(1)$ solutions for $\tilde{v}_0$ (3.20), one can show that the divergence of the heat flux into or out of the vortex in the far-field is zero,

$$\lim_{\tilde{r}\to\infty} \frac{1}{\tilde{r}} \frac{\partial}{\partial \tilde{r}} \left(\tilde{r} \frac{\partial \tilde{T}_1}{\partial \tilde{r}} \right) = 0.$$

Integrating this equation with respect to $\tilde{r}$ gives

$$\tilde{r} \frac{\partial \tilde{T}_1}{\partial \tilde{r}} = \mathcal{C},$$

where $\mathcal{C}$ is an arbitrary constant. In order for this relation to hold $\tilde{T}_1$ will vary as

$$\tilde{T}_1 \sim \mathcal{C} \ln(\tilde{r})$$

in the far-field. But, $\tilde{T}_1 \to 0$ for $\tilde{r} \to \infty$, therefore $\mathcal{C} = 0$, and the far-field heat flux is zero,

$$\lim_{\tilde{r}\to\infty} \tilde{r} \frac{\partial \tilde{T}_1}{\partial \tilde{r}} = 0.$$

Because of this, the net heat flux within the vortex is also zero

$$\int_0^\infty \frac{1}{\tilde{r}} \frac{\partial}{\partial \tilde{r}} \left(\tilde{r} \frac{\partial \tilde{T}_1}{\partial \tilde{r}} \right) \tilde{r} \mathrm{d}\tilde{r} = 0.$$

Regardless of whether or not a weakly compressible vortex is self-similar, if the overall temperature in the core of the vortex increases, the temperature rise is not caused by the conduction of heat from the far-field into the vortex. Instead, it is only caused by viscous dissipation and pressure work[1]. To state this in another way, the form of the perturbation equations limits the solutions to those cases for which one asymptotically obtains a uniform temperature (as the vortex decays) without the "feed" of heat from infinity.

[1]The total viscous work in a flow can be split into a part which is responsible for deforming fluid particles (the dissipation) and second part which accelerates fluid particles [37]. The acceleration part of the viscous work affects the kinetic energy in the flow, but does not increase the temperature of the fluid; see §6.2.

4.2.2 Vorticity

Having determined the form of the $O(1)$ tangential velocity in §3.2 we can now derive an equation for the $O(M^2)$ vorticity. Expanding the tangential velocity in a Rayleigh–Janzen expansion (2.8), we get

$$\tilde{v} = \tilde{v}_0 + M^2\tilde{v}_1 + O(M^4). \tag{4.12}$$

Taking the curl of (4.12) gives

$$\tilde{\omega} = \tilde{\omega}_0 + M^2\tilde{\omega}_1 + O(M^4), \tag{4.13}$$

where

$$\tilde{\omega}_1 = \frac{1}{\tilde{r}}\frac{\partial}{\partial\tilde{r}}\left(\tilde{r}\tilde{v}_1\right). \tag{4.14}$$

Upon taking of the curl of (2.11c) and also using (2.11a) we find the equation governing the $O(M^2)$ vorticity

$$\frac{\partial\tilde{\omega}_1}{\partial\tau} - \frac{1}{\tilde{r}}\frac{\partial}{\partial\tilde{r}}\left(\tilde{r}\frac{\partial\tilde{\omega}_1}{\partial\tilde{r}}\right) = \frac{\partial\tilde{\rho}_1}{\partial\tau}\tilde{\omega}_0 - \left(\frac{\partial\tilde{\rho}_1}{\partial\tilde{r}} + \tilde{u}_1^*\right)\frac{\partial\tilde{\omega}_0}{\partial\tilde{r}} - \tilde{\rho}_1\frac{\partial\tilde{\omega}_0}{\partial\tau}. \tag{4.15}$$

4.2.3 Similarity forms

The similarity variables for the entropy, dissipation, and vorticity are

$$\left.\begin{aligned} \zeta(\eta) &= \tilde{s}_1(\tau+\tau_i)^{(2m+1)}, \\ \delta(\eta) &= \frac{\partial\tilde{s}_1}{\partial\tau}(\tau+\tau_i)^{2(m+1)}, \\ \varpi(\eta) &= \tilde{\omega}_1(\tau+\tau_i)^{(3m+2)}, \end{aligned}\right\} \tag{4.16a–c}$$

respectively. The corresponding decay rates are

$$\tilde{s}_1 \propto \tau^{-(2m+1)}, \quad \frac{\partial\tilde{s}_1}{\partial\tau} \propto \tau^{-2(m+1)}, \quad \tilde{\omega}_1 \propto \tau^{-(3m+2)}, \tag{4.17a,b,c}$$

and we see that the entropy variation decays at the same rate as $\tilde{T}_1$, $\tilde{\rho}_1$, and $\tilde{p}_0$.

In the following subsection the self-similar forms of each of the $O(M^2)$ equations, including (4.8), (4.11), and (4.15) will be derived.

4.3 Perturbation equations

Substituting the similarity forms of the perturbation variables (4.3a–e) into equations (2.11a–c), (2.12), and (2.13), the partial differential equations describing the $O(M^2)$ perturbations are reduced to the following set of ordinary differential equations:

$$\frac{\mathrm{d}}{\mathrm{d}\eta}(\alpha\eta^{\frac{1}{2}}) = \eta\frac{\mathrm{d}\beta}{\mathrm{d}\eta} + (2m+1)\beta, \tag{4.18a}$$

$$2\eta\frac{\mathrm{d}\psi}{\mathrm{d}\eta} = \beta V^2 + 2\phi V, \tag{4.18b}$$

$$\eta\frac{\mathrm{d}^2\phi}{\mathrm{d}\eta^2} + (\eta+1)\frac{\mathrm{d}\phi}{\mathrm{d}\eta} + \left[3(m+\frac{1}{2}) - \frac{1}{4\eta}\right]\phi = \left(\alpha - \beta\eta^{\frac{1}{2}}\right)\Omega - m\beta V, \tag{4.18c}$$

$$\beta = \gamma\mathcal{P} - \sigma, \tag{4.18d}$$

$$\begin{aligned}\frac{\eta}{Pr}\frac{\mathrm{d}^2\sigma}{\mathrm{d}\eta^2} + \frac{(\eta Pr+1)}{Pr}\frac{\mathrm{d}\sigma}{\mathrm{d}\eta} &+ (2m+1)\sigma \\ &= (\gamma-1)\left[(2m+1)\mathcal{P} + \frac{V^2}{2} - \left(\Omega - \frac{V}{\eta^{\frac{1}{2}}}\right)^2\right].\end{aligned} \tag{4.18e}$$

Transforming (2.14a) and (2.14b), gives the boundary conditions for (4.18a–e):

$$\eta = 0 \quad \begin{cases} \alpha = 0, \qquad \phi = 0, \qquad \eta^{\frac{1}{2}}\dfrac{\mathrm{d}\psi}{\mathrm{d}\eta} = 0, \\ \eta^{\frac{1}{2}}\dfrac{\mathrm{d}\sigma}{\mathrm{d}\eta} = 0, \quad \eta^{\frac{1}{2}}\dfrac{\mathrm{d}\beta}{\mathrm{d}\eta} = 0, \end{cases} \tag{4.19a}$$

and

$$\eta \to \infty \quad \begin{cases} \alpha \to 0, \quad \phi \to 0, \quad \psi \to 0, \\ \sigma \to 0, \quad \beta \to 0. \end{cases} \tag{4.19b}$$

The self-similar forms of the equations for the $O(M^2)$ density (4.8), dissipation (4.11), and vorticity (4.15) are

$$\zeta = -(\gamma - 1)\mathcal{P} + \sigma, \tag{4.20a}$$

$$\delta = (\gamma - 1)\left(\Omega - \frac{V}{\eta^{\frac{1}{2}}}\right)^2 + \frac{1}{Pr}\frac{\mathrm{d}}{\mathrm{d}\eta}\left(\eta\frac{\mathrm{d}\sigma}{\mathrm{d}\eta}\right), \tag{4.20b}$$

and

$$\begin{aligned} \eta\frac{\mathrm{d}^2\varpi}{\mathrm{d}\eta^2} + (\eta+1)\frac{\mathrm{d}\varpi}{\mathrm{d}\eta} &+ (3m+2)\varpi \\ &= m\beta\Omega + \eta\frac{\mathrm{d}\beta}{\mathrm{d}\eta}\left(\Omega + \frac{\mathrm{d}\Omega}{\mathrm{d}\eta}\right) + \eta^{1/2}\left(\alpha - \eta^{1/2}\beta\right)\frac{\mathrm{d}\Omega}{\mathrm{d}\eta}. \end{aligned} \tag{4.20c}$$

The homogeneous parts of (4.18e) and (4.20c) have the same form as the similarity equation for the $O(1)$ vorticity (3.8). Therefore, their homogeneous solutions can be written immediately as

$$\sigma_h = B_m \exp(-\eta_1)\mathrm{L}_{2m}(\eta_1) \tag{4.21}$$

and

$$\varpi_h = W_m \exp(-\eta)\mathrm{L}_{3m+1}(\eta), \tag{4.22}$$

where $\eta_1 = \eta Pr$, B_m and W_m are arbitrary constants, and the subscript h refers to the homogeneous part of each solution. Likewise, the homogeneous part of the equation for the $O(M^2)$ tangential velocity (2.11c) and the $O(1)$ tangential velocity equation (2.9b) have the same form. Using (2.9b), (3.18a), and (4.18c) one can show that the forms of ϕ_h and $V(\tau + \tau_i)^{(m+1/2)}$ will be somewhat alike:

$$\phi_h = -\frac{(3m+1)Q_m \exp(-\eta)}{\eta^{\frac{1}{2}}}\left[\mathrm{L}_{3m+1}(\eta) - \mathrm{L}_{3m}(\eta)\right], \tag{4.23}$$

where Q_m is an arbitrary constant.

4.3.1 The behavior of the solutions

Before giving solutions to (4.18a–e) for the Oseen vortex ($m = 0$) and the Taylor vortex ($m = 1$) reference flows, we will use the forms of these equations to reveal some of the physical characteristics of slightly-compressible, self-similar vortices. Specifically, we will examine if these vortices can be isentropic, and briefly look at the Prandtl number dependence of the solutions.

The similarity forms of the reference flow quantities constitute some of the forcing terms of (4.18a–e). The reference flow terms are functions of the viscous timescale τ, and are independent of the Prandtl number. Pr appears explicitly only in (4.18e) — the equation for σ. However, σ and β are directly related by (4.18d), and either σ or β appear as part of the forcing terms in each equation of (4.18a–e). Therefore, all of the $O(M^2)$ terms will vary with both the viscous timescale τ, and the Prandtl number as expected (§1).

Can the compressible self-similar vortex be homentropic? In the homentropic case, $\tilde{s}_1 = \zeta = 0$. If this is true, then (4.20a) requires

$$(\gamma - 1)\mathcal{P} = \sigma. \tag{4.24}$$

Using this relation to replace σ with $\mathcal{P}$ in (4.18e), we see that $\mathcal{P}$ must depend on Pr in order for the vortex to be homentropic. However, since the base flow is incompressible, the base flow pressure must be independent of Pr. Therefore, a slightly-compressible, self-similar vortex cannot be homentropic[2]. The Pr dependence of the solutions is further explored in §§5.1.2 and 5.1.3.

In the next section (4.18–4.23) are used to find self-similar solutions for the $O(M^2)$ compressible perturbations to both an incompressible Oseen vortex and an incompressible Taylor vortex.

[2]If a slightly-compressible vortex is not self-similar, one can specify an initial condition where the vortex is homentropic [12]. However, this condition is only valid at a single instant in time.

Chapter 5

Solutions

5.1 Analytical solutions for the slightly-compressible Taylor vortex

For $m = 1$, (3.16), (3.20), and (3.22), can be used to reduce (4.18e) to the following relation

$$\begin{aligned} \eta_1 \frac{\mathrm{d}^2\sigma}{\mathrm{d}\eta_1^2} + (\eta_1 + 1)\frac{\mathrm{d}\sigma}{\mathrm{d}\eta_1} &+ 3\sigma \\ &= -C_1^2(\gamma - 1)\exp(-2\eta)\left[\eta^2 - \frac{\eta}{2} + \frac{3}{4}\right], \end{aligned} \tag{5.1}$$

where, again, we take $\eta_1 = \eta Pr$. Analytical solutions to (5.1) for a general value of Pr can be found using the Method of Frobenius; the method is outlined in Babister [3]. The particular solution is

$$\sigma_p = -C_1^2(\gamma - 1)\eta_1 \exp(-2\eta_1/Pr)\left[D_0 + 2D_1\eta_1 + 4D_2\eta_1^2 + \sum_{n=3}^{\infty} D_n(2\eta_1)^n\right], \tag{5.2}$$

where

$$\left.\begin{aligned} D_0 &= \frac{3}{4}, \\ D_1 &= \left(\frac{1}{2Pr} - \frac{3}{8}\right), \\ D_2 &= \left(\frac{15Pr^2 - 44Pr + 32}{144Pr^2}\right), \\ &\vdots \\ D_n &= -\frac{(4-2Pr)D_{n-2} + \left[(2n+6)Pr^2 - 4Pr(2n+1)\right] D_{n-1}}{4(n+1)^2 Pr^2}. \end{aligned}\right\} \tag{5.3}$$

Using (4.21) we find that the homogeneous part of the solution for $m = 1$ is

$$\sigma_h = \frac{B_1}{2}\exp(-\eta_1)\left(\eta_1^2 - 4\eta_1 + 2\right), \tag{5.4}$$

and the complete solution is $\sigma = \sigma_h + \sigma_p$. Using (3.22), (4.18$d$) and (4.20$a$), β and ζ are easily found. However, solving equations (4.18a–c) for α, ψ, and ϕ is difficult because (5.2) contains a slowly converging series (see §5.1.2).

Luckily, when $Pr = 1$, it is relatively easy to find simple closed-form solutions for most of the $O(M^2)$ terms. In this case $\eta = \eta_1$, and the particular solution to (5.1) is

$$\sigma_p = -\frac{C_1^2(\gamma - 1)}{4}\exp(-2\eta)(2\eta + 1). \tag{5.5}$$

The total solution for σ is given by

$$\sigma = -\frac{C_1^2(\gamma - 1)}{4}\exp(-2\eta)(2\eta + 1) + \frac{B_1}{2}\exp(-\eta)\left(\eta^2 - 4\eta + 2\right). \tag{5.6}$$

Using this result and (3.22) in (4.18d) and (4.20a) gives the solutions for β and ζ:

$$\beta = \frac{C_1^2}{4}\exp(-2\eta)\left[2\eta(\gamma - 1) - 1\right] - \frac{B_1}{2}\exp(-\eta)(\eta^2 - 4\eta + 2), \tag{5.7}$$

and

$$\zeta = -\frac{C_1^2(\gamma-1)}{2}\eta\exp(-2\eta) + \frac{B_1}{2}\exp(-\eta)(\eta^2 - 4\eta + 2). \tag{5.8}$$

Integrating (4.18a), we find the similarity parameter corresponding to the $O(M^2)$ radial velocity

$$\alpha = \frac{C_1^2\exp(-2\eta)}{4\eta^{\frac{1}{2}}}\left[(2-\gamma) + \eta(1-2\gamma) + 2\eta^2(\gamma-1)\right] - \frac{B_1\eta^{\frac{1}{2}}\exp(-\eta)}{2}\left[\eta^2 - 6\eta + 6\right] + \frac{G_1}{\eta^{\frac{1}{2}}}. \tag{5.9}$$

G_1 is a constant of integration which we will determine from the boundary conditions in (4.19a).

The homogeneous solution for ϕ, which can be found using (4.23), is

$$\phi_h = -\frac{Q_1\eta^{\frac{1}{2}}\exp(-\eta)}{6}(\eta^3 - 12\eta^2 + 36\eta - 24), \tag{5.10}$$

where Q_1 is a constant.

5.1.1 Initial/boundary conditions

C_1 and τ_i are determined so that $\tilde{v}_0 = 1$, at $\tilde{r} = 1$, when $\tau = 0$:

$$\tau_i = \frac{1}{2}, \qquad C_1 = \frac{\exp(1/2)}{2}.$$

The radial velocity in the center of the vortex must be zero (4.19a), so

$$G_1 = -\frac{C_1^2(2-\gamma)}{4}.$$

For this value of G_1, (5.9) shows that far from the vortex core, as $\eta \to \infty$, the radial velocity is

$$\tilde{u}_1^* \sim \frac{G_1}{\eta^{\frac{1}{2}}} = -\frac{C_1^2(2-\gamma)}{4\eta^{\frac{1}{2}}}. \tag{5.11}$$

This result matches the prediction for the far-field radial velocity in the Taylor vortex made by Colonius *et al.* [12].

The solutions for σ, β, and ζ (5.6–5.8) contain polynomials in η. All powers of η in these polynomials are greater than zero. For this reason the boundary conditions (4.19a) are trivially satisfied for any value of B_1. Here we will determine B_1 so that $\tilde{\rho}_1(\tilde{r}=0,\tau=0)$ is close to the value found in the experiments of Mandella [25]. The depth of the vortex density-well is defined as

$$\Delta\rho^* = \frac{\rho(\tilde{r}=0,\tau)-\rho_\infty}{\rho_\infty} = M^2\tilde{\rho}_1(\tilde{r}=0,\tau). \tag{5.12}$$

If, at $\tau=0$, the depth of the density-well is 55.0%, and the Mach number of the vortex is $M=0.67$, then $\tilde{\rho}_1(\tilde{r}=0,\tau=0)=-1.23$. The forms of (5.2) and (5.5) differ, so in order for the series and exact solutions for the $O(M^2)$ density, temperature, and entropy perturbations to match (4.18d), (5.2), and (5.5) require that B_1 for the series solution (denoted B_{1s}), and B_1 for the exact solution (denoted B_{1e}) are related in the following way:

$$B_{1s} = B_{1e} - \frac{C_1^2(\gamma-1)}{4}. \tag{5.13}$$

For an initial density-well depth of 55.0% and $\gamma=1.4$, $B_{1s}=-8.47\times10^{-2}$ and $B_{1e}=-1.67\times10^{-2}$. In §5.1.2 we will show that the series solution for σ (with $Pr=1$) converges to the exact solution when a large number of terms are used in the series. The exact solutions for both the reference flow and the compressible perturbations are plotted in figure 5.1.

The specification of the initial density-well depth is a departure from from the boundary conditions in (4.19a). Rather than only requiring that the gradient of the density is zero at $\tilde{r}=0$, we are also specifying an initial value for the density at the origin. The boundary conditions in (4.19a) are invariant under the transformation group (4.1), but the initial density-well depth condition for $\tilde{\rho}_1$ is not. The resulting shape of the density distribution is dependent on the initial value chosen for $\Delta\rho^*$. Since the coefficient B_1 is determined by this initial $\Delta\rho^*$ the distributions of the self-similar solutions are dependent on the value of B_1 and can differ substantially as B_1 is varied. When B_1 is increased the temperature $\tilde{T}_1$, at $\tilde{r}=0$ increases and can

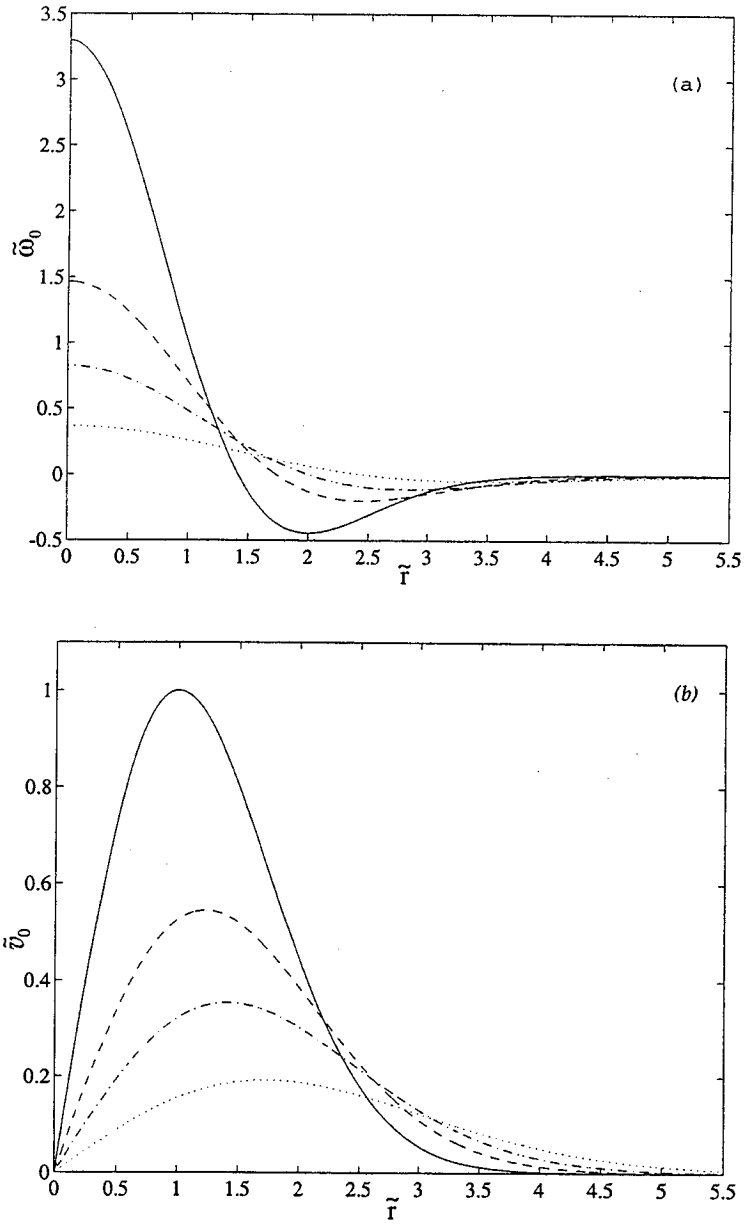

Figure 5.1: *a,b*

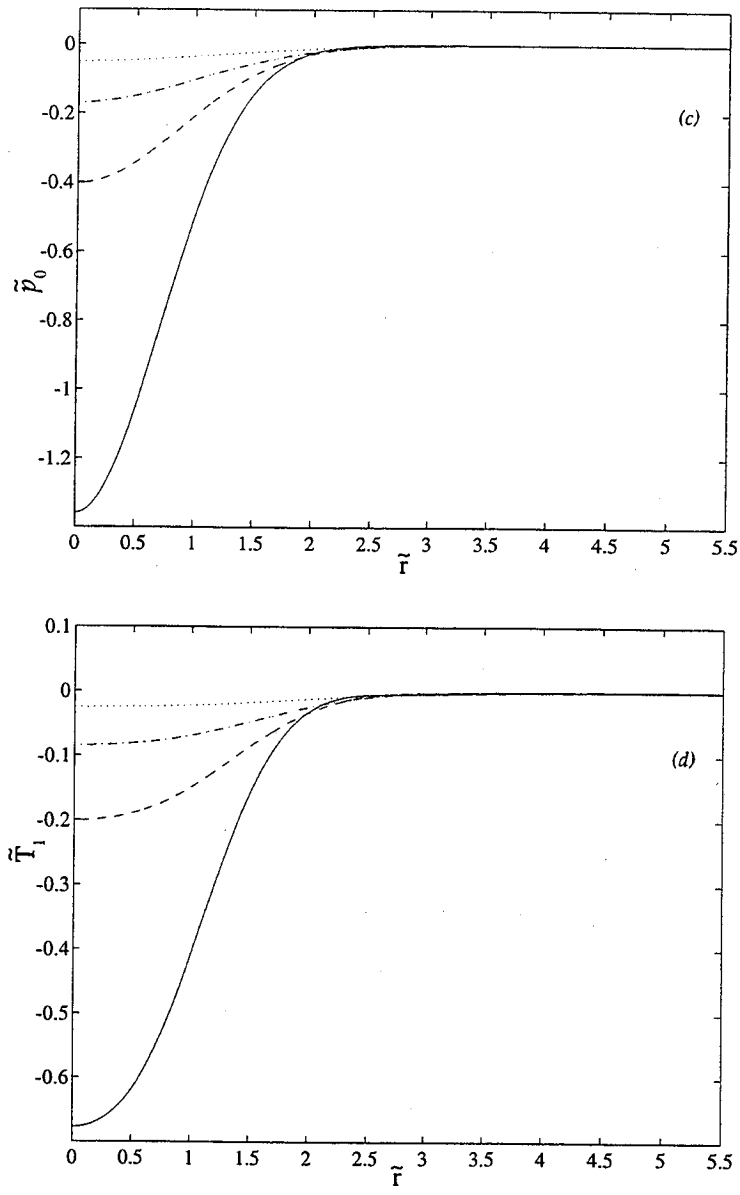

Figure 5.1: c, d

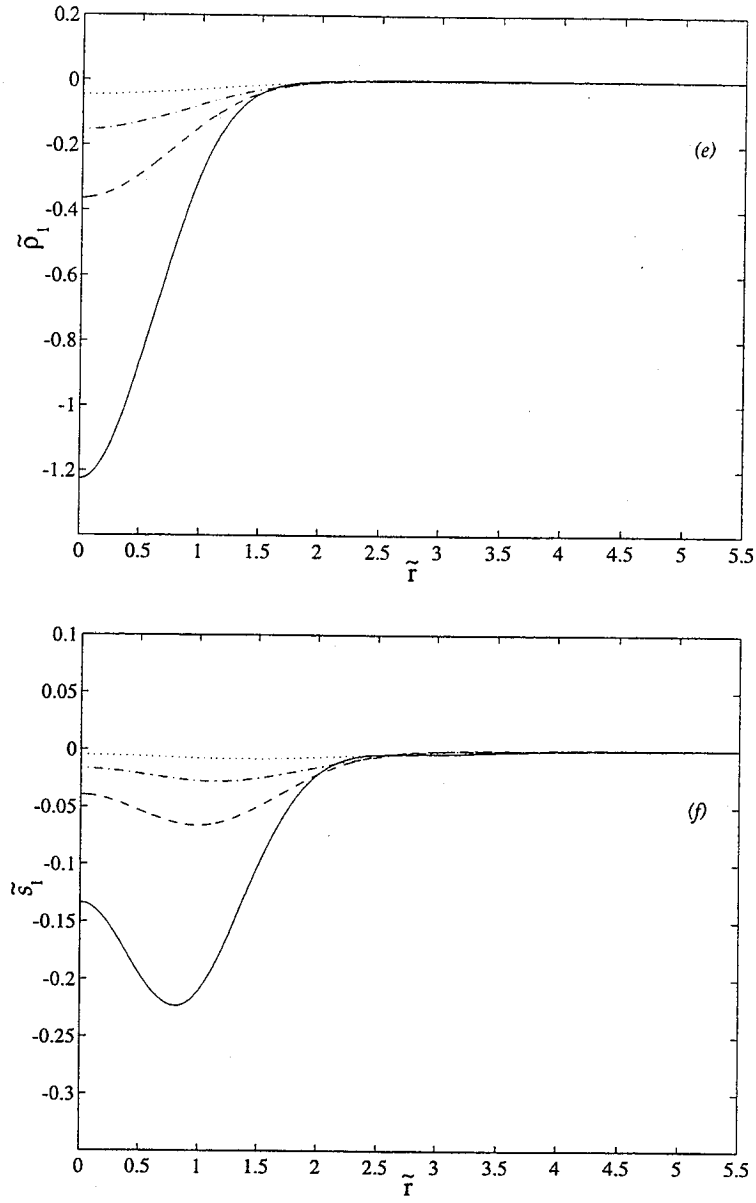
0.2
0
-0.2
-0.4
-0.6
-0.8
-1
-1.2
$\tilde{\rho}_1$
(e)
0 0.5 1 1.5 2 2.5 3 3.5 4 4.5 5 5.5
$\tilde{r}$
0.1
0.05
0
-0.05
-0.1
-0.15
-0.2
-0.25
-0.3
$\tilde{s}_1$
(f)
0 0.5 1 1.5 2 2.5 3 3.5 4 4.5 5 5.5
$\tilde{r}$

Figure 5.1: *e,f*

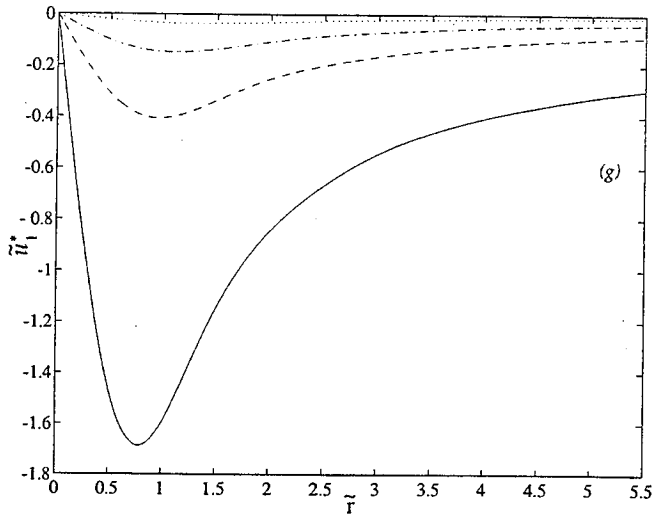

Figure 5.1: Exact solutions for a slightly-compressible Taylor vortex with $\tau_i = 1/2$, $Pr = 1$, $\gamma = 1.4$, $C_1 = \exp(1/2)/2$, $B_{1e} = -1.67 \times 10^{-2}$. Results for four different times are shown: ——, $\tau = 0$; – – – –, $\tau = 1/4$; —·—, $\tau = 1/2$, and ·····, $\tau = 1$. Reference flow quantities are plotted in (a) vorticity, (b) tangential velocity, and (c) pressure. The compressible perturbations are shown in (d) temperature, (e) density, (f) entropy, and (g) radial velocity.

become positive; the corresponding value of density $\tilde{\rho}_1$ decreases. The trends in $\tilde{\rho}_1$ and $\tilde{T}_1$ are reversed when B_1 is reduced (see figure 5.2). Since (4.19a) is still satisfied after applying the initial density-well depth condition, the solutions are self-similar in time.

5.1.2 Convergence rates

To determine the number of terms in the series solution N, required to accurately give the distribution of the $O(M^2)$ quantities,

$$err = \frac{\tilde{T}_{1e} - \tilde{T}_{1s}}{\tilde{T}_{1e}} \tag{5.14}$$

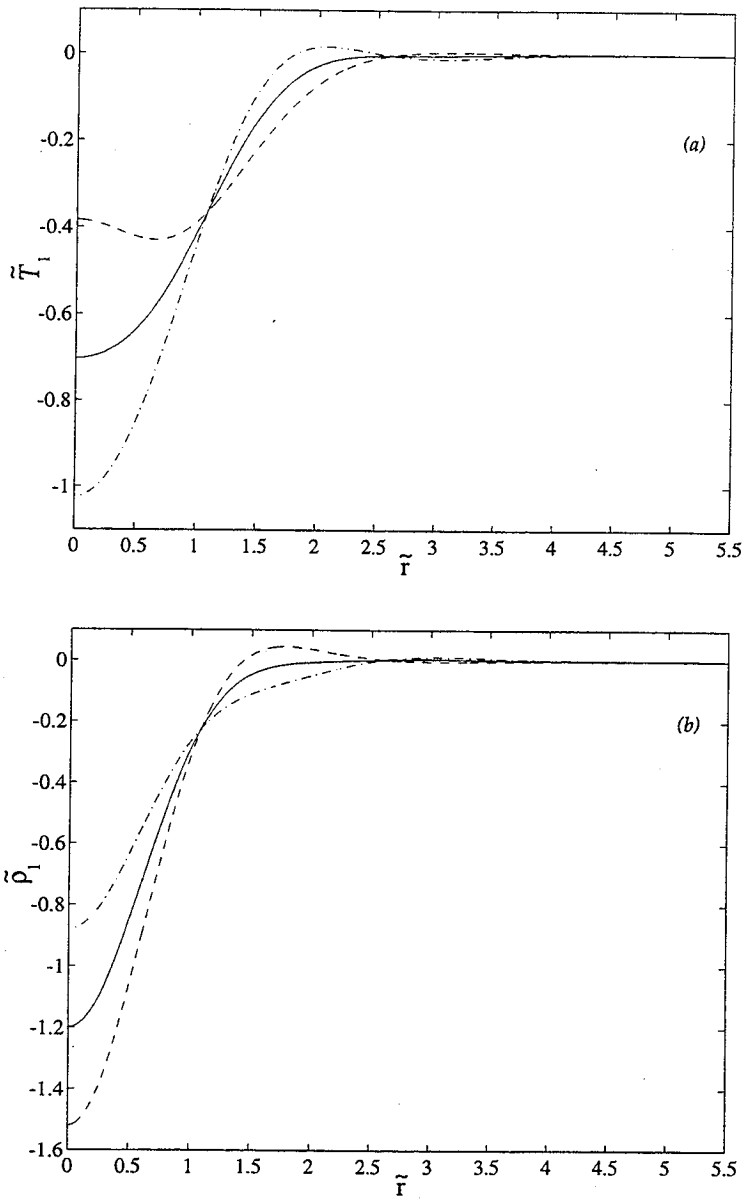

Figure 5.2: *a,b*

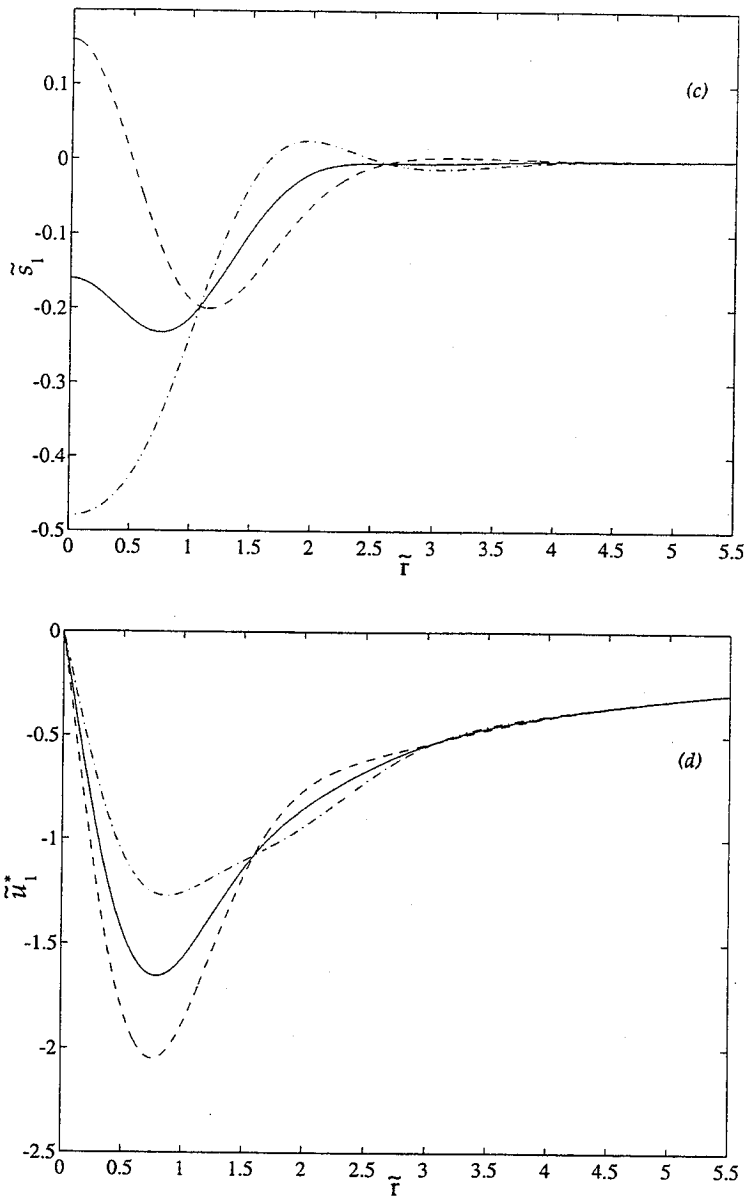

Figure 5.2: Variation of the exact solution with $\tau_i = 1/2$, $\tau = 0$, $Pr = 1$, $\gamma = 1.4$, $C_1 = \exp(1/2)/2$. Radial distributions of $O(M^2)$ (a) temperature, (b) density, (c) entropy, and (d) radial velocity, are shown for three different values of B_{1e}:
– – – –, $B_{1e} = 2 \times 10^{-2}$; ——, $B_{1e} = -2 \times 10^{-2}$; —·—, and $B_{1e} = -6 \times 10^{-2}$.

is plotted in figure 5.3 for $Pr = 1$ and different values of η. The term err is a measure of the relative error in the series solution; $\tilde{T}_{1e}$ and $\tilde{T}_{1s}$ are the exact and series solutions for $\tilde{T}_1$, respectively. The error depends on both the size of N and the value of η at which the solution is evaluated. For larger η, more terms are required to accurately represent the solution (figure 5.4).

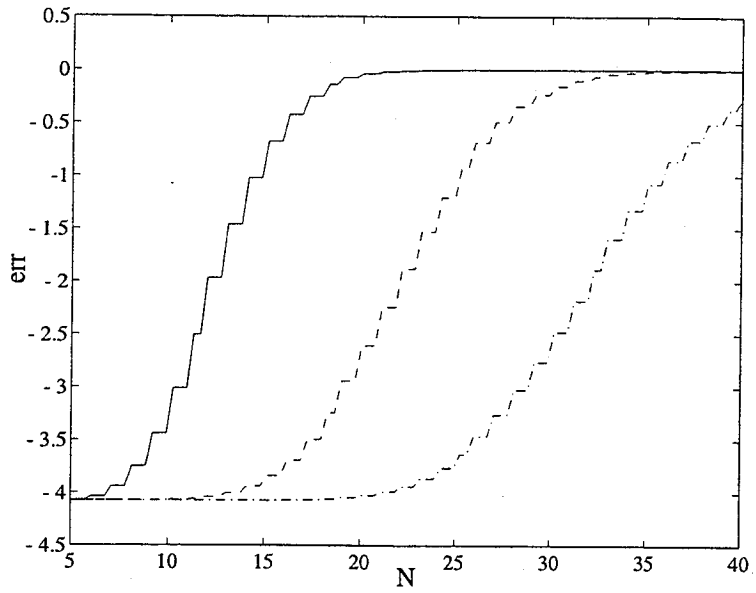

Figure 5.3: Convergence of the series solution as a function of N. Plots show the error (5.14) between the exact and the series solution for $Pr = 1$, $\gamma = 1.4$, $\tau_i = 1/2$, $\tau = 0$, $C_1 = \exp(1/2)/2$, $B_{1s} = -8.47 \times 10^{-2}$, and $B_{1e} = -1.67 \times 10^{-2}$. The error is calculated at three different locations:
——, $\eta = 10$, – – – –, $\eta = 20$, and —·—, $\eta = 30$.

5.1.3 Prandtl number dependence

Consider how the $O(M^2)$ solutions vary with the Prandtl number (figure 5.5). Pr represents the ratio of viscous to thermal diffusion. When $Pr = 1$, heat and viscosity diffuse at the same rate; when $Pr < 1$, heat diffuses faster. Therefore, when the temperature profiles for different values of Pr are plotted on the same graph, and

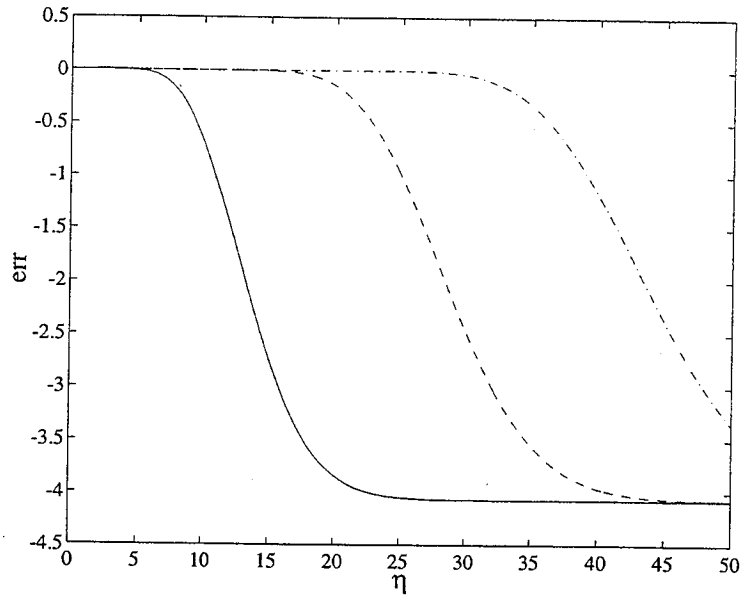

Figure 5.4: Convergence of the series solution as a function of η for different N. Plots show the error (5.14) between the exact and the series solution for $Pr = 1$, $\gamma = 1.4$, $\tau_i = 1/2$, $\tau = 0$, $C_1 = \exp(1/2)/2$, $B_{1s} = -8.47 \times 10^{-2}$, and $B_{1e} = -1.67 \times 10^{-2}$. The error is calculated for: ——, $N = 15$, – – – –, $N = 30$, and —·—, $N = 45$.

each profile is set to the same temperature at $\tilde{r} = 0$ and $\tau = 0$, the temperature distribution for the curve with the smaller value of Pr will extend further from the origin (figure 5.5a). Also, as Pr is lowered, the entropy distribution changes because the heat conduction term in the dissipation equation (4.11) varies inversely with Pr. As Pr decreases, heat conduction has a greater effect on the entropy variation $\tilde{s}$.

In this thesis, values of $Pr = 0.5$, 0.72, and 1.0 are used to get a feel for the behavior of the $O(M^2)$ solutions when Pr is varied over an extreme range. Note that the Pr for most monatomic and diatomic gases at atmospheric pressure lies within the range $0.67 \leq Pr \leq 0.85$ for temperatures between $100\text{K} \leq \text{T} \leq 1300\text{K}$. For a given gas, the Pr is roughly constant, even at large temperatures. The theoretical value of Pr for a monatomic gas is $Pr = 2/3$ [37].

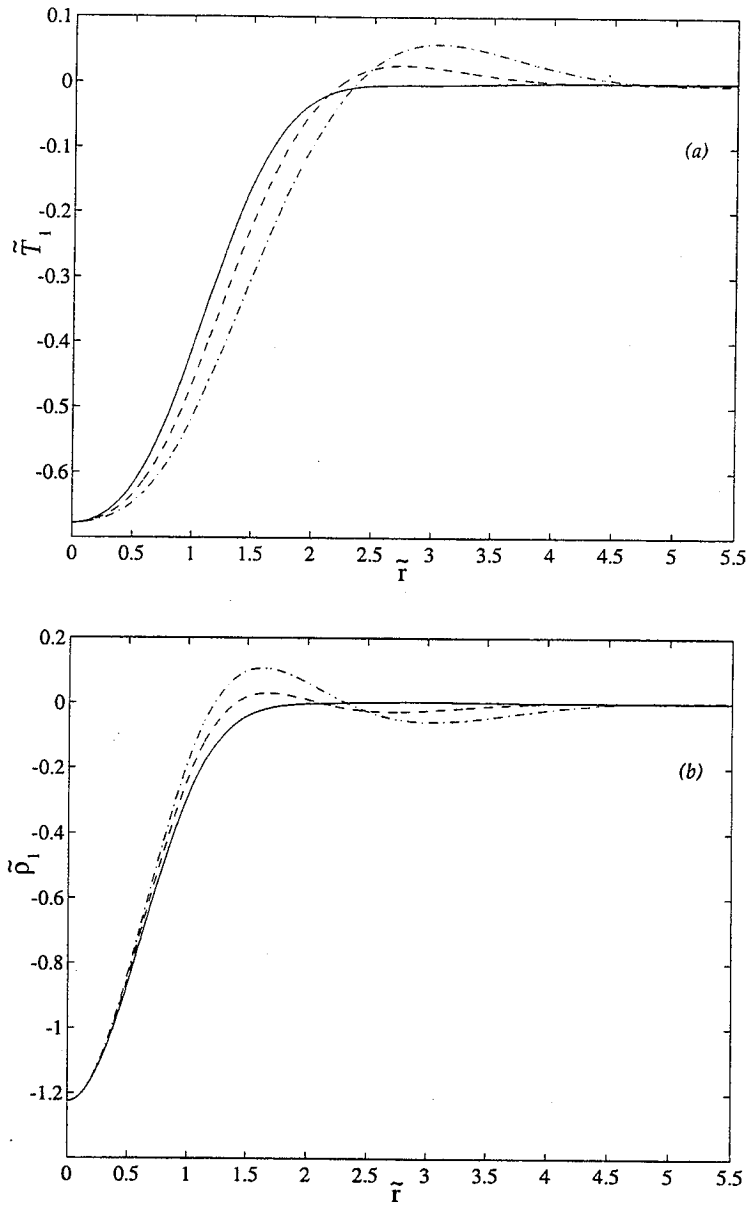
0.1
0
-0.1
-0.2
-0.3
-0.4
-0.5
-0.6
$\tilde{T}_1$
(a)
0 0.5 1 1.5 2 2.5 3 3.5 4 4.5 5 5.5
$\tilde{r}$
0.2
0
-0.2
-0.4
-0.6
-0.8
-1
-1.2
$\tilde{\rho}_1$
(b)
0 0.5 1 1.5 2 2.5 3 3.5 4 4.5 5 5.5
$\tilde{r}$

Figure 5.5: *a, b*

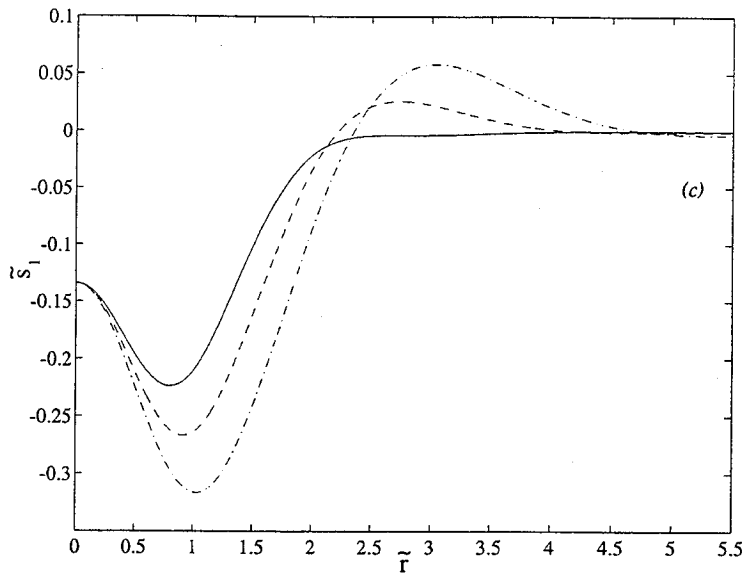

Figure 5.5: Pr dependence of the series solution with $\tau_i = 1/2$, $\tau = 0$, $\gamma = 1.4$, $B_{1s} = -8.47\times10^{-2}$, $C_1 = \exp(1/2)/2$. Radial distributions of $O(M^2)$ (a) temperature, (b) density, and (c) entropy, and are shown for three different values of Pr: ——, $Pr = 1.00$; – – – –, $Pr = 0.72$; and —·—, $Pr = 0.50$.

5.1.4 Entropy production

In accordance with the Second Law of Thermodynamics, the total amount of entropy in the flow must increase. Far from the core of the vortex the entropy is constant, so for $\tilde{r} \to \infty$ the entropy flux is zero. Therefore, the following inequality must hold for the total entropy in the vortex flow:

$$\frac{\mathrm{d}}{\mathrm{d}\tau}\int_0^\infty \tilde{s}_1 \tilde{r}\,\mathrm{d}\tilde{r} \geq 0. \tag{5.15}$$

As a partial check of the $O(M^2)$ perturbation solutions for the Taylor vortex, we use (3.6), (4.16) and (5.8) in integral (5.15) to verify that the Second Law is not violated. The result is

$$\frac{\mathrm{d}}{\mathrm{d}\tau}\int_0^\infty \tilde{s}_1 \tilde{r}\,\mathrm{d}\tilde{r} = \frac{C_1^2(\gamma-1)}{2(\tau+\tau_i)^3}, \tag{5.16}$$

m	C_m	τ_i
0	0.699	0.199
1	$\frac{\exp(1/2)}{2}$	1/2
2	1.6402	0.7964
3	4.5879	1.0922
4	15.507	1.387

Table 5.1: Values of C_m and τ_i that give $\tilde{v}_0(\tilde{r} = 1, \tau = 0) = 1$ for the first five eigenvalues.

which is always ≥ 0 and so satisfies (5.15). Because the total far-field heat flux into or out of the vortex is zero (see §4.2.1), the net entropy produced in the flow is due to viscous dissipation. The magnitude of this dissipation depends on C_1.

5.2 Numerical solutions

The Oseen vortex ($m = 0$) and the Taylor vortex ($m = 1$) are both commonly used to model two-dimensional incompressible vortices. Therefore, it is interesting to compare the self-similar solutions of the compressible perturbations to these reference flows.

The $O(M^2)$ perturbation equations (4.18a, d, e) and (4.20a) are easy to numerically solve. As in §5.1.1 above, the reference flow constants C_m and τ_i are fixed such that $\tilde{v}_0 = 1$ at $\tilde{r} = 1$ when $\tau = 0$. For reference, table 5.1 lists the values of C_m and τ_i which satisfy this condition for the first five eigenvalues. Equation (4.18e) is first numerically integrated to find the similarity parameter σ, which corresponds to the $O(M^2)$ temperature variation. The second order Runge-Kutta Scheme is used to perform the integration for $0 \leq \eta \leq 10$ on a 1000 point grid. The integration is started at $\eta = 0$ and is initialized so that there is no the heat flux at the origin ($\partial \tilde{T}_1/\partial \tilde{r} = 0$), and the temperature variation at $\tilde{r} = 0$ corresponds to a density variation with a density-well depth of 55.0%. The forcing terms in the equations are determined using the analytical solutions for the $O(1)$ velocity (3.20) and pressure (3.22). Equations

(4.3) and (4.16) together with (4.18a, d), and (4.20a) are then used to calculate $\tilde{u}_1^*$, $\tilde{\rho}_1$, and $\tilde{s}_1$, respectively.

The numerical solutions for an Oseen vortex reference flow with $Pr = 0.5, 0.72$, and 1.0 are given in figure 5.6. The numerical solutions of $\tilde{T}_1$, $\tilde{\rho}_1$, and $\tilde{s}_1$ for the Taylor vortex for these values of Pr duplicate the series solutions already shown in figure 5.5. Therefore, only the solution for $\tilde{u}_1^*$ is shown in figure 5.7.

The radial extent of both the Oseen and the Taylor vortex reference flows is larger for smaller values of Pr. However, as shown in figure 5.5 the temperature, density, and entropy distributions for the Taylor vortex exhibit peaks near the core radius at the smaller Prandtl numbers. The entropy distributions of both reference flows contain local maxima at the origin when $Pr = 0.5$ and 0.72, but entropy peaks at the core radius of the vortex do not appear when the reference flow is an Oseen vortex.

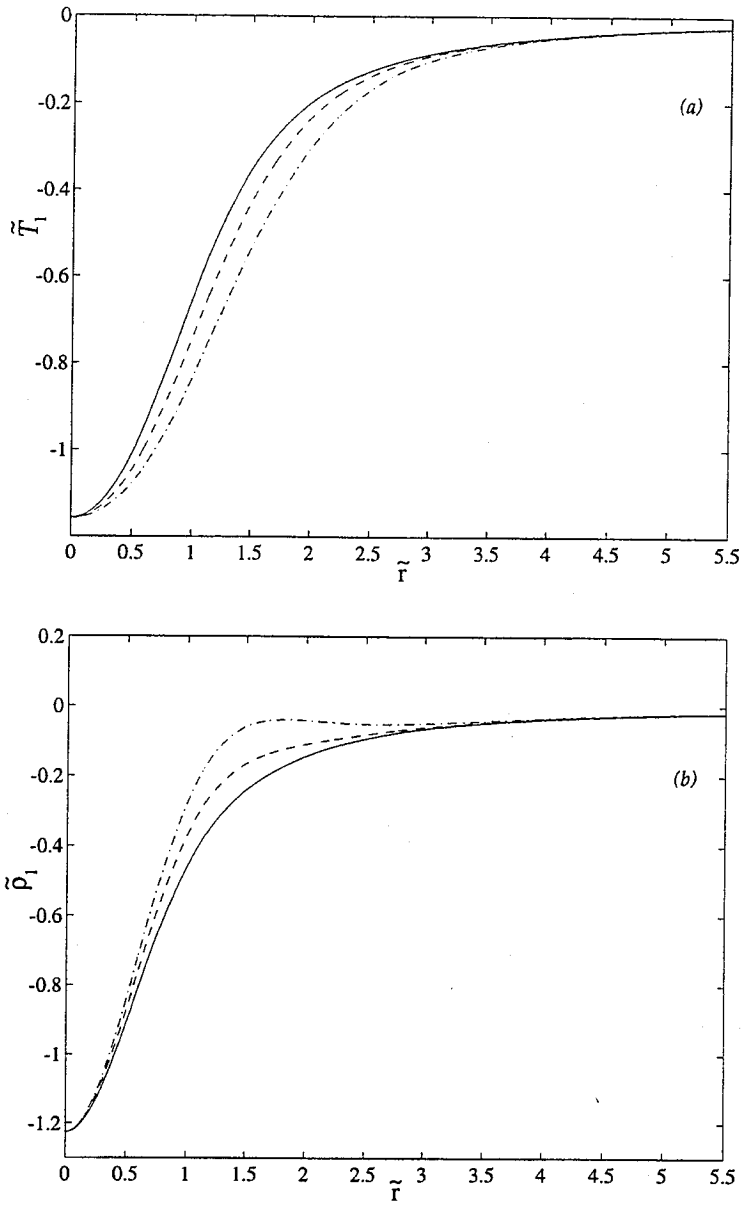

Figure 5.6: a, b

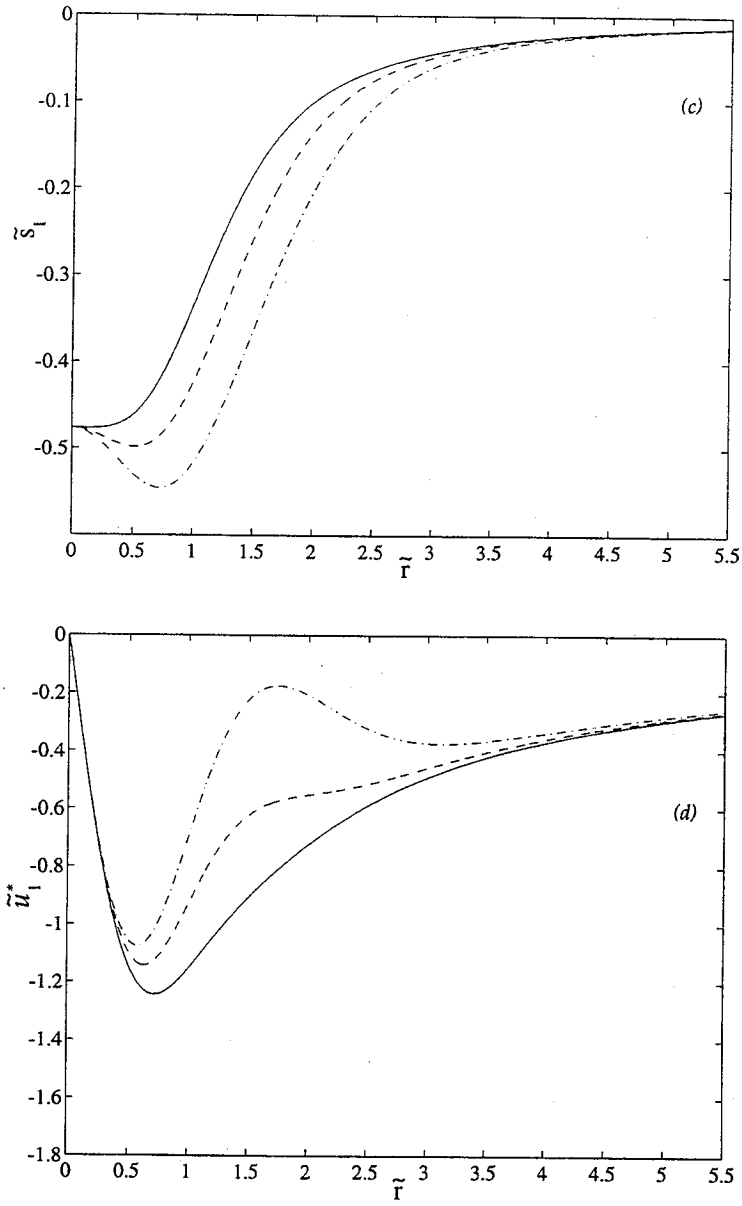

Figure 5.6: Pr dependence of the numerical solution for an Oseen reference flow. $\tau_i = 0.199$, $\tau = 0$, $\gamma = 1.4$, $C_1 = 0.699$. Radial distributions of $O(M^2)$ (a) temperature, (b) density, (c) entropy, and (d) radial velocity are shown for three different values of Pr: ——, $Pr = 1.00$; – – – –, $Pr = 0.72$; —·—, and $Pr = 0.50$.

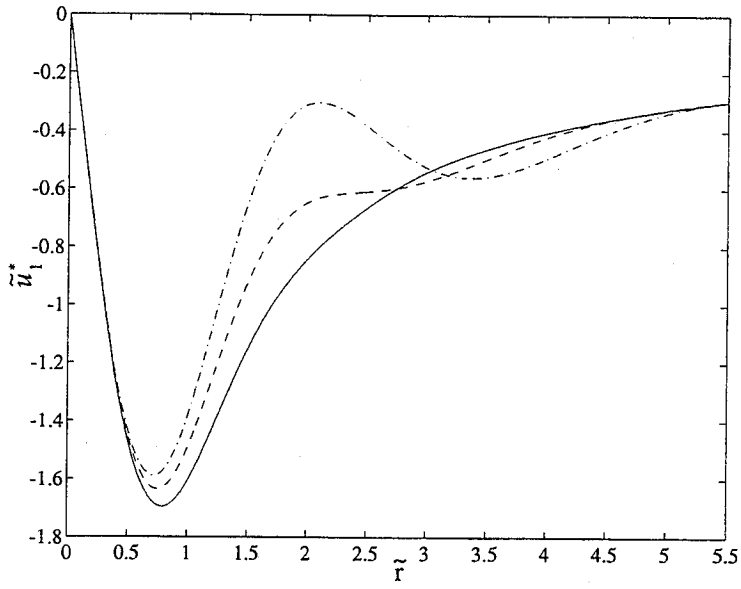

Figure 5.7: Pr dependence of the solution for a Taylor reference flow. $\tau_i = 1/2$, $\tau = 0$, $\gamma = 1.4$, $C_1 = \exp(1/2)/2$. Radial distribution of the $O(M^2)$ radial velocity is shown for three different values of Pr:
——, $Pr = 1.00$; – – – –, $Pr = 0.72$; —·—, and $Pr = 0.50$.

Chapter 6

Discussion

One of the most significant differences between two-dimensional compressible- and incompressible- vortices, is that compressible vortices may possess a radial flow, but incompressible vortices cannot. Therefore, we begin our discussion of the $O(M^2)$ solutions given in §§ 5.1 and 5.2 by considering the radial velocity in a slightly-compressible vortex.

6.1 Radial velocity

The radial velocity $\tilde{u}_1^*$ does not appear in either the $O(1)$ or the $O(M^2)$ radial momentum equations, (2.9a) and (2.11b), respectively. Therefore, the radial velocity does not arise from a force imbalance, such as a difference between the local pressure gradient and the centrifugal force in a rotating vortex flow. Instead, the form of the perturbation equations (2.11a–c),(2.12), and (2.13) and the $O(1)$ reference flow solutions (3.16), (3.20) and (3.21) requires the $O(M^2)$ solutions to have a radial flow. The $O(1)$ reference flow pressure and velocity form the driving terms in the equation for the $O(M^2)$ temperature (2.13). The density $\tilde{\rho}_1$ is, in turn, found from the $O(M^2)$ ideal gas law (2.12), and so is dependent on $\tilde{T}_1$ and $\tilde{p}_0$. The solutions for $\tilde{T}_1$ and $\tilde{p}_0$ necessitate the density in the vortex to increase with time. Therefore, as the vortex decays it is compressed, and the $O(M^2)$ continuity equation (2.11a) requires the radial velocity to convect mass into the vortex. Starting with the $O(M^2)$ temperature

equation (2.13) we can show that far from the core of a slightly-compressible vortex $\tilde{u}_1^*$ is necessarily negative and varies like $\tilde{u}_1^* \sim 1/\tilde{r}$. The volume integral of (2.13), taken over the whole flow-field, is

$$\begin{aligned} \frac{\mathrm{d}}{\mathrm{d}\tau}\int_0^\infty \tilde{T}_1 \tilde{r}\mathrm{d}\tilde{r} \;-\; & \frac{1}{Pr}\int_0^\infty \frac{\partial}{\partial \tilde{r}}\left(\tilde{r}\frac{\partial \tilde{T}_1}{\partial \tilde{r}}\right)\mathrm{d}\tilde{r} \\ = \;& (\gamma-1)\left[\int_0^\infty \left(\frac{\partial \tilde{v}_0}{\partial \tilde{r}} - \frac{\tilde{v}_0}{\tilde{r}}\right)^2 \tilde{r}\mathrm{d}\tilde{r} + \frac{\mathrm{d}}{\mathrm{d}\tau}\int_0^\infty \tilde{p}_0 \tilde{r}\mathrm{d}\tilde{r}\right]. \end{aligned} \tag{6.1}$$

Owing to the fact that there is no net heat flux into or out of the vortex (see §4.2.1), the second integral on the left hand side of this equation is zero. Using the $O(M^2)$ ideal gas law (2.12), (6.1) becomes

$$-\frac{\mathrm{d}}{\mathrm{d}\tau}\int_0^\infty \tilde{\rho}_1 \tilde{r}\mathrm{d}\tilde{r} = (\gamma-1)\int_0^\infty \left(\frac{\partial \tilde{v}_0}{\partial \tilde{r}} - \frac{\tilde{v}_0}{\tilde{r}}\right)^2 \tilde{r}\mathrm{d}\tilde{r} - \frac{\mathrm{d}}{\mathrm{d}\tau}\int_0^\infty \tilde{p}_0 \tilde{r}\mathrm{d}\tilde{r}. \tag{6.2}$$

The second integral on the right hand side of this equation can be expressed in terms of the $O(1)$ tangential velocity by integrating $(2.9a)$:

$$-\frac{\mathrm{d}}{\mathrm{d}\tau}\int_0^\infty \tilde{p}_0 \tilde{r}\mathrm{d}\tilde{r} = \frac{\mathrm{d}}{\mathrm{d}\tau}\int_0^\infty \frac{\tilde{v}_0^2}{2}\tilde{r}\mathrm{d}\tilde{r}. \tag{6.3}$$

Using (6.3) and $(2.11a)$ in (6.2) we find that

$$\lim_{\tilde{r}\to\infty} \tilde{r}\tilde{u}_1^* = (\gamma-2)\int_0^\infty \left[\left(\frac{\partial \tilde{v}_0}{\partial \tilde{r}}\right)^2 + \left(\frac{\tilde{v}_0}{\tilde{r}}\right)^2\right]\tilde{r}\mathrm{d}\tilde{r}. \tag{6.4}$$

Since the terms in the integral are positive definite, and physically realistic values of γ lie in the range $1 < \gamma \leq 5/3$, far from the vortex core the radial velocity is necessarily negative (see Colonius *et al.* [12]).

Note that as $\tilde{r} \to \infty$ the compressible perturbation terms vanish $(2.14b)$, and so the far-field flow is essentially incompressible. Because of this, one would expect the asymptotic behavior of the radial velocity around the vortex to have the same form as the radial velocity around a point mass sink in a two dimensional, incompressible

flow. As we can see from (6.4), the far-field radial velocity has this property: it varies with $\tilde{r}$ as $\tilde{u}_1^* \sim 1/\tilde{r}$.

The far-field behavior of the radial velocity will be the same for all values of m and Pr, and suggests that a slightly-compressible vortex is always compressed. In figure 5.6*d* and figure 5.7 we see that for both the case of the Oseen and the Taylor vortex $\tilde{u}_1^*$ is negative for all values of $\tilde{r}$. The magnitude of $\tilde{u}_1^*$ is zero at $\tilde{r} = 0$, increases almost linearly to a maximum, and in the far-field decreases like $1/\tilde{r}$. However, just outside the vortex core (where $\tilde{r} \approx 1$) the magnitude of the radial velocity decreases non-monotonically for $Pr \neq 1$. In both vortices, $\tilde{\rho}_1$ is larger near the core for the smaller values of Pr used, so the fluid within the core is compressed to a lesser extent — the corresponding radial velocity has a smaller magnitude.

6.2 Vortex energetics

The total amount of pressure work performed on a fluid volume is given by the integral of the product of the pressure and fluid velocity at the volume's surface:

$$\int_{\partial \mathrm{V}} p\vec{u} \cdot \mathrm{d}\vec{\mathrm{S}} = \int_{\mathrm{V}} \vec{\nabla} \cdot (p\vec{u})\, \mathrm{dV} = \int_{\mathrm{V}} \left(\vec{u} \cdot \vec{\nabla} p + p\vec{\nabla} \cdot \vec{u}\right) \mathrm{dV}. \tag{6.5}$$

Here we have used Stokes' Theorem to convert the surface integral into a volume integral and split the total pressure work into two terms. The first term $\vec{u} \cdot \vec{\nabla} p$ represents the work required to move fluid against the pressure gradients in the volume and the second term $p\vec{\nabla} \cdot \vec{u}$ is the work done by pressure forces in locally compressing the fluid at each point within the volume. In the far-field, $u \sim 1/r$, the pressure is constant, and the surface area of the two-dimensional flow field is proportional to r. Therefore, from the surface integral in (6.5) we see that the external pressure field surrounding a slightly compressible free vortex performs a net amount of work on the flow as the vortex decays. As viscous shear stresses decrease the tangential velocity, the centrifugal force of the flow's rotation relaxes and the fluid in the vortex core is compressed by the external pressure field. This pressure work, in addition to heat released by the dissipation of the flow's kinetic energy, increases both the temperature

and density of the vortex. To see this in more detail, we will consider the two parts of the total pressure work and their separate effects on the kinetic and internal energy of the flow.

The scalar product of the velocity and the momentum equations gives an expression for the balance of kinetic energy in a flow. Note that the kinetic energy associated with the radial component of the velocity does not enter our analysis because it is $O(M^4)$. Integrating the product of $\tilde{v}_0$ and the tangential momentum equation $(2.9b)$ gives an expression for the total $O(1)$ kinetic energy in the vortex:

$$\frac{\mathrm{d}}{\mathrm{d}\tau}\int_0^\infty \frac{\tilde{v}_0^2}{2}\tilde{r}\mathrm{d}\tilde{r} = -\int_0^\infty \left(\frac{\partial \tilde{v}_0}{\partial \tilde{r}} + \frac{\tilde{v}_0}{\tilde{r}}\right)^2 \tilde{r}\mathrm{d}\tilde{r}. \tag{6.6}$$

We see that since the reference flow is incompressible, only the work involved in viscous dissipation decreases the total $O(1)$ kinetic energy of the flow [21].

The product of $\tilde{v}_0$ and $(2.11c)$, as well as the use of $(2.9a)$, gives an equation for the $O(M^2)$ kinetic energy:

$$\begin{aligned} \tilde{\rho}_1\frac{\partial}{\partial\tau}\left(\frac{\tilde{v}_0^2}{2}\right) \;+\; & \tilde{u}_1^*\frac{\partial}{\partial\tilde{r}}\left(\frac{\tilde{v}_0^2}{2}\right) + \frac{\partial}{\partial\tau}\left(\tilde{v}_0\tilde{v}_1\right) \\ = \; & -\tilde{u}_1^*\frac{\partial\tilde{p}_0}{\partial\tilde{r}} + \tilde{v}_1\frac{\partial}{\partial\tilde{r}}\left[\frac{1}{\tilde{r}}\frac{\partial}{\partial\tilde{r}}\left(\tilde{r}\tilde{v}_0\right)\right] + \tilde{v}_0\frac{\partial}{\partial\tilde{r}}\left[\frac{1}{\tilde{r}}\frac{\partial}{\partial\tilde{r}}\left(\tilde{r}\tilde{v}_1\right)\right]. \end{aligned} \tag{6.7}$$

Integrating this expression over the entire flow field we find the total $O(M^2)$ kinetic energy in the flow

$$\begin{aligned} \frac{\mathrm{d}}{\mathrm{d}\tau}\int_0^\infty \left(\frac{\tilde{\rho}_1\tilde{v}_0^2}{2} + \tilde{v}_1\tilde{v}_0\right)\tilde{r}\mathrm{d}\tilde{r} \;=\; & -\int_0^\infty \tilde{u}_1^*\frac{\partial\tilde{p}_0}{\partial\tilde{r}}\tilde{r}\mathrm{d}\tilde{r} \\ & - \; 2\int_0^\infty \left(\frac{\partial\tilde{v}_0}{\partial\tilde{r}} + \frac{\tilde{v}_0}{\tilde{r}}\right)\left(\frac{\partial\tilde{v}_1}{\partial\tilde{r}} + \frac{\tilde{v}_1}{\tilde{r}}\right)\tilde{r}\mathrm{d}\tilde{r}. \end{aligned} \tag{6.8}$$

From this equation, (3.6), $(3.18a)$, and $(4.3b,d)$, we see that the time derivative of the total $O(M^2)$ kinetic energy varies as $1/\tau^{4m+2}$. Since the total $O(M^2)$ kinetic energy is a perturbation to the total $O(1)$ kinetic energy, it may be either positive or negative in sign. Since this term may be negative, the second term on the right hand

side of (6.8), which represents the contribution of viscous forces, is not necessarily positive-definite. However, in the case of both the Oseen and the Taylor vortex, the first term on the right hand side of (6.8), which gives the $\vec{u}\cdot\vec{\nabla}p$ part of the pressure work in (6.5), always increases the $O(M^2)$ kinetic energy of the vortex. The reason this happens is because the radial velocity in these two vortices is negative for $\tilde{r}>0$.

Turning now to the internal energy of the flow e, let $\tilde{e}=C_vT_\infty e$. With this choice of scaling, $\tilde{e}=\tilde{T}$ and from $(2.11d)$ we find an equation for the balance of internal energy in the flow

$$\frac{\partial\tilde{e}_1}{\partial\tau}=\gamma(\gamma-1)\left(\frac{\partial\tilde{v}_0}{\partial\tilde{r}}-\frac{\tilde{v}_0}{\tilde{r}}\right)^2+\frac{\gamma}{Pr}\frac{1}{\tilde{r}}\frac{\partial}{\partial\tilde{r}}\left(\tilde{r}\frac{\partial\tilde{T}_1}{\partial\tilde{r}}\right)-\frac{(\gamma-1)}{\tilde{r}}\frac{\partial}{\partial\tilde{r}}(\tilde{r}\tilde{u}_1^*). \tag{6.9}$$

Integrating this expression over the entire flow field gives

$$\frac{\mathrm{d}}{\mathrm{d}\tau}\int_0^\infty\tilde{e}_1\tilde{r}\mathrm{d}\tilde{r}=\gamma(\gamma-1)\int_0^\infty\left(\frac{\partial\tilde{v}_0}{\partial\tilde{r}}-\frac{\tilde{v}_0}{\tilde{r}}\right)^2\tilde{r}\mathrm{d}\tilde{r}-(\gamma-1)\int_0^\infty\frac{1}{\tilde{r}}\frac{\partial}{\partial\tilde{r}}\left(\tilde{r}\tilde{u}_1^*\right)\tilde{r}\mathrm{d}\tilde{r}; \tag{6.10}$$

note that the integral of the heat flux is zero (see §4.2.1).

Because the first term on the right hand side of this equation is positive definite, and since fluid is moving into the vortex, the total internal energy of the vortex always increases in time. The second term on the right hand side of (6.10) is proportional to the $O(M^2)$ divergence of the flow and represents the total amount of work performed by the pressure in compressing the fluid within the vortex. To see this note that, to $O(M^2)$, the term $-p\vec{\nabla}\cdot\vec{u}$ in (6.5) is given by

$$-p\vec{\nabla}\cdot\vec{u}\rightarrow-\frac{1}{\tilde{r}}\frac{\partial}{\partial\tilde{r}}\left(\tilde{r}\tilde{u}_1^*\right), \tag{6.11}$$

where (2.7) has been used to make the terms non-dimensional, and the Rayleigh-Janzen expansion (2.8) was applied.

6.3 The entropy distribution

For the initial and boundary conditions chosen in §5.1.1, the far-field entropy is larger than the entropy in the core of the vortex. What could produce a vortex with this feature? Once again, consider the formation of the vortex studied by Mandella & Bershader [26]. The experimental vortex isn't necessarily self-similar, but here we will use Mandella's results to provide some insight into the entropy distributions in compressible vortices. Figures 3.2-3.3 show the formation of a vortex by shock diffraction. When the vortex forms, the shock passing beneath the airfoil diffracts around the trailing-edge of the airfoil (see §3.3). The diffracting shock expands almost cylindrically around the sharp corner and becomes highly curved. During this process, the shock weakens substantially, and the entropy difference across it decreases. The vortex core forms at the trailing-edge of the airfoil, and is surrounded by fluid of higher entropy which wraps around the core as it rotates. The part of the shock passing over the upper section of the airfoil collides with the diffracted lower shock, and the resulting structure knocks the vortex away from the airfoil. The fluid surrounding the vortex has a larger amount of entropy, because the fluid comprising this region passes through the less-curved parts of the upper and lower shocks. Both the upper shock and the majority of the lower shock are stronger than the part of the shock which diffracts around the airfoil's trailing-edge. Additionally, any portion of a shock which passes through the vortex, such as the shock structure which forms from the collision of the upper and lower shocks, is considerably weakened as it travels through the low pressure region of the vortex core. In this scenario one would expect the vortex to contain a local "cold spot" with less entropy than the surrounding fluid. If this is the case, does the experimental data reported by Mandella [25] support this conclusion?

Mandella [25] presents formulae for curves fit to experimental measurements of pressure and density in a compressible vortex:

$$\rho(r) = \rho_\infty - \frac{\Delta\rho}{1 + \left(\frac{r}{\Delta r}\right)^2}, \tag{6.12}$$

and

$$p = p_\infty - \frac{\Delta p}{1 + \left(\frac{r}{\Delta r_p}\right)^2}. \tag{6.13}$$

Here, $\Delta r_p = 0.117$ cm is a length scale for the pressure profile, and $\Delta r = 0.166$ cm is a length scale related to the density profile. The other parameters include:

$$\rho_\infty = 1.787 \text{ kg m}^{-3}, \quad \Delta\rho = 1.076 \text{ kg m}^{-3}, \tag{6.14}$$

and

$$p_\infty = 152100 \text{ N m}^{-2}, \quad \Delta\text{p} = 107300 \text{ N m}^{-2}. \tag{6.15}$$

Also note that Mandella gives a core size $l_i \approx 0.93$mm based on his estimate of the tangential velocity.

We can use these formulae to calculate the entropy $\tilde{s}$, in the vortex. Evaluating (4.5) with these parameters gives the curve shown in figure 6.1*d*. For the values given in the above curve-fits, the entropy in the center of the vortex is larger than in the far-field. However, Mandella estimates that the pressure curve-fit is accurate to within $\pm 5.6\%$. Note what happens when Δp is increased by 2.0% and then by 4.0% from the value given in (6.15). The entropy in the center of the vortex decreases as Δp increases, and can become less than s_∞. This demonstrates that the entropy distribution is very sensitive to small variations in the values of pressure and density. Therefore, one must be extremely careful to take into account the accuracy of the experiment. While the curve-fits may give reasonable measures of the pressure and density, they cannot be used to conclusively determine the exact values of $\tilde{s}$ in the vortex; the prediction that the far-field entropy is larger than the core entropy lies within the accuracy of the experiment.

6.4 Entropy production

Most of the local entropy changes occurring in the core of a self-similar, slightly-compressible Taylor vortex are caused by heat conduction; since there is no net heat

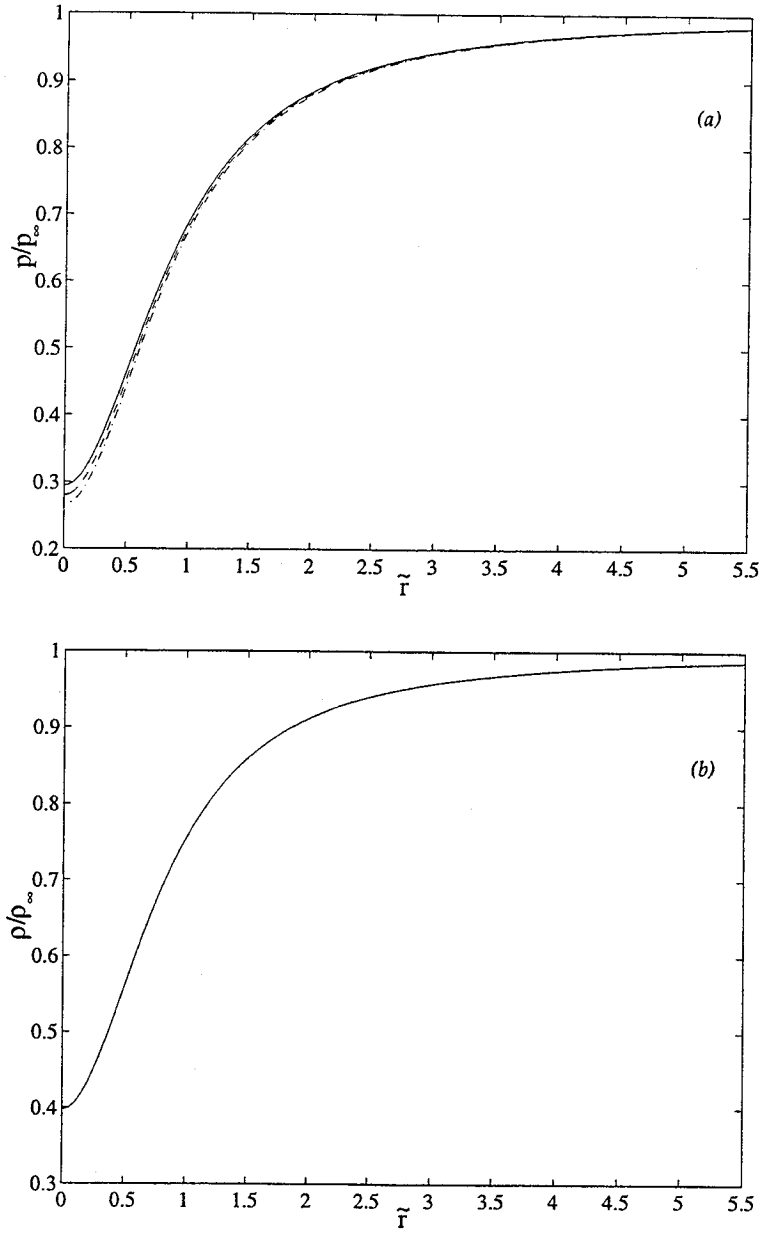

Figure 6.1: *a,b*

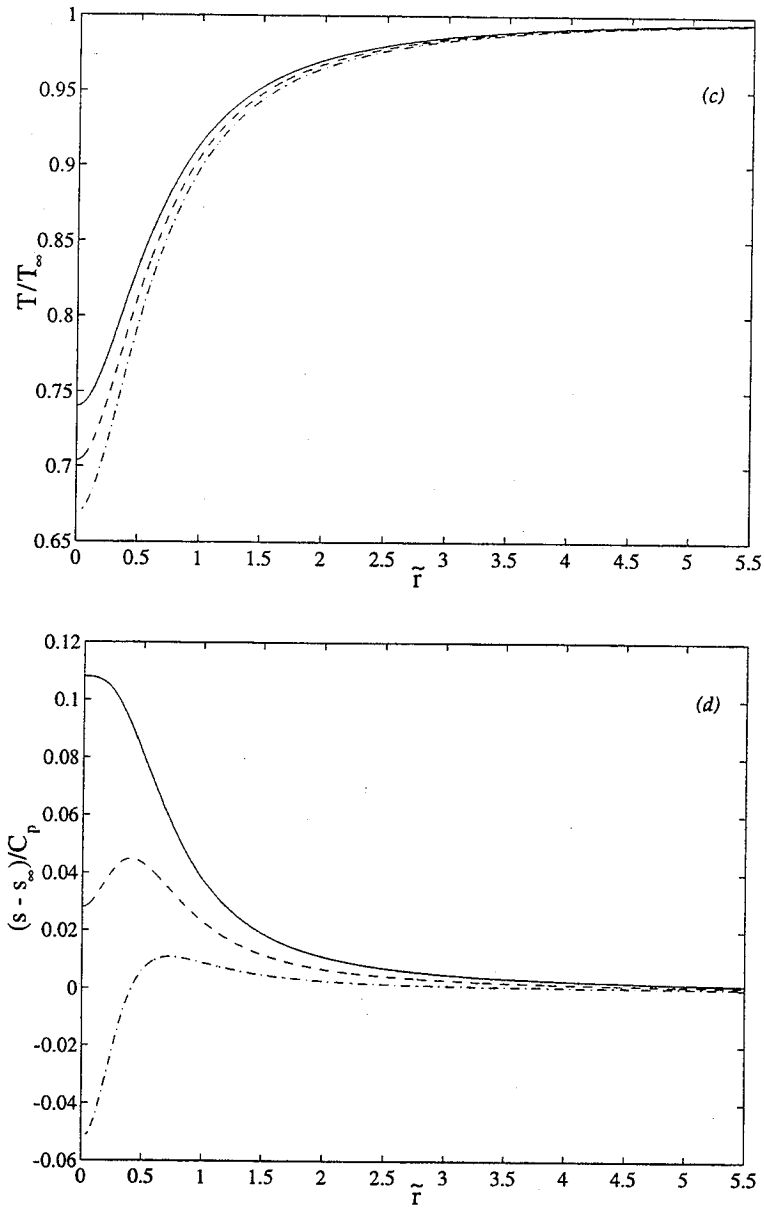

Figure 6.1: Radial profiles of (a) pressure, (b) density, (c) temperature, and (d) entropy from curve-fits of experimental data (Mandella 1987). Small variations in the pressure are given by:
——, $\Delta p = 107300$ N/m^2 nominal pressure curve; – – –, $\Delta p = 109500$ 2.0% increase at $\tilde{r} = 0$, —·—, $\Delta p = 111600$ N/m^2 4.0% increase at $\tilde{r} = 0$.

flux into the vortex the total dissipation produced by heat conduction is zero. To see this, examine the dissipation equation (4.11). The rate of change of entropy is plotted in figure 6.2 for $Pr = 1$ at several different times. The maxima of $\partial\tilde{s}_1/\partial\tau$ correspond to the minima of $\tilde{s}_1$ (figure 5.1f). In figure 6.3 each of the terms in (4.11) is plotted separately. This allows us to compare the relative magnitudes of the rate of entropy changes due to viscous dissipation and due to heat conduction. In the core of the vortex $\tilde{r} \leq 1$, the magnitude of the heat conduction term is larger than the viscous dissipation term. Note that the part of $\partial\tilde{s}_1/\partial\tau$ due to heat conduction is larger than zero, because heat is flowing into the cold core of the vortex. For $\tilde{r} \approx 1$ and longer, the rate of entropy change from heat conduction is less than zero because heat is flowing away from this region and into the vortex core. The rate of dissipation from viscous diffusion is, of course, always greater than zero. As shown in figure 6.3, the series solution for σ_p, (5.2), can be used with (4.16a) and (4.20b) to reveal that the rate of entropy change from heat conduction increases in magnitude as the Prandtl number decreases; when μ is constant, heat diffuses faster, but the rate of viscous diffusion remains the same.

6.5 Similarity and decay rates

In §§4.1.1 and 4.2.3 the similarity forms of the $O(M^2)$ flow variables are used to determine the decay rates of the self-similar solutions. Barenblatt [5] shows several examples of physical phenomena which do not have self-similar initial conditions, but which asymptotically approach a self-similar solution at large times. Here we test this idea, and check to see if the self-similar solutions for the slightly-compressible vortex represent the limiting behavior of compressible vortices which are not initially self-similar.

Consider the decay of the $O(M^2)$ flow quantities governed by (2.11a–c), (2.12), and (2.13). We will assume that the $O(1)$ flow is self-similar because, as discussed in §3.2.4, we cannot superpose the $O(1)$ reference flows for different eigenvalues m and still find self-similar solutions for the $O(M^2)$ terms. Since the reference flow is self-similar and the forcing terms in (2.11a–c), (2.12), and (2.13) are $O(1)$ flow

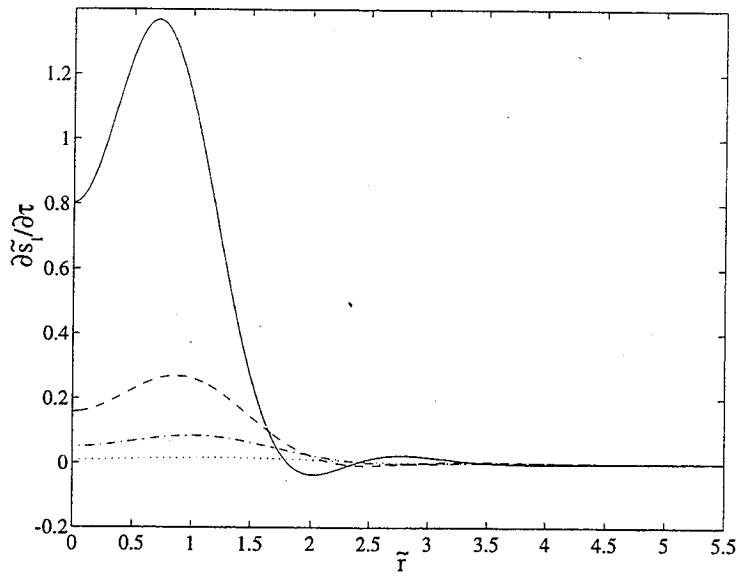

Figure 6.2: Entropy production in the Taylor vortex when $Pr = 1$, $C_m = \exp(1/2)/2$, $\tau_i = 1/2$. ——, $\tau = 0$; – – – –, $\tau = 1/4$, —·—, $\tau = 1/2$, ·····, $\tau = 1$.

variables, the forced parts of the $O(M^2)$ solutions will also be self-similar. Note that these equations are linear in the $O(M^2)$ terms and the Laguerre polynomials, which constitute our solutions, are a mathematically complete set of functions. Therefore, after determining the corresponding particular solution, we can superpose the $O(M^2)$ homogeneous self-similar solutions to construct a solution for any $O(M^2)$ initial condition. At large times the vortex flows resulting from such a superposition process will be governed by the most slowly decaying self-similar component of the flow.

For example, consider the decay rate of the $O(M^2)$ temperature $\tilde{T}_1$ from an initial condition which is not self-similar. Let the $O(1)$ base flow be a Taylor vortex $m = 1$, so that the self-similar part of the solution for the temperature $\tilde{T}_{1ss}$ is given by $(4.3a)$ and (5.6). We can alternatively represent this part of the solution by

$$\tilde{T}_{1ss} = \frac{f_1(\eta)}{(\tau + \tau_i)^3}. \tag{6.16}$$

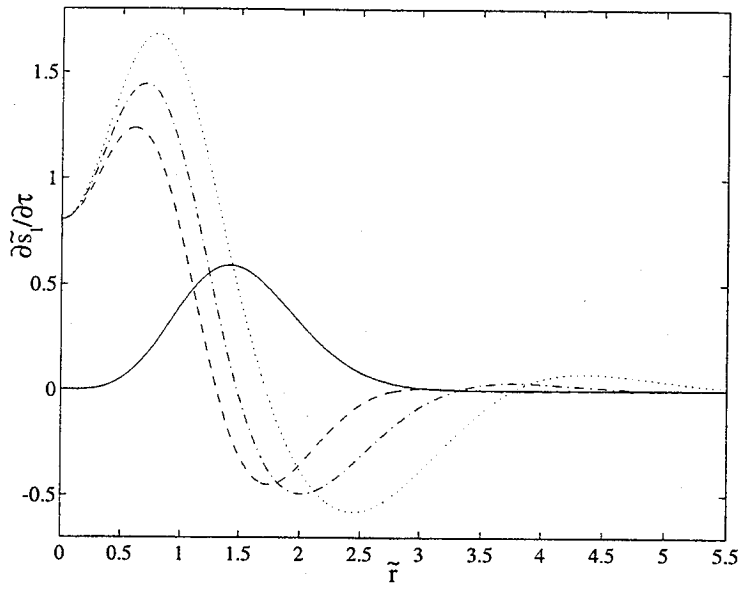

Figure 6.3: Comparison of entropy production by heat conduction and viscous dissipation in the Taylor vortex when $\tau = 0, C_m = \exp(1/2)/2, \tau_i = 1/2$: ——, viscous dissipation terms, and heat conduction terms for – – – –, $Pr = 1$, —·—, $Pr = 0.72$, ·····, $Pr = 0.5$.

We add another self-similar term

$$\tilde{T}_{1ns} = \frac{f_2(\eta)}{(\tau + \tau_i)}, \tag{6.17}$$

to $\tilde{T}_{1ss}$ so that the complete solution represents the evolution of the $O(M^2)$ temperature from an initial condition which is not self-similar

$$\tilde{T}_1 = \tilde{T}_{1ss} + \tilde{T}_{1ns} = \frac{f_1(\eta)}{(\tau + \tau_i)^3} + \frac{f_2(\eta)}{(\tau + \tau_i)}. \tag{6.18}$$

This expression shows that the limiting behavior of the solution for $\tilde{T}_1$ is dominated by its most slowly decaying component, which in this case is $\tilde{T}_{1ns}$.

From (4.3a–e) and (4.16a–c)we see that the decay rates of the $O(M^2)$ self-similar terms decrease as the eigenvalue m decreases. Therefore, the motion of a decaying vortex which is not initially self-similar, will asymptotically approach the self-similar solution corresponding to the component of the superposed solutions with the lowest eigenvalue. If a vortex under computational or experimental investigation is not initially self-similar, a self-similar solution will still give a close approximation to its motion at large times.

Chapter 7

Conclusions & Recommendations

7.1 Conclusions

The objective of this thesis is the development of a simple analytical description of a compressible free vortex. Applying group methods to the Navier-Stokes equations, it is found that they are not invariant under translations in the thermodynamic variables and so do not admit self-similar solutions for compressible free vortex flow. However, the equations governing a slightly-compressible free vortex possess this invariance property; these equations describe a set of incompressible reference flows and the compressible perturbations to each reference flow. The perturbation equations are derived under the assumptions that the viscosity and thermal conductivity of the fluid are constant, the far-field is quiescent with constant values of pressure, density and temperature, and that the flow evolves on a viscous timescale. The reference flow vorticity satisfies an eigenvalue problem in which each eigenvalue corresponds to a different self-similar incompressible vortex. An integral invariant for each vortex solution is determined.

Using the perturbation equations it is shown that, generally: a self-similar slightly-compressible vortex cannot be homentropic; the far-field radial velocity in the vortex is negative and inversely proportional to the radial coordinate; and there is no heat flux into or out of the vortex in the far-field.

A three parameter group, which leaves the reference flow equations and the perturbation equations invariant, is identified. This group is used to convert the flow variables to similarity form and to reduce the perturbation equations from PDE's to ODE's. The similarity forms of the flow variables are used to reveal their decay rates and it is found that all of the thermodynamic quantities decay like $1/\tau^{2m+1}$. Additionally, it is shown that superposed similarity solutions are not self-similar, and that slightly-compressible vortices will asymptotically decay to a self-similar state from arbitrary initial conditions.

A self-similar solution for an Oseen vortex reference flow is found numerically, and both numerical and analytical solutions for a Taylor vortex reference flow are given. For general values of Pr the analytical solutions for the Taylor vortex are composed of infinite series. However, when $Pr = 1$ the solutions are simple closed-form expressions. The closed-form solutions are used to measure the convergence rate of the corresponding series solutions (with $Pr = 1$), and it is found that for $0 \leq \eta \leq 10$ the sum of the first twenty-two terms of the series gives an approximation to the exact solution with an error of less than 1%.

The solutions for the Oseen and Taylor vortices reveal that varying the Prandtl number has a significant effect on the distributions of temperature, density, entropy, and radial velocity in a slightly-compressible vortex. For $Pr = 0.5$, and 0.72 the radial temperature distribution for the Taylor vortex exhibits peaks near the core radius of the vortex. For these values of Pr, the magnitude of the radial velocity in both the Oseen and the Taylor vortex reference flows decreases non-monotonically from a maximum value near the core radius; in contrast, when $Pr = 1$ the decrease in the magnitude of the radial velocity is monotonic. It is shown that the non-monotonic decrease of the radial velocity's magnitude, for $Pr \neq 1$, is due to local variations in the compressibility of these vortices.

The density in the self-similar solutions is initialized so its minimum value in the vortex core corresponds to the minimum density in the vortex studied by Mandella [25]. With this choice of density at $\tilde{r} = 0$, the entropy in the core of the self-similar vortex is less than the entropy of the surrounding fluid. It is shown that this prediction for the entropy distribution lies within the accuracy of Mandella's experiment and

that the entropy in the core of the vortex is extremely sensitive to small pressure and density variations.

The dissipation in the Taylor vortex is split into two terms to show that most of the local entropy changes in the vortex core are caused by heat transfer. However, since there is no net heat flux into the vortex for $\tilde{r} \to \infty$, heat conduction does not increase the total entropy in the vortex; instead it only redistributes the existing entropy. For the slightly-compressible vortex, the total entropy produced in the flow comes from viscous dissipation alone.

An examination of the kinetic and internal energy in a slightly-compressible vortex shows that to $O(1)$ all of the kinetic energy in the vortex is consumed by viscous dissipation. However, to $O(M^2)$ the far-field pressure compresses the fluid within the viscously decaying vortex, thereby increasing the density in the vortex core. Part of this pressure work $\vec{u} \cdot \vec{\nabla} p$, together with viscous dissipation, increases the internal energy and temperature in the vortex. The other part of the pressure work, $p\vec{\nabla} \cdot \vec{u}$, increases the $O(M^2)$ perturbation of the vortex's total kinetic energy.

The search for self-similar solutions has yielded simple analytical expressions for the Taylor vortex, and a set of ODE's which can be numerically integrated to find solutions for the compressible perturbations to a great number of different incompressible vortex reference flows. From a theoretical standpoint, the results of the above analysis provide a rich description of the basic physical properties of a slightly-compressible vortex and a foundation for understanding compressible vortices in general. From a practical standpoint, the use of the closed form Taylor vortex solutions is a quick and simple means of validating and initializing numerical simulations of flows containing a free two-dimensional compressible vortex.

7.2 Future work

A couple of important questions have arisen from this work and represent possible extensions of the current study.

Here, it is assumed that the viscous diffusivity and thermal conductivity of the fluid are constant. In reality both of these quantities are temperature dependent.

An interesting continuation of the present work would be to include the temperature dependence of μ and κ by using power law models [41]

$$\mu = \mu_0 T^{n1} \quad and \quad \kappa = \kappa_0 T^{n2};$$

for air $n1 = 2/3$ and $n2 = 0.81$, and for Argon $n1 = 0.72$ and $n2 = 0.73$. Combined with a Rayleigh-Janzen expansion of the temperature, such models may permit one to derive a set of low Mach number perturbation equations which can be solved analytically.

The analysis above does not account for the effects of acoustic waves in the flow. A theoretical study that couples the propagation of acoustic waves and the dynamics of a viscously decaying compressible vortex may help to explain some of the discrepancies between the findings of Mandella [25] and those of Colonius *et al.* [12] (see Appendix A). Such a solution may also be useful for predicting/modelling the circular acoustic waves which arise in shock/vortex interaction [18].

Additionally, a full characterization of the flow during the formation and subsequent evolution of the compressible vortex studied by Mandella [25], [26], has still not been done[1]. Since compressible vortices are present in many flows of engineering and physical interest (see chapter 1), a thorough knowledge of the formation process and structure of a single compressible free vortex is of fundamental importance. Therefore, future computational and experimental effort should also be directed towards more fully understanding the flow studied by Mandella & Bershader.

[1] See §3.3.

Appendix A

Angular Momentum

In §6.1 it is shown that the radial velocity in a slightly-compressible vortex arises from the form of the perturbation equations (2.11a–c),(2.12), and (2.13) and the $O(1)$ reference flow solutions (3.16), (3.20) and (3.21). Mandella & Bershader [26] suggest that the radial velocity in the vortex they investigated arises to counteract the outward spread of angular momentum by viscous diffusion. To further explore these ideas, consider the following preliminary investigation of the conservation of angular momentum in a compressible vortex.

A dimensional analysis of the angular-momentum transport occurring in compressible vortices reveals three flow regimes into which their time evolution can be characterized. Each flow regime is determined by the magnitude of the radial velocity and the core size of the vortex. Note that the main part of this thesis focuses on self-similar, slightly-compressible vortices, but the following analysis applies more broadly to compressible vortices in general.

A.1 Angular momentum transport

For a two-dimensional and cylindrically symmetrical fluid flow, the equation governing the conservation of angular momentum, expressed in cylindrical coordinates, is:

$$\rho r^2 \frac{\partial}{\partial t}\left(\frac{v}{r}\right) + \rho u \frac{\partial}{\partial r}(rv) - \frac{1}{r}\frac{\partial}{\partial r}\left[r^3 \mu \frac{\partial}{\partial r}\left(\frac{v}{r}\right)\right] = 0. \qquad \text{(A.1)}$$

The first term in this equation is the local time rate of change of angular momentum, the second its convection by radial mass flux, and the final term is its rate of change due to viscous torque. Using the constants l_i, τ_t, ρ_∞, μ, u_m, and v_m, the angular momentum conservation equation can be cast in the following non-dimensional form:

$$\bar{\rho}\bar{r}^2\frac{\partial}{\partial\bar{t}}\left(\frac{\bar{v}}{\bar{r}}\right)+\left\{\frac{\tau_t u_m}{l_i}\right\}\bar{\rho}\bar{u}\frac{\partial}{\partial\bar{r}}(\bar{r}\bar{v})-\left\{\frac{\mu\tau_t}{\rho_\infty {l_i}^2}\right\}\frac{1}{\bar{r}}\frac{\partial}{\partial\bar{r}}\left[\bar{r}^3\bar{\mu}\frac{\partial}{\partial\bar{r}}\left(\frac{\bar{v}}{\bar{r}}\right)\right]=0. \qquad \text{(A.2)}$$

For the analysis, numerical values characteristic of Mandella's experimental results [25] are used for l_i, ρ_∞, μ, and v_m (see table A.1). Note that v_m cancels from the expression, and that the analysis yields the values for the time constant of angular momentum transport τ_t, and the radial velocity (at l_i) u_m. An examination of the orders of magnitude of the two resulting dimensionless groups (bracketed terms), suggests that there are three flow regimes into which the transport of angular momentum within a vortex can be categorized: convective, convective/diffusive, and diffusive.

Constant	Value	Description
l_i	9.3×10^{-1} mm	Vortex core radius
ρ_∞	$1.8\,\mathrm{kg\,m^{-3}}$	Free-stream density
μ	$1.9\times10^{-5}\,\mathrm{N\,s\,m^{-2}}$	Coefficient of viscosity (air)
v_m	$2.3\times10^{2}\,\mathrm{m\,s^{-1}}$	Tangential velocity at l_i

Table A.1: Physical constants characteristic of the experimental vortex [26].

A.1.1 Convective: $\tau_t u_m/l_i \sim 1.0 \gg \mu\tau_t/(\rho_\infty {l_i}^2)$

In this flow regime convection is the dominant process by which angular momentum is transferred within the vortex. By eliminating τ_t in the inequality, approximate values may be found for the radial velocity: $u_m \gg 1.1\times10^{-2}\ \mathrm{m\,s^{-1}}$ or more roughly $u_m > 3.0\times10^{-2}\ \mathrm{m\,s^{-1}}$. Estimates for the time scale of this motion are given by $\tau_t \sim l_i/u_m$, which yields a time scale of $\tau_t \ll 8.2\times10^{-2}$ s or approximately $\tau_t < 3.0\times10^{-2}$ s. Note that the radial velocities predicted by Mandella $u_m \sim 0.3\ \mathrm{m\,s^{-1}}$ lie in the convective range, and that for the experimental vortex

under investigation, when u_m is negative (inward flow) the angular momentum in the vortex is increasing.

A.1.2 Convective/diffusive: $\tau_t u_m/l_i \sim 1.0 \sim \mu\tau_t/(\rho_\infty {l_i}^2)$

When the magnitude of each dimensionless group is on of the order of 1.0, both the effects of viscosity and convection must be considered in determining angular momentum transport within the vortex. An approximate value of u_m in this region is given by: $3.0 \times 10^{-3}\ \mathrm{m\,s^{-1}} \leq \mathrm{u_m} \leq 3.0 \times 10^{-2}\ \mathrm{m\,s^{-1}}$. The radial velocities reported by Colonius et al. [12] $u_m \sim 6.8 \times 10^{-3}\ \mathrm{m\,s^{-1}}$ lie in this range. The time scale for these effects is $\tau_t \approx 7.9 \times 10^{-2}$ s, which is the same as the viscous time scale of the incompressible reference flow solutions found in §3.1.

A.1.3 Diffusive: $\tau_t u_m/l_i \ll 1.0 \sim \mu\tau_t/(\rho_\infty {l_i}^2)$

In the diffusive regime viscosity is mostly responsible for the spreading of angular momentum. When slight compressibility is present radial velocities in the range $u_m \ll 1.1 \times 10^{-2}\ \mathrm{m\,s^{-1}}$ or around $u_m < 3.0 \times 10^{-3}\ \mathrm{m\,s^{-1}}$ are expected for this regime.

A.2 Discussion

The magnitude of the radial velocity measured by Mandella suggests that convection is the dominant mode of angular momentum transport in the vortex he describes. However, Colonius *et al.* suggest that the radial velocity should be around two orders of magnitude smaller than that determined by Mandella; in this case the angular velocity transport regime would be convective/diffusive. The discrepancy in the magnitude of the radial velocity may be due to unsteady variations in the experimental ambient flow conditions. In the computational study, the external pressure, density, and temperature are fixed — the only mechanism for changes to occur in the vortex is viscosity. In the experiment the vortex forms in a complex, unsteady flow field (§3.3). The vortex is created in the low-pressure region behind an airfoil, and after being traversed by a shock, is convected away from the airfoil. The radial pressure

gradient across the vortex is approximately balanced by its tangential velocity. If there are acoustic waves present in the flow, they could create small changes in the vortex far-field pressure. Such pressure variations might cause the tangential velocity profile to change, and the radial convection of angular momentum may be the mechanism responsible. Please see von Ellenrieder *et al.* [40] for a more complete discussion of how variations of the far-field flow conditions may affect the transport of angular momentum and the distribution of entropy in a free vortex.

Appendix B

Introduction to One-Parameter Lie Groups

This appendix gives a brief introduction to the basic ideas behind Lie (pronounced "lee") group methods. Much of the material presented here has been adapted from Prof. Brian Cantwell's course notes for AA218 "Introduction to Symmetry Analysis" [10]. A more complete description of the theory is presented in the course notes, and also in the text by Bluman & Kumei [8].

B.1 Basic definitions

A *Lie group* is simply a collection of parametrically-defined transformations on the variables in an equation[1]. An equation is *invariant* under a Lie group if the equation is symmetric under the set of transformations in the group. In geometry and art we say that an object is symmetric if we can perform an operation on it, such as a rotation or translation, and after the operation the object has the same appearance. In an analogous way, an equation is *symmetric* if we can substitute transformed variables into the equation and the resulting expression appears the same as the

[1] In general a group may also be applied to a system of equations.

original equation. For example, take the equation

$$\frac{\mathrm{d}y}{\mathrm{d}x} = \frac{y}{x}, \tag{B.1}$$

and the transformation group

$$\tilde{x} = \mathrm{e}^s x, \quad \tilde{y} = \mathrm{e}^s y, \tag{B.2}$$

where s is known as the *group parameter.*

The differentials of x and y in (B.2) transform as

$$\mathrm{d}\tilde{x} = \mathrm{e}^s \mathrm{d}x, \quad \mathrm{d}\tilde{y} = \mathrm{e}^s \mathrm{d}y.$$

On substituting the transformed variables into (B.1) we find

$$\frac{\mathrm{e}^{-s}\,\mathrm{d}\tilde{y}}{\mathrm{e}^{-s}\,\mathrm{d}\tilde{x}} = \frac{\mathrm{e}^{-s}\,\tilde{y}}{\mathrm{e}^{-s}\,\tilde{x}}, \tag{B.3}$$

and after canceling the exponential terms we get

$$\frac{\mathrm{d}\tilde{y}}{\mathrm{d}\tilde{x}} = \frac{\tilde{y}}{\tilde{x}}. \tag{B.4}$$

Aside from the tildes, (B.4) and (B.1) look the same; they are functionally equivalent. Therefore, (B.1) is invariant under the transformation group (B.2).

A Lie group has four main traits, the group: 1) has an identity, 2) has an inverse, 3) is invariant under composition (also known as "closure") and 4) is associative. These properties are important in the development of self-similar solutions because they allow us to derive an invariant functional relationship between the variables in an equation. This functional relationship can then be used to simplify the equation.

Let's dissect the preceding paragraph by first examining the first four properties of a Lie group more closely. Returning to the example transformation group (B.2),

we see that when $s = 0$, $e^s = 1$. So for a given value of the group parameter s, the group becomes an *identity* transformation.[2]

Next, consider a second transformation group for the transformed variables $\tilde{x}$ and $\tilde{y}$ in (B.2) above:

$$\tilde{\tilde{x}} = e^t \tilde{x}, \quad \tilde{\tilde{y}} = e^t \tilde{y}. \tag{B.5}$$

Rewriting (B.5) in terms of the variables x and y we get

$$\left.\begin{aligned} \tilde{\tilde{x}} &= e^t (e^s x) = e^{t+s} x, \\ \tilde{\tilde{y}} &= e^t (e^s y) = e^{t+s} y. \end{aligned}\right\} \tag{B.6}$$

Here we see that if $t = -s$, then $\tilde{\tilde{x}} = x$ and $\tilde{\tilde{y}} = y$. So the group (B.2) has an *inverse* which "takes you back" from the transformed variables $\tilde{x}$ and $\tilde{y}$ to the original variables x and y. Additionally, note that we can define a new variable $u = t + s$, such that

$$\tilde{\tilde{x}} = e^u x, \quad \tilde{\tilde{y}} = e^u y. \tag{B.7}$$

The transformation (B.6), which is a composite of the transformations (B.2) and (B.5), appears the same as the original transformation (B.2) when expressed in terms of the "dummy variable" u in (B.7). Thus, the group (B.2) is *invariant under composition.*

Now suppose that in forming the composite transformation (B.6) we had first transformed the transformation and then applied the result to x and y

$$\left.\begin{aligned} \tilde{\tilde{x}} &= (e^t e^s)\, x = e^{t+s} x, \\ \tilde{\tilde{y}} &= (e^t e^s)\, y = e^{t+s} y; \end{aligned}\right\} \tag{B.8}$$

the composite transformation remains the same. Thus, the group is *associative.*

To show how self-similar solutions to an equation can be found using a Lie group, let's assume that an invariant functional relationship between the variables in an

[2]In general, a Lie group can always be mathematically manipulated so that when the group parameter is zero the group becomes an identity transformation.

equation exists. Using the vectorial representation of a Lie group

$$\tilde{\mathbf{x}} = \mathbf{X}(\mathbf{x}; s), \tag{B.9}$$

the invariant relationship between the quantities is given by

$$\Psi(\tilde{\mathbf{x}}) = \Psi(\mathbf{X}(\mathbf{x}; s)) = \Psi(\mathbf{x}). \tag{B.10}$$

Ψ defines a family of characteristic surfaces or level curves such that Ψ is constant when the invariant relationship between the variables is satisfied. The variables which compose the vector $\mathbf{x}$ then become parametric functions of s (figure B.1).

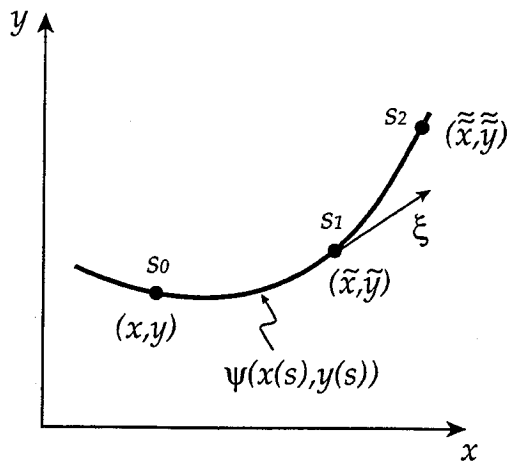

Figure B.1: Along the invariant curve ψ is constant and x and y are parametric functions of s. Lie group transformations map the point s_0 to the points s_1 and s_2. ξ is the vector of infinitesimals and is tangent to the curve ψ.

A convenient way of determining Ψ is to arrange the group (B.9) so that $s = 0$ corresponds to the identity transformation, and then expand the transformation in a

Taylor series near $s = 0$:

$$\tilde{\mathbf{x}} = \mathbf{x} + \left.\frac{\partial \mathbf{X}}{\partial s}\right|_{s=0} s + O(s^2). \tag{B.11}$$

The derivative in the second term, taken in the limit $s \to 0$, is known as an *infinitesimal* and is given by

$$\xi(\mathbf{x}) = \left.\frac{\partial \mathbf{X}}{\partial s}\right|_{s=0} = \left[\left.\frac{\partial \mathbf{X}}{\partial x_i}\frac{\partial x_i}{\partial s}\right|_{s=0} = \left.\frac{\mathrm{d}\mathbf{x}}{\mathrm{d}s}\right|_{s=0}. \tag{B.12}$$

Here the subscript i denotes the i^{th} component of the vector $\mathbf{x}$. The sum of the first two terms in expansion (B.11) is called an *infinitesimal transformation*

$$\tilde{\mathbf{x}} = \mathbf{x} + \xi s. \tag{B.13}$$

Substituting the infinitesimal transformation into (B.10) we get

$$\begin{aligned} \Psi(\tilde{\mathbf{x}}) &= \Psi(\mathbf{x} + s\xi) \\ &= \Psi(\mathbf{x}) + s\left.\frac{\partial \Psi}{\partial s}\right|_{s=0} + \frac{s^2}{2!}\left.\frac{\partial^2 \Psi}{\partial s^2}\right|_{s=0} + \frac{s^3}{3!}\left.\frac{\partial^3 \Psi}{\partial s^3}\right|_{s=0} + \cdots. \end{aligned} \tag{B.14}$$

With the relation

$$\left.\frac{\partial}{\partial s}\right|_{s=0} = \left[\left.\frac{\partial X_i}{\partial x_i}\frac{\partial x_i}{\partial s}\right|_{s=0}\frac{\partial}{\partial x_i} = \xi_i(\mathbf{x})\frac{\partial}{\partial x_i}, \tag{B.15}$$

(B.14) reduces to

$$\begin{aligned} \Psi(\tilde{\mathbf{x}}) = \Psi(\mathbf{x}) + s\xi_i\frac{\partial \Psi}{\partial x_i} &+ \frac{s^2}{2!}\xi_j\frac{\partial}{\partial x_j}\left(\xi_i\frac{\partial \Psi}{\partial x_i}\right) \\ &+ \frac{s^3}{3!}\xi_k\frac{\partial}{\partial x_k}\left[\xi_j\frac{\partial}{\partial x_j}\left(\xi_i\frac{\partial \Psi}{\partial x_i}\right)\right] + \cdots. \end{aligned} \tag{B.16}$$

So a necessary and sufficient condition for Ψ to be an invariant function is that

$$\xi_i \frac{\partial \Psi}{\partial x_i} = 0. \tag{B.17}$$

Geometrically, the gradient of each invariant surface in Ψ is orthogonal to the corresponding vector field of the surface's infinitesimals ξ. Since the gradient of a surface is parallel to the surface's normal, the infinitesimals form a vector ξ which is tangent to the surface (figure B.1).

If there are n components in the vector of transformations (B.9), the partial differential equation (B.17) has an associated system of characteristic equations given by

$$\frac{\mathrm{d}x_1}{\xi_1} = \frac{\mathrm{d}x_2}{\xi_2} = \frac{\mathrm{d}x_3}{\xi_3} = \cdots = \frac{\mathrm{d}x_n}{\xi_n}. \tag{B.18}$$

The solutions of these equations determines the family of invariant surfaces Ψ. There are n variables in the transformation group, and only $(n-1)$ characteristic relations between them. Therefore, once the solutions ψ_j to the characteristic equations are determined, a group of n variables can be specified by $(n-1)$ terms $\Psi = \Psi(\psi_1, \psi_2, \ldots, \psi_{n-1})$. As we will show below, this is where the power of Lie groups for simplifying and solving equations comes from.

As an example let's find Ψ for the transformations given in (B.2). The infinitesimals are

$$\xi_1 = \left.\frac{\mathrm{d}x}{\mathrm{d}s}\right|_{s=0} = x, \quad \text{and} \quad \xi_2 = \left.\frac{\mathrm{d}y}{\mathrm{d}s}\right|_{s=0} = y. \tag{B.19}$$

The associated characteristic equations are

$$\frac{\mathrm{d}x}{x} = \frac{\mathrm{d}y}{y}, \tag{B.20}$$

and so the solution for Ψ is given by

$$\Psi = \Psi(\psi_1), \quad \text{where} \quad \psi_1 = \ln(y/x) \tag{B.21}$$

is a constant of integration. However ψ_1, which is called *an invariant*, should not be strictly thought of as a constant, but as a parameter that determines which invariant curve the solution lies on. Along each curve the invariant will have a constant value.

Let's alternatively represent the family of invariant curves as

$$\Psi = \Psi(y/x).$$

If we let $\bar{\psi}_1 = y/x$ the relation between x and y everywhere on an invariant surface is given by

$$y = \bar{\psi}_1 x. \tag{B.22}$$

Therefore, the family of surfaces Ψ corresponds to a set of rays centered at the origin (figure B.2). As we vary the invariant $\bar{\psi}_1$ we move from one ray to another. But, along any given ray $\bar{\psi}_1$ is fixed.

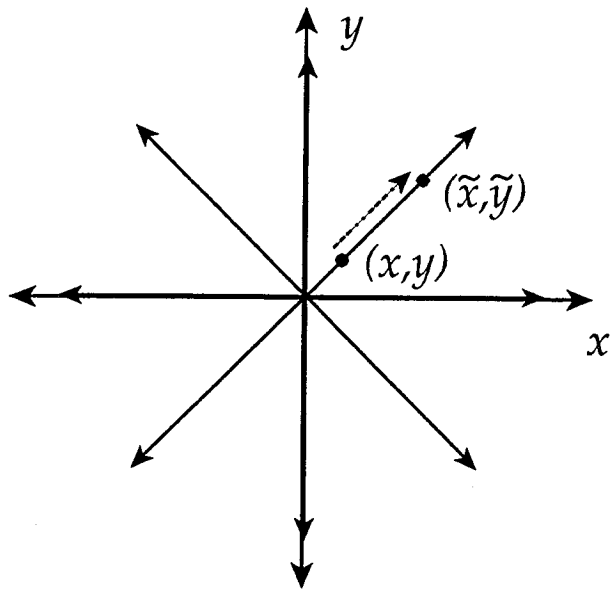

Figure B.2: The transformation (B.2) maps points along rays centered at the origin. Each ray is specified by the numerical value of $\bar{\psi}_1$.

B.2 Simplifying/solving equations

In the simple example above there is only one dependent and one independent variable. Therefore, the relationship between x and y given by (B.22) is also the solution[3] to (B.1).

When there are more than two variables in an equation, the solution for Ψ can be used to simplify the equation by reducing the number of variables required to specify a solution. In this case, the relation between the invariant surfaces can be rewritten as

$$\psi_1 = f(\psi_2, \psi_3, \ldots, \psi_{n-1}). \tag{B.23}$$

Take, for example, the linear, one dimensional, heat equation

$$\frac{\partial \phi}{\partial t} = \frac{\partial^2 \phi}{\partial x^2}. \tag{B.24}$$

This equation is invariant under the following Lie group

$$\tilde{\phi} = \phi, \quad \tilde{x} = \mathrm{e}^s x, \quad \tilde{t} = \mathrm{e}^{2s} t, \tag{B.25}$$

and the corresponding infinitesimals are

$$\xi_1 = 0, \quad \xi_2 = x, \quad \xi_3 = 2t, \tag{B.26}$$

respectively. Since ϕ is already an invariant, let $\psi_1 = \phi$, we don't need to include it in the characteristic equations. The characteristic relations between x and t are

$$\frac{\mathrm{d}x}{x} = \frac{\mathrm{d}t}{2t}. \tag{B.27}$$

Therefore, the second invariant relation is given by

$$\psi_2 = x/\sqrt{t}, \tag{B.28}$$

[3]Note that when solving a problem in which boundary conditions are specified, the Lie group must leave both the equations and its boundary conditions invariant.

and the family of invariant surfaces is defined by

$$\Psi = \Psi(\psi_1, \psi_2). \tag{B.29}$$

As mentioned above, we can alternatively rewrite the relation for the family of invariant surfaces as $\psi_1 = f(\psi_2)$. Therefore, solutions to the heat equation can be found where

$$\phi = f(x/\sqrt{t}). \tag{B.30}$$

If we set $\eta = x/\sqrt{t} = \psi_2$, the partial differential equation (B.24) can be recast as a very simple, readily solvable, ordinary differential equation

$$\frac{\mathrm{d}^2\phi}{\mathrm{d}\eta^2} = -\eta\frac{\mathrm{d}\phi}{\mathrm{d}\eta}. \tag{B.31}$$

One of the features of these solutions (B.30), which holds in general when the relation B.23 is used to simplify an equation, is that they are self-similar. In fact, one can generally say that the identification of a Lie group which leaves an equation invariant guarantees that the equation has a self-similar solution.

Lastly, it should be noted that Lie groups provide an extremely powerful means of solving nonlinear differential equations. They are often used to identify integrating factors for such equations. However, these topics are beyond the scope of this simple introduction; the interested reader should consult the references listed at the beginning of this appendix.

Appendix C

The Integral Invariants A_j

In §3.1 solutions for the reference flow similarity parameter $\Omega(\eta)$ and the corresponding integral invariants $\bar{A}_j$ are given for even values of the eigenvalue/stretching-parameter j. This appendix contains a more detailed explanation of the solution for $\Omega(\eta)$ and a proof that for positive, odd values of j, the integral invariants $\bar{A}_j$ are unbounded.

Equation (3.8) is a form of Kummer's equation [1] and its general solution is

$$\Omega(\eta) = \mathrm{e}^{-\eta}\left[\bar{C}_j \bar{\mathrm{M}}(-\frac{j}{2};1;\eta) + \bar{D}_j \bar{U}(-\frac{j}{2};1;\eta)\right]. \tag{C.1}$$

Here $\bar{C}_j$ and $\bar{D}_j$ are constants and $\bar{U}(-j/2;1;\eta)$ is

$$\bar{U}(-\frac{j}{2};1;\eta) = \frac{\pi}{\sin(\pi)}\left[\frac{\bar{\mathrm{M}}(-j/2;1;\eta)}{\Gamma(-j/2)\Gamma(1)} - \frac{\bar{\mathrm{M}}(-j/2;1;\eta)}{\Gamma(-j/2)\Gamma(1)}\right],$$

which is mathematically "undefined". Therefore, we take $\bar{D}_j = 0$ and there is only one independent solution [3], which is given by (3.9). The hypergeometric function can be expanded to give

$$\bar{\mathrm{M}}(-\frac{j}{2};1;\eta) = \sum_{n=0}^{\infty} \frac{(-j/2)_n \eta^n}{(1)_n n!}. \tag{C.2}$$

$(\ )_n$ is Pochhammer's symbol [1] where

$$(f)_n = \frac{\Gamma(f+n)}{\Gamma(f)} = f(f+1)(f+2)\cdots(f+n-1),$$

f represents any number, and

$$(1)_n = n! \quad \text{and} \quad (f)_0 = 1.$$

Using (C.2) in the invariant integral (3.10) gives

$$\bar{A}_j = 4^{(j+2)/2}\pi\bar{C}_j \sum_{n=0}^{\infty} \frac{(-j/2)_n}{(n!)^2} \int_0^{\infty} \eta^{j/2+n} \mathrm{e}^{-\eta} \mathrm{d}\eta. \tag{C.3}$$

Evaluating this integral, we find that

$$\bar{A}_j = 4^{(j+2)/2}\pi\bar{C}_j \sum_{n=0}^{\infty} \frac{(-j/2)_n}{(n!)^2} \Gamma(\frac{j}{2}+n+1). \tag{C.4}$$

First, let's look at odd values of j. Both $\Gamma(j/2+n+1) > 0$ and $(n!)^2 > 0$, but the sign of

$$(-\frac{j}{2})_n = (-\frac{j}{2})(-\frac{j}{2}+1)(-\frac{j}{2}+2)\cdots(-\frac{j}{2}+n-1)$$

depends on the value of n. For odd j, $(-j/2)_n$ changes sign only once as n increases from $n = 0$ to $n \to \infty$. Because of this, the summation in (C.4) is unbounded.

When j is even, $(-j/2)_n = 0$ for $n \geq j/2+1$ and the series in (C.4) truncates. Taking j to be even gives a finite value of $\bar{A}_j$ and leads to the reference flow solutions found in §3.1.

Appendix D

Similarity at Higher Orders

In chapter 4 the $O(M^2)$ compressible perturbation equations are shown to be invariant under the action of the same three-parameter Lie group (3.4) which leaves the reference flow equations invariant. In this appendix we will explore the similarity of the compressible perturbation equations for higher orders of approximation in the Rayleigh-Janzen expansion (2.8):

$$\tilde{f} = \tilde{f}_0 + M^2\tilde{f}_1 + M^4\tilde{f}_2 + M^6\tilde{f}_3 + \cdots. \tag{D.1}$$

We will find that the $O(M^4)$ equations for the compressible perturbations are also invariant under the same group; the invariance of the perturbation equations may actually exist at each level of approximation in (D.1).

To $O(M^4)$ the equations governing the compressible perturbations are

$$\frac{\partial\tilde{\rho}_2}{\partial\tau} + \frac{1}{\tilde{r}}\frac{\partial}{\partial\tilde{r}}(\tilde{r}\tilde{u}_2^* + \tilde{\rho}_1\tilde{u}_1^*\tilde{r}) = 0, \tag{D.2a}$$

$$\frac{\partial\tilde{p}_2}{\partial\tilde{r}} = \frac{\tilde{\rho}_2\tilde{v}_0^2}{\tilde{r}} + \frac{2\tilde{\rho}_1\tilde{v}_0\tilde{v}_1}{\tilde{r}} + \frac{2\tilde{v}_0\tilde{v}_2}{\tilde{r}} + \frac{\tilde{v}_1^2}{\tilde{r}}, \tag{D.2b}$$

$$\tilde{\rho}_2\frac{\partial\tilde{v}_0}{\partial\tau} + \tilde{\rho}_1\frac{\partial\tilde{v}_1}{\partial\tau} + \frac{\partial\tilde{v}_2}{\partial\tau} + \frac{(\tilde{\rho}_1\tilde{u}_1^* + \tilde{u}_2^*)}{\tilde{r}}\frac{\partial}{\partial\tilde{r}}(\tilde{r}\tilde{v}_0) + \frac{\tilde{u}_1^*}{\tilde{r}}\frac{\partial}{\partial\tilde{r}}(\tilde{r}\tilde{v}_1) = \frac{\partial}{\partial\tilde{r}}\left[\frac{1}{\tilde{r}}\frac{\partial}{\partial\tilde{r}}(\tilde{r}\tilde{v}_2)\right], \tag{D.2c}$$

$$\frac{\partial \tilde{T}_2}{\partial \tau} + \tilde{\rho}_1 \frac{\partial \tilde{T}_1}{\partial \tau} + \tilde{u}_1^* \frac{\partial \tilde{T}_1}{\partial \tilde{r}} + (\gamma - 1)\frac{(\tilde{\rho}_1 + \tilde{T}_1)}{\tilde{r}} \frac{\partial}{\partial \tilde{r}}(\tilde{r}\tilde{u}_1^*) + \frac{(\gamma - 1)}{\tilde{r}} \frac{\partial}{\partial \tilde{r}}(\tilde{r}\tilde{u}_2^*)$$
$$= 2\gamma(\gamma - 1)\left(\frac{\partial \tilde{v}_0}{\partial \tilde{r}} - \frac{\tilde{v}_0}{\tilde{r}}\right)\left(\frac{\partial \tilde{v}_1}{\partial \tilde{r}} - \frac{\tilde{v}_1}{\tilde{r}}\right) + \frac{\gamma}{Pr}\frac{1}{\tilde{r}}\frac{\partial}{\partial \tilde{r}}\left(\tilde{r}\frac{\partial \tilde{T}_2}{\partial \tilde{r}}\right), \tag{D.2d}$$

$$\gamma \tilde{p}_1 = \tilde{\rho}_2 + \tilde{T}_2 + \tilde{\rho}_1 \tilde{T}_1. \tag{D.3}$$

Here, each of the $O(M^4)$ terms is denoted by the subscript 2.

The similarity forms of the $O(M^2)$ flow quantities are given in table D.1. Note that for each similarity variable, the next higher order similarity variable differs by a factor of $(\tau + \tau_i)^{(2m+1)}$. We will not pursue this pattern any further here, but it is quite possible that it persists at successively higher orders of approximation.

$O(1)$	$O(M^2)$	$O(M^4)$
——	$\sigma = \tilde{T}_1(\tau + \tau_i)^{(2m+1)}$	$\sigma_2 = \tilde{T}_2(\tau + \tau_i)^{(4m+2)}$
——	$\beta = \tilde{\rho}_1(\tau + \tau_i)^{(2m+1)}$	$\beta_2 = \tilde{\rho}_2(\tau + \tau_i)^{(4m+2)}$
——	$\alpha = \tilde{u}_1^*(\tau + \tau_i)^{(2m+3/2)}$	$\alpha_2 = \tilde{u}_2^*(\tau + \tau_i)^{(4m+5/2)}$
$V = \tilde{v}_0(\tau + \tau_i)^{(m+1/2)}$	$\phi = \tilde{v}_1(\tau + \tau_i)^{(3m+3/2)}$	$\phi_2 = \tilde{v}_2(\tau + \tau_i)^{(5m+5/2)}$
$P = \tilde{p}_0(\tau + \tau_i)^{(2m+1)}$	$\psi = \tilde{p}_1(\tau + \tau_i)^{(4m+2)}$	$\psi_2 = \tilde{p}_2(\tau + \tau_i)^{(6m+3)}$

Table D.1: Similarity forms.

The similarity forms of the $O(M^4)$ equations are:

$$\eta \frac{\mathrm{d}\beta_2}{\mathrm{d}\eta} + (4m + 2)\beta_2 - \frac{\mathrm{d}}{\mathrm{d}\eta}\left(\alpha_2 \eta^{1/2} + \alpha\beta\eta^{1/2}\right) = 0, \tag{D.4a}$$

$$2\eta \frac{\mathrm{d}\psi_2}{\mathrm{d}\eta} = \beta_2 V^2 + 2\beta V\phi + 2V\phi_2 + \phi^2, \tag{D.4b}$$

$$
\begin{aligned}
-\beta_2\left[\eta\frac{\mathrm{d}V}{\mathrm{d}\eta}+\left(m+\frac{1}{2}\right)V\right] &- \beta\left[\eta\frac{\mathrm{d}\phi}{\mathrm{d}\eta}+\left(3m+\frac{3}{2}\right)\phi\right]-\left[\eta\frac{\mathrm{d}\phi_2}{\mathrm{d}\eta}+\left(5m+\frac{5}{2}\right)\phi_2\right] \\
&+ (\beta\alpha+\alpha_2)\frac{\mathrm{d}}{\mathrm{d}\eta}\left(\eta^{1/2}V\right)+\alpha\frac{\mathrm{d}}{\mathrm{d}\eta}\left(\eta^{1/2}\phi\right) \\
&= \eta^{1/2}\frac{\mathrm{d}^2}{\mathrm{d}\eta^2}\left(\eta^{1/2}\phi_2\right), \qquad \text{(D.4}c\text{)}
\end{aligned}
$$

$$
\gamma\psi = \beta_2+\sigma_2+\beta\sigma, \qquad \text{(D.4}d\text{)}
$$

$$
\begin{aligned}
-\left[\eta\frac{\mathrm{d}\sigma_2}{\mathrm{d}\eta}+(4m+2)\,\sigma_2\right] &- \beta\left[\eta\frac{\mathrm{d}\sigma}{\mathrm{d}\eta}+(2m+1)\,\sigma\right]+\alpha\eta^{1/2}\frac{\mathrm{d}\sigma}{\mathrm{d}\eta} \\
&+ (\gamma-1)(\sigma+\beta)\frac{\mathrm{d}}{\mathrm{d}\eta}\left(\eta^{1/2}\alpha\right)+(\gamma-1)\frac{\mathrm{d}}{\mathrm{d}\eta}\left(\eta^{1/2}\alpha_2\right) \\
&= \frac{2\gamma(\gamma-1)}{\eta}\left[\eta\frac{\mathrm{d}V}{\mathrm{d}\eta}-\frac{V}{2}\right]\left[\eta\frac{\mathrm{d}\phi}{\mathrm{d}\eta}-\frac{\phi}{2}\right] \\
&+ \frac{\gamma}{Pr}\frac{\mathrm{d}}{\mathrm{d}\eta}\left(\eta\frac{\mathrm{d}\sigma_2}{\mathrm{d}\eta}\right). \qquad \text{(D.4}e\text{)}
\end{aligned}
$$

Note that even though each level of approximation in the compressible perturbation equations may be invariant, the sum of terms of different orders for a given variable will not be self-similar; this is because each level of approximation has a different decay rate. From a physical standpoint, we would not expect the sum of several different orders of compressible perturbations to be self-similar, because as discussed in § 2.1.1 above, the full Navier-Stokes equations do not admit similarity solutions for a free compressible vortex.

Bibliography

[1] M. ABRAMOWITZ & I. A. STEGUN, *Handbook of Mathematical Functions.* Dover, 1972.

[2] K. ARDALAN, D. I. MEIRON & D. I. PULLIN, Steady compressible vortex flows: the hollow-core vortex array. *Journal of Fluid Mechanics*, **301**:1–17, 1995.

[3] A. W. BABISTER, *Transcendental Functions Satisfying Nonlinear Differential Equations.* Macmillon Co., 1967.

[4] H. BATEMAN, *Differential Equations.* Longmans, Green and Co., 1918.

[5] G. I. BARENBLATT, *Scaling, Self-similarity, and Intermediate Asymptotics.* Cambridge University Press, 1996.

[6] P. G. BELLAMY-KNIGHTS, Viscous compressible heat conducting spiraling flow. *Quarterly Journal of Mechanics and Applied Mathematics*, **33**:321–336, 1980.

[7] D. B. BERSHADER, Compressible vortices. In *Fluid Vortices.* (ed. S. I. Green). Kluwer Academic Publishers, 1995.

[8] G. W. BLUMAN & S. KUMEI, *Symmetries and Differential Equations.* Springer-Verlag, 1989.

[9] S. N. BROWN, The compressible inviscid leading-edge vortex. *Journal of Fluid Mechanics*, **22**:17–32, 1965.

[10] B. J. CANTWELL, *Introduction to Symmetry Analysis*. Course notes for AA218 "Similitude in Engineering Mechanics", Dept. Aeronautics & Astronautics, Stanford University, 1997.

[11] G. CHIOCCHIA, A hodograph approach to the rotational compressible flow of an ideal fluid. *Quarterly of Applied Mathematics*, **47:3**, 513–528, 1989.

[12] T. COLONIUS, S. K. LELE & P. MOIN, The free compressible viscous vortex. *Journal of Fluid Mechanics*, **230**:45–73, 1991.

[13] A. DE NEUFVILLE, The dying vortex. In *Proceedings of the Fifth Midwestern Conference on Fluid Mechanics*. pp. 365–375. University of Michigan, 1957.

[14] P. G. DRAZIN & W. H. REID, *Hydrodynamic Stability*. Cambridge University Press, 1981.

[15] T. E. FABER, *Fluid Dynamics for Physicists*. Cambridge University Press, 1995.

[16] N. GOLDENFELD, *Lectures on Phase Transition and the Renormalization Group*. Addison–Wesley, 1992.

[17] L. HOWARTH, Some aspects of Rayleigh's problem for a compressible fluid. *Quarterly Journal of Mechanics and Applied Mathematics*, 4(2):157–169, 1951.

[18] C. T. KAO, Experimental and computational studies of two-dimensional compressible vortex-shock interaction. PhD. thesis, Dept. of Aeronautics & Astronautics, Stanford University, 1996.

[19] A. M. KEUTHE & C. Y. CHOW, *Foundations of Aerodynamics: Bases of Aerodynamic Design, 3rd Ed.* Wiley, 1976.

[20] H. LAMB, *Hydrodynamics, 6th Ed.* Cambridge University Press, 1932 (*Reprinted 1995*).

[21] L. D. LANDAU & E. M. LIFSHITZ, *Fluid Mechanics, 2nd Ed.* Pergamon Press, 1987.

[22] P. A. LAGERSTROM, *Laminar Flow Theory.* Princeton University Press, 1996.

[23] L. M. MACK, The compressible viscous heat-conducting vortex. *Journal of Fluid Mechanics*, 8:284–292, 1960.

[24] S. MAHALINGAM, Non-premixed combustion: full numerical simulation of a coflowing axisymmetric jet, inviscid and viscous stability analysis. PhD. thesis, Dept. of Mechanical Engineering, Stanford University, 1989.

[25] M. J. MANDELLA, Experimental and analytical studies of compressible vortices. PhD. thesis, Dept. of Applied Physics, Stanford University, 1987.

[26] M. J. MANDELLA & D. B. BERSHADER, Quantitative study of the compressible vortex: generation, structure, and interaction with airfoils. *AIAA Paper* **87**–0328, 1987.

[27] E. W. MAYER & K. G. POWELL, Similarity solutions for viscous vortex cores. *Journal of Fluid Mechanics*, **238**:487–507, 1992.

[28] P. A. MCMURTRY, W. -H. JOU, J. J. RILEY & R. W. METCALFE, Direct numerical simulations of a reacting mixing layer with chemical heat release. *AIAA Paper* **85**–0143, 1985.

[29] Y. J. MOON & H. C. YEE, Numerical simulation by TVD schemes of complex shock reflections from airfoils at high angle of attack. *AIAA Paper* **87**–0350, 1987.

[30] C. W. OSEEN, Über Wirbelbewegung in einer reibenden Flüssigkeit. *Ark. f. Mat. Astron. Fys.*, **7**, 14, 1912.

[31] P. G. SAFFMAN, *Vortex Dynamics.* Cambridge University Press, 1995.

[32] B. STURTEVANT & V. A. KULKARNY, The focusing of weak shock waves. *Journal of Fluid Mechanics*, **230**:651–681, 1975.

[33] M. SIBULKIN, Unsteady, viscous, circular flow: I. The line impulse of angular momentum. *Journal of Fluid Mechanics*, **11**:291–308, 1961.

[34] K. STEWARTSON, On the impulsive motion of a flat plate in a viscous fluid. *Quarterly Journal of Mechanics and Applied Mathematics*, **4**(2):182–198, 1950.

[35] S. TANEDA, The development of the lift of an impulsively started elliptic cylinder at incidence. *Journal of the Physical Society of Japan*, **33**:1706–1711, 1972.

[36] G. I. TAYLOR, On the dissipation of eddies, 1918. Reprinted in *The Scientific Papers of Sir Geoffrey Ingram Taylor. Vol II. Mechanics of Fluids: Misc. Papers.* (ed. G. K. Batchelor). Cambridge University Press, 1971.

[37] P. A. THOMPSON, *Compressible-Fluid Dynamics.* RPI, 1988.

[38] M. VAN DYKE, *Perturbation Methods In Fluid Mechanics.* Parabolic Press, 1975.

[39] M. VAN DYKE, Impulsive motion of an infinite plate in a viscous compressible fluid. *Zeitschrift für Angewandt Mathematik und Physik*, **3**:343–353, 1952.

[40] K. VON ELLENRIEDER, C. T. KAO, & D. BERSHADER, Physics of a shock-generated freely moving compressible vortex. In *Proceedings of the* $20^{\underline{th}}$ *International Symposium on Shock Tubes and Waves.* World Scientific Press, 1996.

[41] F. M. WHITE, *Viscous Fluid Flow,* $2^{\underline{nd}}$ *Ed.* McGraw-Hill, 1991.

[42] H. T. YANG & L. LEES, *Journal of Mathematics and Physics*, **35**:195–235, 1956.